ASSESSING THE CURRENT LIVE FIRE TRAINING STRUCTURE ENVIRONMENT IN ETHEKWINI USING CFD

THOMAS BENJAMIN BAYLISS CLARKE

SUBMITTED IN FULFILMENT OF THE REQUIREMENTS OF THE DEGREE OF MASTER OF ENGINEERING: MECHANICAL IN THE FACULTY OF ENGINEERING, SCIENCE AND THE BUILT ENVIRONMENT AT THE DURBAN UNIVERSITY OF TECHNOLOGY

.....	.....
SUPERVISOR	DATE
PROFESSOR MARK WALKER	
[redacted]	
.....	.....
CO-SUPERVISOR	12th March, 2020 DATE
DOCTOR FRANK MENDHAM	

DURBAN, SOUTH AFRICA

MARCH 2020

DECLARATION

I declare that this thesis is my own unaided work except where due acknowledgement is made to others. This thesis is being submitted for the Degree of Master of Engineering to the Durban University of Technology and has not been previously submitted for any other degree or examination.

....

Thomas Benjamin Bayliss Clarke Date

ACKNOWLEDGEMENTS

I wish to thank Professor Mark Walker and Dr Frank Mendham for their guidance. I would like thank Alex Gloster, Training Manager at eThekwini Metro Council Fire & Emergency Services, for providing me with information on the existing eThekwini live fire training structure. I would like to thank my parents for their continued support, and I would like to thank Valeska Roelofse for her encouragement throughout this study.

ABSTRACT

eThekwini Fire and Emergency Services currently uses a repurposed structure to train their firefighters. This study identifies fire related hazards for trainee firefighters when using the ground and first floor of the existing structure. The purpose is to prevent shortcomings being repeated in the design of future firefighter training structures.

The fire related hazards have been identified by using Computational Fluid Dynamics (CFD) to simulate fires in the existing structure. The fundamentals of CFD, as well as the selected CFD based fire model, have been summarized. CFD is selected due to its flexibility, accuracy, and cost effectiveness [1]. The Fire Dynamics Simulator (FDS) is the selected CFD based fire model as it has been extensively validated in the past decade [2], which is an important factor should the CFD code claim any credibility [3]. It was developed by the National Institute of Standards and Technology (NIST) to model fire driven fluid flow. It does this by numerically solving a form of the Navier Stokes equations appropriate for thermally driven low Mach flow [4].

Appropriate inputs required for FDS were investigated specifically for live fire training structures. A unique heat release rate (HRR) was investigated and subsequently proposed for a fire on both the ground floor and first floor. The HRR was assessed to find a rate that will be safe from inducing ventilation-controlled conditions and therefore preventing the occurrence of an explosive backdraught. This was investigated by monitoring the effect of the existing structure on a t-

squared fire. A t-squared fire uses a selected growth coefficient to estimate the fire's HRR when the data on the actual fire is not available. Also, the suitability of selecting the emissivity of soot for surfaces was investigated. This was done because it is expected that there would be residual soot deposits in the existing structure. The investigation used the soot modelling capabilities of FDS. This identified the soot density on exposed surfaces and provided an indication on the number of fires required to cover the majority of the exposed surfaces with soot.

The simulations performed in this study were within the required validation range. This included using a selected numerical grid size that was within the validation range for the plume resolution index. There is a range of grid sizes that are valid for the plume resolution index and so to assist in the selection of a suitable grid size from the range of valid grid sizes, the implications of time constraints to complete a simulation were investigated. The investigation compared the accuracy of FDS results when having to restart the simulation multiple times due to limited computer access time, with the accuracy of FDS when using a coarser grid.

From the fire induced environment, the heat flux and gas temperature were estimated to assess the safety of training firefighters. After examining past firefighter deaths, it was considered necessary to include normal civilian tenable limits in the study to identify the time to incapacitation should mistakes occur during training. The structure's surface temperature was also measured to assess possible structural damage due to the concern that the existing structure has been damaged from repeated heating and cooling.

The fire related hazards to trainee firefighters were assessed according to how the safe available time to trainee firefighters was limited. This assessment included the location of the trainee firefighter, the time spent in the location, the time entering the location after the fire is ignited, and the probability of the FDS estimated value exceeding the critical value.

To understand the probability of the FDS estimated value exceeding the critical value, the probability of firefighters being injured at an actual fire incident was considered. In the controlled environment created in the live fire training structure, a firefighter should be less likely to sustain an injury than when attending an actual fire incident, therefore, an acceptable probability was considered when it was less than the probability of a firefighter being injured at an actual fire incident.

Significant post processing of the FDS results were performed to define the hazards firefighters face from heat flux exposure. The selected method for finding the time to a critical heat flux level would have to incorporate the protection provided by the firefighter's protective garments. The best available method was found to be the use of the Thermal Protective Performance (TPP) test used for rating firefighter garments, against an appropriate TPP value.

The commonly used Thermal Dose Unit (TDU) method, used for assessing heat flux exposure damage, was compared to the use of the TPP method. This was done by assessing the standard deviation found in results of both the TDU and TPP method. This thesis further investigated the time required for second degree burns to occur through protective fabrics when exposed to appropriate firefighter heat

flux exposures. An appropriate TPP value was developed by comparing known firefighter working conditions with the resulting heat flux exposure from recommended TPP values.

This study has led to a better understanding of the fire environment created during the live fire training at eThekwini's existing live fire training structure. The relatively unknown conditions experienced by eThekwini's trainee firefighters have now been suitably estimated and extensively detailed. Also, exposed surfaces in the structure have been identified that require additional thermal protection. This study has identified shortcomings that can be avoided in the design of future live fire training structures and which can be considered when training exercises are being planned.

Chapter 1 provides a review of live fire training, fundamentals of CFD and FDS, the design fire, firefighter safety during live fire training, and the scope of this research. Chapter 2 discusses the inputs required for an appropriate FDS model of the existing live fire training structure and explains the output measurements taken from the FDS simulation. Chapter 3 presents and discusses the results of the fire related hazards for trainee firefighters and the need for the structure to receive thermal protection. Chapter 4 concludes the work carried out in this study. Chapter 5 presents recommendations and opportunities upon which future work may be based on the current study.

TABLE OF CONTENTS

LIST OF FIGURES

LIST OF TABLES

NOMENCLATURE

E	Energy
EMC	Equilibrium moisture content
D_α	Diffusion coefficient
f_b	External force vector
F	Exposure energy heat flux
h	Enthalpy
h_s	Sensible enthalpy
H	Relative humidity
k	Thermal conductivity
K, K_1, K_2, W	Coefficients of absorption model
$\dot{m}_\alpha'''$	Mass production rate per unit volume of species α by chemical reactions
$\dot{m}_b'''$	External mass input rate
M	Molecular weight of gas mixture
MLR	Mass loss rate
P	Probability
p	Pressure
$\bar{p}$	Background pressure
$\tilde{p}$	Perturbation pressure
$\dot{q}''$	Heat flux vector
$\dot{q}_r''$	Radiative heat flux
$\dot{q}'''$	HRR per unit volume

$\dot{q}_b'''$	Energy transfer to subgrid particles
$\dot{Q}_s$	Heat source
R	Universal gas constant
$\dot{R}_s$	Reaction source
S_ϕ	Source term
t	Time
T	Temperature
TPP	Thermal protective performance
u, v, w	Velocity component
u_{dep}	Total deposition velocity
X	Position vector (x, y, z)
x_c	Critical value
Y_α	Mass fraction of species α
Z_α	Species mixture α

Greek letters

α	Gas species index
Γ_ϕ	Diffusion coefficient
δ	Bias factor
Δh_c	Effective heat of combustion
$\Delta h_{f,\alpha}$	Heat of formation of the respective species (α)
μ	Dynamic viscosity
μ_a	Mean average

ϕ	General variable
τ_{ij}	Viscous stress tensor
ρ	Density
σ	Standard deviation
$\tilde{\sigma}_M$	Relative standard deviation
Φ	Dissipation function

CHAPTER 1: LITERATURE REVIEW

1.1 Introduction

Firefighters have an inherently dangerous occupation [5]. Raimundo and Figueiredo [6] explain that they are subjected to thermal radiation and have a high metabolic heat production. This, they say can lead to introversion, various degrees of burns, heat stroke, brain damage and even death. It is obvious that firefighters need suitable training to ensure they are ready for such a dangerous occupation. It is also commonly identified as a research area requiring attention [7-9].

Live fire training structures provide important training to firefighters. They provide a space where fire behaviour can be studied, and rescue operations can be conducted in realistic conditions [10]. They allow the simulation of various occupancies and provide the setting for various training objectives to be carried out, such as fire suppression [10].

Live fire training structures simulate a realistic firefighter environment and are therefore dangerous. Firefighters are training for real fire incidents, which is where they receive the most injuries [11], [12]. Before trainee firefighters can train in these realistic environments, they must complete the required prerequisite training. The National Fire Protection Association (NFPA) specify that all training firefighters receive the appropriate training before they are permitted to undertake live fire training [13]. This includes training in health and safety, fire dynamics,

fundamentals of fire behaviour, fire development in a compartment, nozzle techniques and door control.

However, injury and death still occur during live fire training. Madrzykowski [14] identifies two firefighters that died during live fire training due to untenable firefighter conditions exceeding the design capabilities of their protective equipment. The live fire training took place in an acquired structure. The fire was later recreated to understand the fire environment and it was subsequently found that both heat flux and gas temperatures were excessive for tenable firefighter conditions. This tragedy could be avoided if the firefighter's training environment was better estimated prior to training taking place. This can be achieved by use of existing technologies, such as fire models, which can be used to provide the required information [15].

The National Fallen Firefighters Foundation provides "*16 Firefighter Life Safety Initiatives*" that can be used as a guide to reduce injuries and deaths of working firefighters [16].

Included in their "*16 Firefighter Life Safety Initiatives*" is:

> *"(8) Utilize available technology wherever it can produce higher levels of health and safety."*

1.2 Computational fluid dynamics

This section offers a summary on the fundamentals of Computational Fluid Dynamics (CFD) and introduces the concept of using CFD for fire related applications. An in-depth discussion of CFD is avoided here as it is purely used to gather data for this study. In CFD, fluid dynamic based equations are processed through numerical methods on computers to derive an approximate solution [17].

Solving problems involving fluid flow and heat transfer can generally be approached with one of three methods [1].

1. Theoretical method: governing equations are used to produce analytical solutions.
2. Experimental method: a model of a real object is used in a staged experiment to produce a solution.
3. Numerical method: computational procedures are used to produce a solution.

Method 3 is selected due to its flexibility, accuracy, and cost [1]. If used correctly, CFD models can provide detailed fire models in complex geometries and are typically used for estimating time to tenable conditions [15].

Figure 1 breaks down the numerical solution method and details the procedure required to reach an approximate solution.

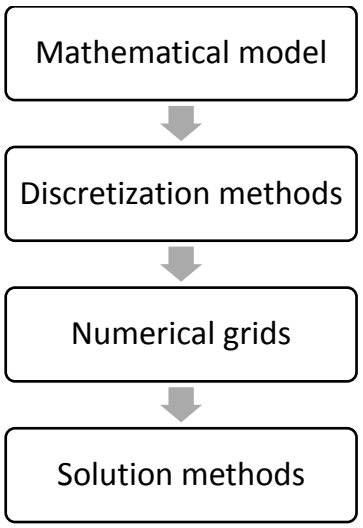

Figure 1: Numerical solution method for hydrodynamic

1.2.1 Mathematical model

The mathematical model is the initial component of the numerical solution. Here the set of governing equations are specified in the form of partial differential equations [18]. The dependent variables are reliant on the natural independent variables of continuum mechanics, which are three-dimensional space and time [19]. This allows the dependant variables to be estimated through the computational domain as time progresses.

Universal laws of conservation are applied to fluid flow to develop the fundamental equations of fluid dynamics [20]. How these governing equations are calculated is dependent on the target application, i.e. is the flow compressible, turbulent, three dimensional, etc. [18].

Conservation of mass

Applying the conservation of mass law to fluid flow produces the continuity equation [20]. For the produced equation to satisfy the conservation of mass law, the following requirement is made:

The rate of increase of mass within the fluid element is equal to the net rate at which mass enters the elemental volume [17].

Conservation of momentum (Newtons Second Law of Motion)

Applying Newton's Second Law to fluid flow produces the momentum equation [20]. For the produced equation to satisfy Newton's Second Law, the following requirement is made:

The rate increase of momentum of the fluid element is equal to the sum of the forces acting on the fluid element [17].

Conservation of energy (First Law of Thermodynamics)

Applying the First Law of Thermodynamics to fluid flow produces the energy equation [20]. For the produced equation to satisfy the First Law of Thermodynamics, the following requirement is made:

The rate of change of energy is equal to the net rate of heat addition, plus the heat rate of work done, plus the rate of heat added or removed by a heat source [17].

Yeoh and Yuen [17] detail the governing equations for time dependent fluid flow in three dimensions as well as heat transfer of a compressible Newtonian fluid. Their equations, Equation 1, Equation 2, and Equation 3, are shown below and have been expressed in symbolic form for simplicity.

Continuity equation

$$\frac{\partial \rho}{\partial t} + u.\nabla(\rho) = 0 \qquad (1)$$

Momentum equation

$$\frac{\partial (\rho u)}{\partial t} + u.\nabla(\rho u) = -\nabla p + \nabla.\tau_{ij} + \sum F_{body\ forces} \qquad (2)$$

Energy equation

$$\frac{\partial (\rho E)}{\partial t} + \nabla.(\rho E) = -u.\nabla(p) + \Phi + \dot{Q}_s - \nabla.\dot{q}'' \qquad (3)$$

CFD is used as a tool to solve complicated problems. Tu, Yeoh and Liu [21] explain that a general form of the governing equations is needed to allow complicated problems to be solved with CFD. This is done by the above equations being represented in a single equation known as the transport equation, Equation 4, is a generic form of the governing equations [17].

$$\frac{\partial(\rho\phi)}{\partial t}+\frac{\partial(\rho u\phi)}{\partial x}+\frac{\partial(\rho v\phi)}{\partial y}+\frac{\partial(\rho w\phi)}{\partial z} \quad (4)$$

$$=\frac{\partial}{\partial x}\left[\Gamma_\phi\frac{\partial\phi}{\partial x}\right]+\frac{\partial}{\partial y}\left[\Gamma_\phi\frac{\partial\phi}{\partial y}\right]+\frac{\partial}{\partial z}\left[\Gamma_\phi\frac{\partial\phi}{\partial z}\right]+S_\phi$$

The equation uses the general variable (ø) to replace any variable quantity in the governing equations. Most of the equation is derived from the common features in the governing equations, with the source term (S_ϕ) comprising of terms that are not shared between the governing equations [17].

To close the system, Pletcher, Tannehill and Anderson [20] specify further equations that are required to establish relationships between fluid properties. They identify the equations of state, Equation 5, as a common equation used to do this. The equation shows the relationship between temperature, pressure, and density.

$$\rho=\frac{pM}{RT} \quad (5)$$

1.2.2 Discretization methods

The method of discretization is chosen after the mathematical model is defined. The discretization method is a process of approximating the governing equations by a system of algebraic equations for the variables at a specific time and space location [18]. The chosen discretization method changes the generic form of the governing equation from a problem involving calculus to an algebraic problem [20].

Ferziger and Peric [18] discuss what the effects are of what they consider to be the most important discretization methods. These are the finite difference method, finite volume method and finite element method. They explain that the chosen method is often selected according to the attitude of the developer with some methods being better suited than others to some classes of problems.

The chosen discretization method will have an effect on the grid type [18].

1. The finite element method uses an unstructured grid.
2. The finite volume method is possible with either a structured or unstructured grid.
3. The finite difference method is most commonly used with structured grids.

After selecting the appropriate grid type, approximations are chosen to be used in the discretization process [18].

1. In the finite volume method, the process of surface and volume integrals being approximated is selected.
2. In the finite element method, weighting functions and shape functions are selected.
3. In the finite difference method, approximations for the derivatives at the grid points are chosen.

1.2.3 Numerical grid

There are a couple of common terms possible here. Here the term grid is used instead of mesh and the term cell is used instead of element.

The basics of the numerical grid discussed here are explained by Blazek [22]. He describes the calculation domain being subdivided into smaller subdomains (cells), forming a grid. This is used to provide specific locations for variables to be calculated. It is noted that three dimensional grids are commonly constructed from cells that are tetrahedra, hexahedra, pyramids, or prisms. When creating a grid, he explains that it is important that grids have no holes, that they do not overlap and have no sudden changes in the cell's volumes. Also, there must be no large bends in the grid lines for quadrilateral and hexahedral cells. This reduces numerical errors [22].

Two common grid types used in CFD are the unstructured grid and the structured grid type [21]. The advantages and disadvantages of each have been collected from Tu, Yeoh and Liu [21].

Structured grid advantages:

1. The grid points of a cell can be simply addressed by using triple indices (i,j,k).
2. The connectivity of a cell is simple due to adjacent cells to a specific cell face being identified by these indices.
3. Easy data management and simple connectivity make programming of the grid easy when used in simple geometries.

Structured grid disadvantages:

1. Use with curved boundaries commonly result in numerical instabilities.

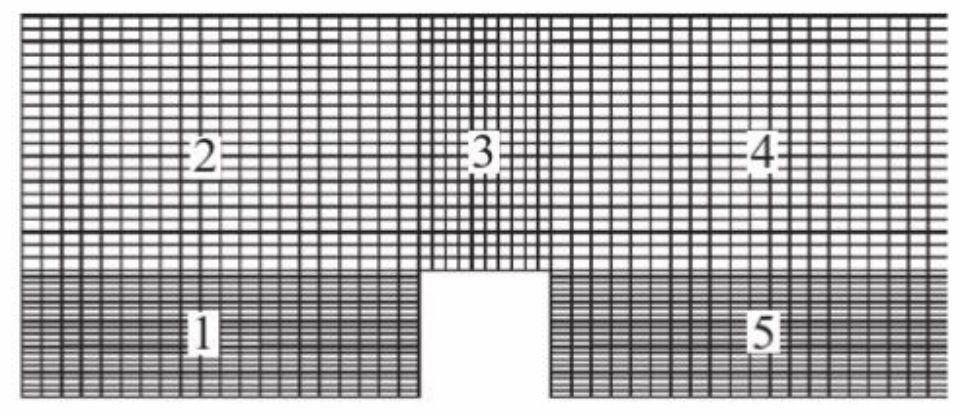

Figure 2: An example of 5 structured 2D grids being used to include a 2D rectilinear domain [21]

Unstructured grid advantages:

1. Highly flexible, especially with curved boundaries.

Unstructured grid disadvantages:

1. Connectivity information for each cell face must be appropriately stored in a table.
2. A cell may have a random amount of attaching cells, making the connection to neighbouring cells difficult.
3. The difficulties of cell connectivity and data handling are associated with more complex solution algorithms for flow field variables.
4. Resolving wall boundary layers is commonly unsuccessful with hexahedral cells.

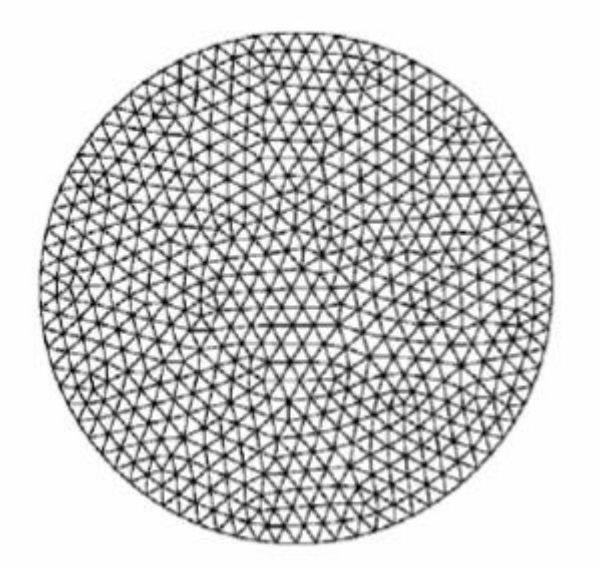

Figure 3: An unstructured grid being used to include a 2D circular domain [21]

1.2.4 Solution methods

A summary of the solution methods discussed by Ferziger and Peric [18] are explained below.

After the chosen discretization process, there is a system of algebraic equations which need to be solved. They may be either linear or non-linear depending on the equations they were derived from in the mathematical model. In the direct solution method, matrices are used to solve the linear equations. In the iterative method, both linear and non-linear equations may be solved. In this method, a solution is guessed and then steadily improved on. If there are few iterations and the effort to perform each iteration is low, then the iterative method may be more favourable over the more accurate direct method.

The solution of unsteady flow is based on methods used for initial value problems in ordinary differential equations. These methods include the explicit Euler method, the implicit Euler method and the trapezoid rule. A combination of the methods forms the predictor corrector method. This is done by one method predicting the solution at a new time step and another method correcting it. For example, a popular predictor-corrector method, called the predictor corrector method, is by the explicit method being used as the predictor and the trapezoid rule being used as the corrector. This method is shown to be second order accurate, meaning the error in the approximated solution is reduced by a factor of four with an increasing grid resolution.

1.3 CFD based fire model

The below diagram identifies the aspects of the components required for a CFD based fire model to be produced. These components are explained in the following sections for the chosen CFD based fire model. The chosen CFD based fire model for this study is the Fire Dynamic Simulator, developed by the NIST. It is chosen as it has been extensively validated in the past decade [2]. Validation of a specific CFD code is necessary should that CFD code claim any credibility [3]. Hasib *et al.* [3] explains that CFD code users have increased confidence in their CFD code when it has been validated with experimental data.

Refer to FDS Technical Reference Guide Volume 1 [23] for an in-depth review of FDS. What is presented here is the fundamentals of FDS and how it compares to the general CFD that is discussed in 1.2 Computational Fluid Dynamics. Figure 4

shows an adapted schematic from Yeoh and Yuen [17] of the components used in CFD based fire models as discussed in 1.2 CFD based fire model.

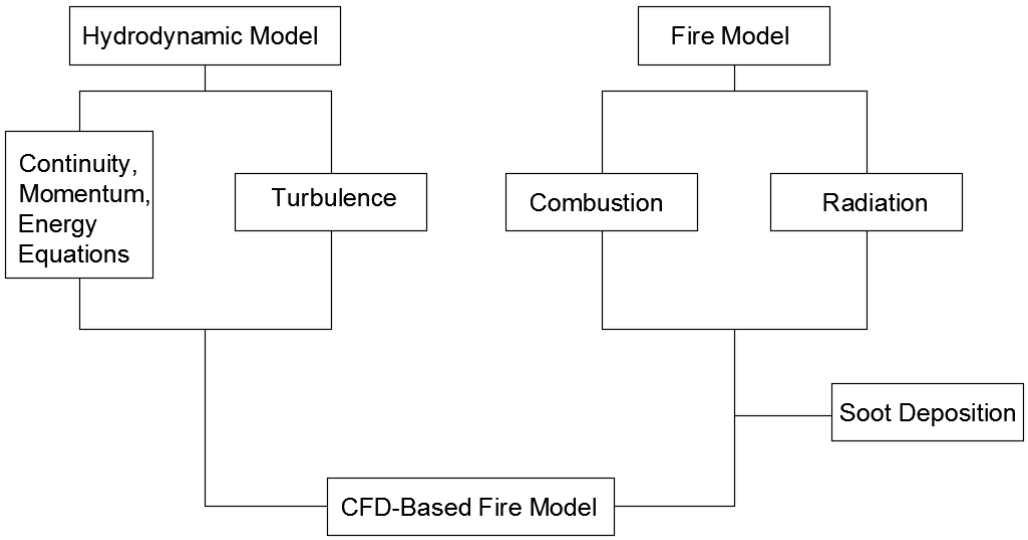

Figure 4: Schematic showing the components of a CFD-based fire model

1.3.1 FDS description

FDS is used for modelling fire driven fluid flow by numerically solving a form of the Navier Stokes equations appropriate for thermally driven low Mach flow [4]. The program is written in Fortran. It works by receiving input parameters from a text file, then it uses the governing equations to compute a numerical solution and writes data to files as an output [24]. An additional program called Smokeview produces visualizations of the numerical predications from the FDS created data files [25].

Within the text file, the parameters defining the fire environment are set for which the simulation will be modelled in. Solid surfaces are detailed with specific thermal

properties for which the user must assign. In this study, the fire's HRR is user specified, which is done by detailing the HRR over time. In defining the fire for this study, the user must specify the size and location of the fire and must specify the fuel chemistry used in the fire along with the post combustion yields for soot and carbon monoxide [24]. In the text file the user will define the outputs that are of interest and the location for the outputs to be gathered.

The software was publicly released in February 2000. This study uses version 6, released in September 2013. The minor release is version 6.6.0, released in October 2017.

FDS limitations

McGrattan *et al.* [26] identify the following prominent limitations within FDS:

1. FDS is to be used for low Mach flow (<0.3) with an emphasis on smoke and heat transport from fires.
2. The grid used in FDS can't perfectly match curved geometry.
3. The model is less accurate when using a predicted HRR compared to a specified HRR.
4. In an under ventilated compartment fire or if a suppression agent like water mist is introduced, fuel and oxygen can mix but not burn. This is being governed in FDS by a few simple empirical rules until reliable models are developed.

5. Targets positioned far away from a growing fire may be subject to a nonuniform distribution of radiant energy.

1.3.2 Governing equations

McDermott [27] explains fire driven flow as a low speed, variable density fluid. Baum and Rehm [28] introduced these equations in 1978, which describe flows that are created by a slow addition of heat.

Like the general CFD governing equations, the governing equations presented here are also based on the universal laws of conservation. Equation 6, Equation 7, Equation 8, and Equation 9 are found in the FDS Technical Reference Guide [23].

Continuity equation

$$\frac{\partial \rho}{\partial t} + u.\nabla(\rho) = \dot{m}_b''' \qquad (6)$$

Here the equation is specified as being equal to the external mass input rate $\dot{m}_b'''$ [29].

Momentum equation

$$\frac{\partial (\rho u)}{\partial t} + u.\nabla(\rho u) = -\nabla \tilde{p} + \nabla.\tau_{ij} + \rho g + f_b \qquad (7)$$

Here the equation is the same except that the sum of the body forces has been identified as the gravitational force (ρg) and external forces such as drag exerted by liquid droplets (f_b).

Energy equation

$$\frac{\partial(\rho h_s)}{\partial t} + \nabla.(\rho h_s u) = \frac{D\bar{p}}{Dt} + \dot{q}''' + \dot{q}_b''' - \nabla.\dot{q}'' \qquad (8)$$

1. Here the energy equation is expressed in terms of the sensible enthalpy. This is derived from the thermal energy equation, which is further derived from the subtraction of the kinetic energy equation from the total energy equation [19].
2. The dissipation function is left out as it is small in comparison to the heat released from the fire.
3. In FDS, the HRR per unit volume from a chemical reaction ($\dot{q}'''$) replaces the HRR from a source ($\dot{Q}_s$) in the general CFD energy equation.
4. In the heat flux vector ($\dot{q}''$), there is the addition of the diffusive and radiative heat fluxes to the conductive heat flux used in the general CFD energy equation.
5. The energy transferred to subgrid-scale particles and droplets are included ($\dot{q}_b'''$).
6. Source terms for radiation and combustion are later included in the energy equation.

Equation of state

$$\rho = \frac{\bar{p}_m M}{RT} \tag{9}$$

The pressure in the general CFD equations for state and energy is replaced with the background pressure due to the formulation of low Mach flow. Background pressure $(\bar{p})$ is extracted from pressure (p) along with perturbation pressure $(\tilde{p})$. The perturbation pressure is a fluctuating hydrodynamic pressure that drives local fluctuations in the flow field [27].

Using the background pressure, filters out acoustic waves [30]. Baum and Rehm [28] explain that such filtering allows important features of buoyant flow to be included in the model equations while avoiding the long computation times incurred by high frequency sound waves when numerically integrated.

The relationship between the background pressure and perturbation pressure are shown in Equation 10, representing the pressure field for the *m*th zone [23].

$$p(\mathrm{X}, t) = \bar{p}_m(z, t) + \tilde{p}(\mathrm{X}, t) \tag{10}$$

The governing equations form part of what is known as the hydrodynamic model in FDS.

1.3.3 Numerical grid

The governing equations are approximated in FDS by using second order accurate finite differences on a collection of uniformly spaced three dimensional grids. Various variables associated with the flow are located in each grid cell [23].

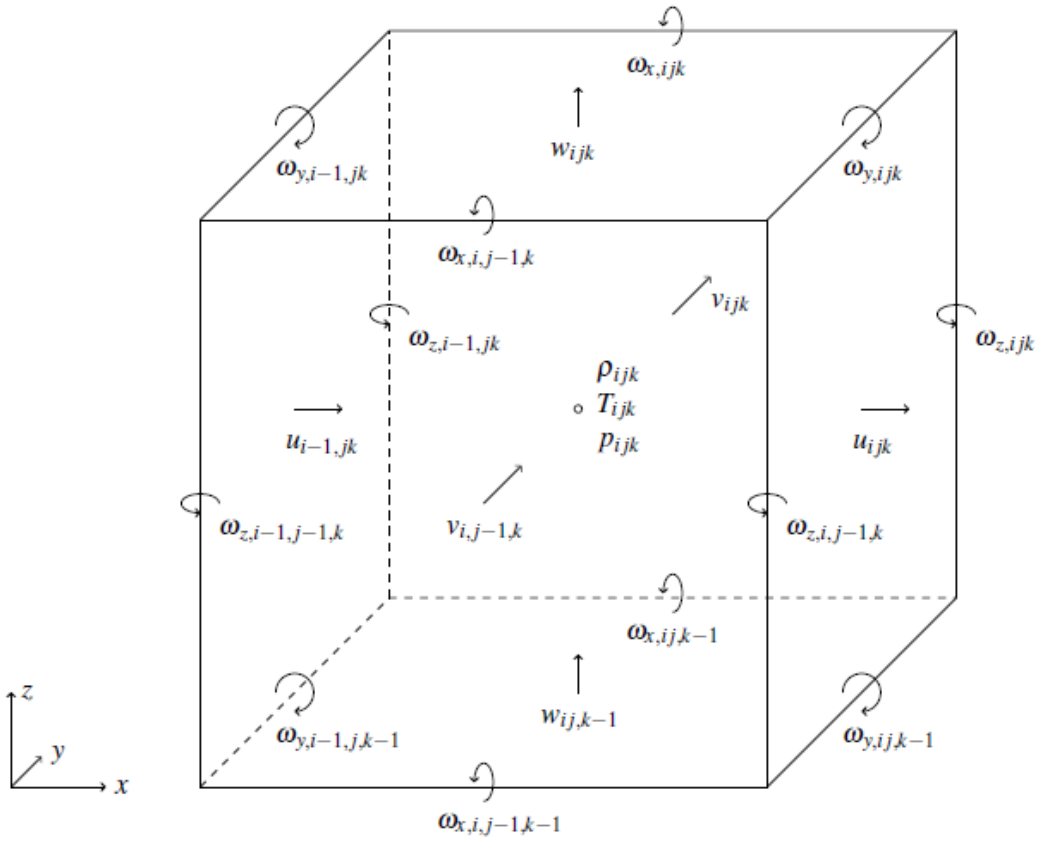

Figure 5: Position of flow variables in grid cell ijk [23]

In FDS, the location of the variables are as follows [31]:

1. Vector quantities are located at the cell's surface. Velocity components are located at the surface of the cell and vorticity components are located at the cell's edge.
2. Scalar quantities are located at the centre of the cell (density, temperature, pressure).

This is referred to as a staggered grid. Morinishi *et al.* [32] identify this grid type to be one of the three common classes of structured computational grids, which conventional numerical algorithms are based on. They differentiate the staggered grid by the velocity components being distributed around the pressure points. Unlike the regular and collected grids having the velocity components located at the pressure points [32].

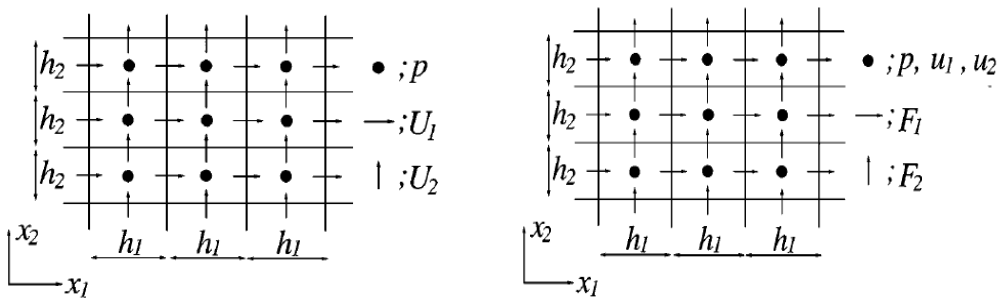

Figure 6: Variable location shown within a staggered grid (left) and a collated grid (right) [32]

The primary purpose of the staggered grid being used is to prevent "checker-boarding" in pressure-velocity coupling. The effect of "checker-boarding" pressure

field is that it indicates no pressure force. Thus, having no effect on the momentum equations even though the pressure field is not uniform [33].

In FDS, grid stretching or shrinking is possible in two of the possible three coordinates, but excessive transformations to the grid should be restricted to prevent computational instabilities [31]. Transforming of a grid cell in one coordinate reduces the computational efficiency and transforming the grid in two coordinates reduces the computational efficiency even further [24]. A uniform grid is therefore preferred, producing a grid with cubic cells.

1.3.4 Solution method

An explicit second order predictor corrector scheme is used to advance the flow variables in time [23]. More information on this solution method is found in section 1.2.4 Solution Method. McGrattan *et al.* [23] have detailed the step by step predictor and corrector method for FDS.

1.3.5 Turbulence

Part of the hydrodynamic model is how turbulent flow is treated. In FDS, turbulence can be treated with the use of either a Large Eddy Simulation (LES) or Direct Numerical Simulation (DNS) [26].

Ferziger and Peric [18] explain that DNS is the most accurate method to simulating turbulence and from a theoretical aspect it is the simplest approach. In this

simulation all of the motions contained in the flow are resolved and produces very detailed results about the flow [18]. The negative associated with DNS is that the grid resolution must be considerably fine to resolve the included small-scale turbulences [34]. Thus, increasing simulation times.

For LES, Ferziger and Peric [18] explain that the large-scale motions are focused on because they are generally more energetic, making them more effective in transporting the conserved properties. They explain that by applying a filter to the velocity field, the large-scale motions are focussed on. The filters have a width and when eddies are bigger than the filter width, they are considered to be large eddies [18]. The large eddies are directly represented in LES, and the effects of smaller scale motions are modelled [35]. Filtering can be either implicit or explicit [34]. In FDS, implicit filtering is applied, which is the practice of making the filter width equal to the grid cell's width [23].

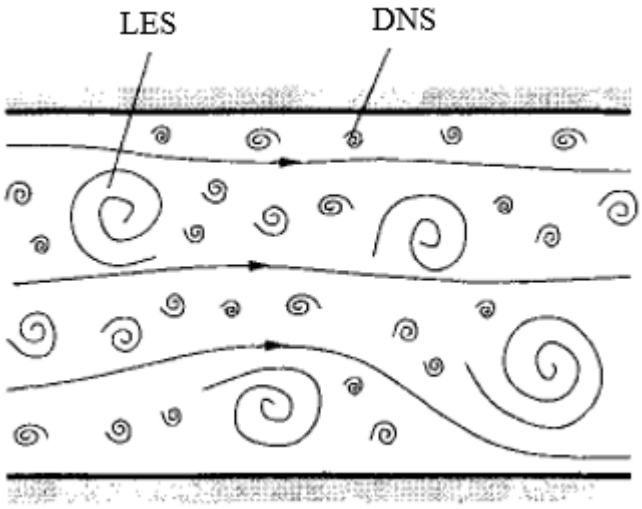

Figure 7: Schematic representation of turbulent flow [18]

1.3.6 Combustion model

Typically, FDS's combustion model is based on mixing limited, infinitely fast reacting lumped species [26]. The FDS Technical Reference Guide explains that FDS uses a lumped species approach, which combines species that will transport and react together as a group [23]. Lumped species are identified in the Guide as a mixture of primitive species that occur only in certain proportions in the flow. The benefit of forming lumped species is noted in the Guide due to it reducing the number of transport equations needed to be solved and therefore reduces the calculation time.

The mean chemical production rate of species per unit volume ($\dot{m}_\alpha'''$) is explained in the FDS Technical Reference Guide as being determined from the combustion model. After $\dot{m}_\alpha'''$ is determined, the HRR per unit volume ($\dot{q}'''$) can be determined from Equation 11 as expressed in the Guide. In the formula, the sum of the species mass production rates is multiplied with the heat of formation of the respective species ($\Delta h_{f,\alpha}$) [23].

$$\dot{q}''' = -\sum_\alpha \dot{m}_\alpha''' \Delta h_{f,\alpha} \qquad (11)$$

1.3.7 Thermal radiation

McGrattan *et al.* [23] explain that thermal radiation and conduction in the gas phase is represented by the heat flux vector ($\dot{q}''$) in the energy equation. As mentioned

above, this is the sum of the conductive, diffusive, and radiative heat fluxes. In Equation 12 [23], conductive and diffusive heat flux are represented by the first and second terms respectively on the right of the equals. The last term on the right of the equals is the radiative heat flux.

$$\dot{q}'' = -k\nabla T - \sum_{\alpha} h_{s,\alpha}\rho D_{\alpha}\nabla Z_{\alpha} + \dot{q}_r'' \qquad (12)$$

Solving radiation in FDS results in the computation of the radiative loss term at all gas phase cells and the radiative heat flux at solid boundaries [23]. The technique of solving the radiation transport equation is similar to that used for convective transport in finite volume methods for fluid flow and has therefore been named the Finite Volume Method [36].

1.3.8 Soot deposition

In a fire analysis, soot deposits are important. The removal of soot by deposition can impact occupant visibility and activation times of devices like smoke detectors [23]. It is also important as it has the possibility of changing the thermal properties of a compartment's boundaries. This is due to the potential change of emissivity from repeated soot deposits forming in a building that has fires repeatedly ignited in. Jahna, Reina and Toreroa [37] found in their study that the effects of boundary emissivity change made a difference in their surface temperature readings.

It is noted that soot deposits will build on boundaries during the compartment's first fire, thus potentially changing the emissivity of the boundaries during the first fire

[38]. However, the extent of the boundary surfaces covered in soot deposit is not known and which surfaces need to change to the emissivity of soot.

Kennedy [39] has discussed soot production in his study on models of soot formation and oxidation. He explains that soot is produced during the pyrolysis of hydrocarbons, which develops aromatic species that grow into polyaromatic hydrocarbons (PAH). Further growth of PAH produces the smallest recognizable soot particle of 1 nm. After this phase soot can grow further by other mechanisms [39].

Overholt, Floyd and Ezekoye [40] detail the computational modelling of aerosol deposition in FDS. They explain that by adjusting the species transport equation to one dimensional flux towards a surface, the rate that soot is deposited onto a wall surface ($\dot{m}''$) can be determined by Equation 13. Using this boundary condition allows for the soot to be removed from the gas phase and deposited onto a surface should the soot enter a gas phase cell that is adjacent to a surface [23].

$$\dot{m}'' = \rho Y_{\alpha} u_{dep} \qquad (13)$$

The total deposition velocity (u_{dep}) is the sum of the respective deposition velocities from the following deposition mechanisms [40]:

1. Gravitation settling

   Particles are acted on by the force of gravity, inducing a gravitational settling velocity in a downward direction.

2. Thermophoretic deposition

   Particles are attracted or repelled from a surface due to a temperature gradient near a surface.

3. Turbulent deposition

   Particles with sufficient inertia separate from turbulent flow, impact a surface and remain deposited on the surface.

1.4 Design fire

1.4.1 Type of fuel

Only wood-based products should be used during live fire training and should be used in amounts that are insufficient to cause a ventilation-controlled fire [13]. A ventilation-controlled fire can be identified by the simulated HRR deviating from the specified HRR [41]. If a fire becomes ventilation controlled it can lead to the occurrence of an explosion known as a backdraft [42]. It can also result in a flameover or flashover, which are fire phenomena that can lead to a dangerous increase in thermal energy being transferred to firefighters [13].

The arrangement and mass of wood used should be standardized to allow a single fire scenario to be repeated and produce similar results from each repetition. Wood pallets allow for a repeatable fire scenario [43]. They are also commonly used in live fire training and firefighter tests [14, 44, 45].

1.4.2 Heat of combustion

The heat of combustion is the amount of heat released for every kilogram of fuel consumed. There has been some discussion over what the heat of combustion for wood should be. The heat of combustion specified in handbooks is often determined from tests performed in an oxygen bomb calorimeter. This is considered inappropriate for realistic fires as the oxygen bomb calorimeter ensures complete combustion of a specimen by burning it in a 100 % oxygen atmosphere [46]. In reality, only 70-80 % of the wood is completely burnt. Charred wood remains, which when consumed in an oxygen bomb calorimeter, produce a heat of combustion similar to carbon at approximately 30 MJ/Kg [47].

A high heat of combustion is frequently used in FDS for simulating wood burning products [48-51]. Heskestad and Delichatsios [52] specified using 12.5 MJ/kg as an actual heat of combustion for wood pallets. This is further confirmed in viewing the heat of combustion for pine, a common wood used in pallets. Janssens [53] showed in his studies that the heat of combustion for white pine, during the flaming period, is at an average of 12.5 MJ/kg. This average is from the flaming period, which reflects the effective heat of combustion [46].

1.4.3 Heat release rate

The fire's HRR, or fire size, is rather specified than predicted by the Fire Dynamic Simulator (FDS). This is done due to FDS not being as accurate when it is predicting the HRR and it is noted as a limitation of the software [26]. A realistic

fire size is required to adequately train firefighters, which will therefore require the correct number of wood pallets to be burnt. As shown in Table 1, the amount of wood required cannot be based on an occupancies typical fire load because the amount of fuel does not directly correspond to the appropriate fire size. Table 1 is using the results from a study performed by Bwalya, Zalok and Hajisophocleous [54]. The importance of fuel composition and fuel arrangement for fires with the same ventilation is noted from this study.

Table 1: Fire load compared to peak HRR

Recreated fire	**Fire load density (MJ/m2)**	**Peak HRR (kW)**
Book store	5,305	1,200
Fast food restaurant/kitchen	881	1,592

The enclosure that the fire is measured in is also of importance. Saber and Kashef [55] demonstrated this in a CFD study whereby duplicates of the same fire were simulated with different ventilation opening sizes and positions. In one of the ventilation scenarios, one window and one door opening on the opposite wall was simulated. It was found that a larger window allowed for more oxygen into the compartment. This resulted in a fire with a larger HRR and a shorter burn duration due to efficient burning. In another scenario with just one door opening, the HRR was significantly less and a longer burn duration was achieved.

The pallet fire tests documented by Krasner (cited in Lee [56]) provide the most comprehensive pallet stack height range [57]. However, this document was not

found to be available for viewing at the time of this study. The below information from Krasner has been compiled according to the cited information by Lee [56].

The pallet tests consisted of a single stack of pallets. The individual pallet size was 1.22 m x 1.22 m x 0.14 m and had a mass of 31.75 kg. Table 2: Pallet mass loss rates details the observed average maximum mass loss rates.

Table 2: Pallet mass loss rates

Test #	**# Pallets**	**Stack height (m)**	**Mass loss rate (kg/sec)**	
1	2.00	0.28	0.06	0.07 (Average)
2	2.00	0.28	0.08	
3	3.00	0.42	0.14	
4	5.00	0.70	0.20	
5	5.00	0.70	0.22	
6	7.00	0.98	0.26	
7	9.00	1.26	0.33	
8	11.00	1.54	0.42	

This information then allows the peak HRR to be calculated from Equation 14

$$HRR = \Delta h_c \times MLR \qquad (14)$$

where h_c is the effective heat of combustion (kJ/kg) and MLR is the mass loss rate (kg/s) [58].

A typical HRR curve is determined from known HRR curves for pallet fires. Averill *et al.* [43] documented the HRR curves generated from a single stack of pallets that ranged in stack heights from 0.44 m to 0.88 m. The individual pallet dimensions

where approximately 1 m x 1.3 m x 0.11 m. Of interest is the free burn pallet tests as theses HRR results compare well with the tests documented in Lee [56]. The HRR for these free burn pallet tests are shown in Figure 8 and Figure 9. Also documented by Averill *et al.* [43] is the ignition source, slender wood shavings lit by electronic match (the remote lighting of a match by electric current). For a fast ignition fire, approximately 1 kg of wood shavings for every 9 kg of pallet and wood shavings to be placed in every pallet. For a slow ignition fire, approximately 1 kg of wood shavings is to be placed in the top pallet.

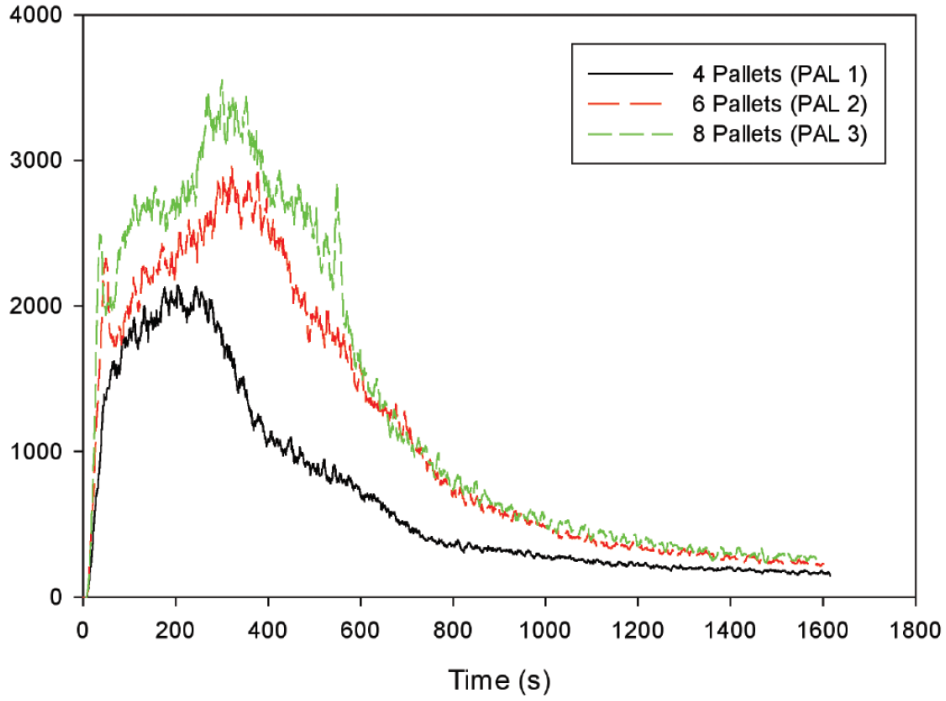

Figure 8: Free burn, fast ignition scenario, pallet fire test

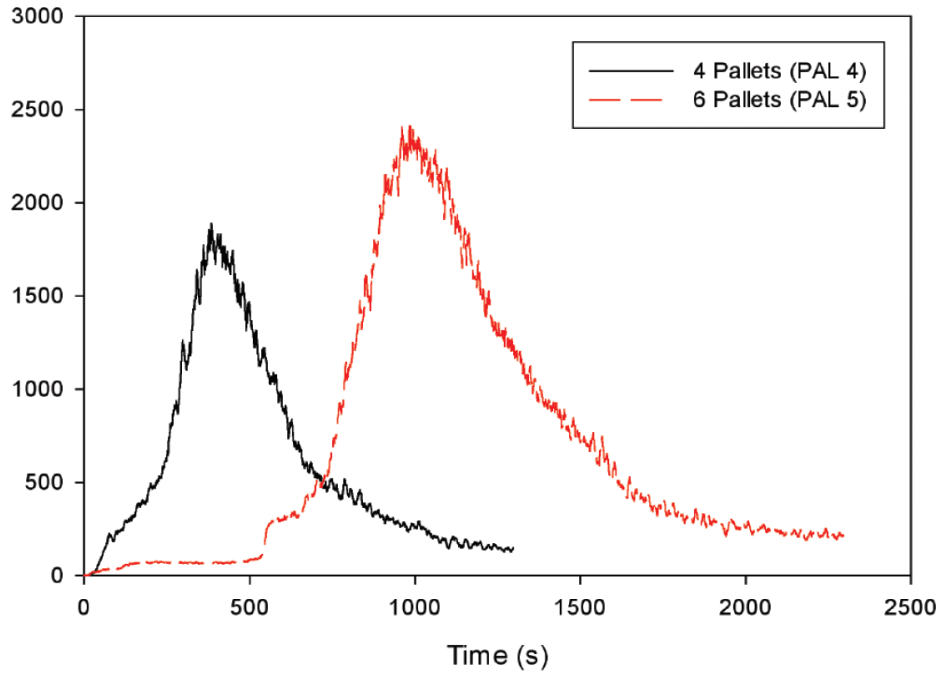

Figure 9: Free burn, slow ignition scenario, pallet fire test

A short pallet stack (0.46 m high) is considered to have medium to fast fire growth and a tall pallet stack 1.52 m high is considered to have a fast fire growth [59]. The growth time of the short pallet stack compares well to the short pallet stack conducted by Averill *et al.* [43]; however, their tall pallet stacks had an ultra-fast fire growth time. This is considered to be because they were conducted with substantially more wood shavings in their ignition of the pallets than what was used in the short pallet stack.

The moisture content of wood reduces the HRR [60]. The moisture content of wood expressed here is relative to the oven dry moisture content of the wood. It is derived from the equilibrium moisture content that is achieved from the environment that the wood is stored in [61]. This is the moisture content that the wood will naturally balance to due to its environment's relative humidity and temperature. The average annual relative humidity in the eThekwini area is 77 % [62] and the average annual

temperature is 21 °C [63]. Using Equation 15 [61], the equilibrium moisture content for wood is 15 %, which is higher than the normal 6 % - 12 % wood pallet moisture content [59], [43]. Thus, a fire simulated in the eThekwini area, which uses the above HRR information, is expected to provide results that are conservative to an actual fire.

$$EMC\ (\%) = \frac{1800}{W}\left(\frac{KH}{1-KH} + \frac{K_1KH + 2K_1K_2K^2H^2}{1 + K_1KH + K_1K_2K^2H^2}\right) \quad (15)$$

In Equation 15, the variables K, K_1, K_2, and W are coefficients of an adsorption model that are determined from the air temperature [61]

1.5 Firefighter safety

1.5.1 Hazards experienced by firefighters

In a study of U.S. firefighter injuries, the leading cause of injury to firefighters was from overexertion/strain. This accounted for 26 % of all injuries and was followed by 21 % of all injuries being from exposure to hazard. Together, these two causes of injury accounted for nearly 50 % of the annual average of injuries, approximately 14,236 injuries per year, between 2010 and 2014 [64].

Exposure to hazards in a fire situation, typically means exposure to smoke and heat. Firefighters protect themselves from these exposures by using a breathing

apparatus to prevent smoke inhalation [65] and thermal protective clothing to protect from burn injuries [66]. The protective clothing provides a limited amount of protection from hot gases, direct contact with hot surfaces, and thermal radiation [67]. It is therefore required to provide a high level of heat insulation. However, requirement also reduces the amount of metabolic heat that can be dissipated to the environment [68].

Various demanding tasks attributed to firefighting leads to significant heat and cardiovascular strain [69]. The carrying of various equipment, operating in protective clothing, and dealing with the various tasks that different scenarios require, results in a large energy expenditure from the individual firefighter [70]. The expenditure of energy causes the body core temperature to rise. To help regulate the core temperature, the heart beats faster to increase the volume of blood flow to the skin, thus increasing cardiovascular strain [68]. If the body is unable to keep its core temperature at the required temperature, heat strain is caused [71], which may lead to adverse health effects such as fatigue, exhaustion, stroke, and even death [72].

To help lower the body temperature, sweat is produced. Firefighters tend to sweat profusely as their tasks require a high energy expenditure while wearing heavy, restrictive personal protective equipment (PPE) [69]. For firefighters, sweating causes further complications to firefighter safety. Lawson [67] explains that moisture trapped in a firefighters' clothing, may decrease the thermal protection offered by the clothing, as wet clothing results in a higher heat transfer rate through the clothing. Lee and Barker [73] found that wet heat resistant fabric decreases in

thermal protective performance with high radiant heat exposure; however, they also found that wet heat resistant fabric experiences the opposite when the radiant heat exposure is low. This is explained due to the increased thermal capacity of the wet fabric overcoming its increased efficiency to transfer heat from a low radiant heat source. Additionally, Barker *et al.* [74] found that the amount of moisture in firefighter clothing affects thermal protective performance. They identified that an added moisture of 15 % clothing system mass, produced the greatest negative impact and that increasing the moisture content past this, resulted in longer times to achieve second degree burns. In a study performed on UK firefighters in live fire training scenarios, it was found that the firefighters sweated at a rate of approximately 0.03 l/min or 1.8 l/hr [75]. Additional wetting of the clothing may also come from firefighting operations as water spray splashes back onto the firefighter [67].

1.5.2 Safety of firefighters during live fire training

The environment of a live fire training structure is considered to be very dangerous. Realistic firefighter environments are recreated to prepare for the actual event. There have been few recorded deaths in live fire training structures, with the significant incidents summarized below:

1. Two firefighters die in the same incident after being caught in a fire flashover while training in an acquired structure. This happened while doing search and rescue training in a live fire training structure. One firefighter had not yet completed his first week of training at the fire department [76].

It follows that firefighters should not perform search and rescue training when exposed to heat flux in excess of 10 kW/m^2 [77], which is the case with flashover fires [78]. Training firefighters should have completed their training before being approved to participate in live fire training. In doing so they would have learnt about what causes flashover fires and the impact of fuel on fire development in a compartment [13].

2. A young firefighter recruit died of smoke inhalation during a training exercise in an acquired live fire training structure. The firefighter is suspected to have removed his facepiece due to the burns that were identified on his face [76].

   Due to the facility being used for persons receiving training, there is an inherent risk that trainee firefighters will make mistakes. Mistakes made during live fire training may result in the loss of life. The effect of removing the protective clothing, either on purpose or by being accidentally dislodged, should be identified. The tenability of the environment will be drastically reduced to that which would be expected for a normal civilian

3. A firefighter dies of smoke inhalation and burns when igniting the fuel in an acquired live fire training structure. The firefighter used the wrong fuel which resulted in a flash fire blocking him from escaping the training structure [79].

   An appropriate fuel should be designed for the specific burn room used. The design of the fuel should include the type of fuel, fuel arrangement, fuel

location and compartment ventilation as per 1.3 Design Fire. Using a prescribed fuel that has been designed for the purpose of live fire training will control the occurrence of flash fires and flashovers.

4. A firefighter recruit died of heat stroke from a live fire training exercise. The recruit was operating a hose stream in a shipboard simulator [76].

   To protect against the effects of elevated body core temperature, it is advised that the travel distance made by firefighters be limited [75]. The horizontal travel distance should be limited to 34 m for a ground floor and is reduced as the number of floors are climbed.

Tenable limits without PPE

For a firefighter that has removed his breathing apparatus, incapacitation can be expected from toxic combustion gases. Fractional Effective Dose (FED) is used to evaluate if the exposure received from combustion gases is considered sufficient to cause incapacitation [24]. Traina *et al.* [80] specifies using a FED equal to 0.3 to characterize incapacitation to young children, the elderly, and unhealthy occupants. Su *et al.* [81] specifies using a FED equal to 1.0 to characterize incapacitation for healthy adults. Additionally, if a firefighter breaths air in from the atmosphere during live fire training, they may receive thermal burns to their respiratory tract due to the raised air temperatures that are experienced in a compartment fire.

The required air temperature for thermal burns to occur to the respiratory tract is above 60 °C and at 100 °C, severe burns will occur [82]. This is for air that has a high humidity, which is possible to occur as a result of firefighting activities creating steam when putting water on a fire [83].

If any other item of protective clothing is removed, exposing skin, the radiant heat flux experienced must be below 2.5 kW/m^2 and the air temperature must be below 121 °C for it to be considered safe for several minutes [82]. Skin exposure to a radiant heat flux above 2.5 kW/m^2 or air temperatures exceeding 121 °C will cause pain, followed by burns [82].

Burns that extend through the skin's epidermis and into the dermis is classified as a second-degree burn [84]. Severe incapacitation is expected under such conditions that produce second degree burns [82]. The time it takes for incapacitation to occur identifies when tenable conditions have been lost [85]. Pain is expected to be experienced before a second-degree burn is achieved for sufficiently low heat fluxes. Thus, providing the firefighter with a means of detecting exposed skin. On receipt of pain, it is expected that the firefighter will begin their exit of the live fire training structure. Firefighter garments complying with NFPA 1971 are tested to provide 17.5 seconds until a second degree burn will occur, and is measured from the time when they are confronted by a flashover fire [86]. Applying the same safe time duration of 17.5 seconds, it was found that a maximum heat flux of 4.5 kW/m^2 can be sustained by exposed skin. This is due to 4.5 kW/m^2 heat flux causing skin pain in 12.5 seconds [87] and second degree burns in 30 seconds [67]. Thus,

allowing the firefighter 17.5 seconds to remove themselves from the heat flux exposure before becoming incapacitated as shown in Figure 10.

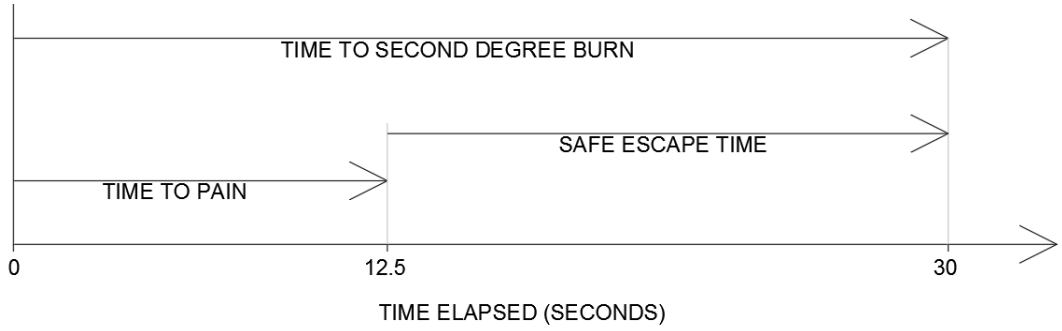

Figure 10: Safe escape time from 4.5 kW/m^2 heat flux exposure

Tenable limits with PPE

Should none of the firefighter's protective garments and equipment be removed, the tenability limit is established according to the level of protection provided by the protective clothing and equipment worn by the firefighter.

Firefighter garments typically consist of three layers of fabric. Song, Mandal and Rossi [88] explains the following about these three layers.

1. The first layer is the outer shell. This helps to keep the integrity of the fabric assembly when exposed to flame, radiant heat, and hot surfaces. It also has a high mechanical strength structure to resist tears and punctures.
2. The middle layer is a moisture barrier. It prevents the transmission of hot liquids, but it may also allow sweat vapour to escape from the firefighter's body.

3. The last layer is the inner layer in contact with the firefighter's body. It raises the overall thermal insulation of the fabric assembly because it traps dead air, further insulating the firefighter from heat.

To prevent injuries and damage to PPE, air temperatures above 260 °C must be monitored [10]. For protection against high heat flux exposure, NFPA 1971 specifies a Thermal Protective Performance (TPP) rating of 35 for firefighter garments comprising of these three fabric layers [86]. TPP measures the thermal insulation provided by clothing until the exposed heat flux results in a second-degree burn and is calculated as shown in Equation 16 [86].

$$TPP_{rating;\,value} = F \times t \qquad (16)$$

Where F is the exposure energy heat flux measured in cal/cm^2/s, and t is the time to burn measured in seconds.

There are two alternatives to using the TPP rating. They are the Thermal Dose Unit (TDU) method or by use of the Protective Clothing Performance Simulator [89].

The TDU method uses an equation similar to Equation 16 except that the heat flux has an exponent of 4/3 [90]. By using the work of Su *et al.* [91], it was found that the results from the TDU method had a higher standard deviation than the results from the TPP rating. This is shown in Table 3 and Table 4. The study by Su *et al.* [91] found the time to second degree burns for three different fire protective fabrics when exposed to a heat flux of 8.5, 30, and 84 kW/m^2. This range in heat flux is

important. The TPP rating used in NFPA 1971 is calculated from a heat flux of 84 kW/m^2 [86] whereas the heat flux expected for tenable firefighter conditions is in the 8.5 kW/m^2 region [77]. This allows for both the TDU and TPP rating to be calculated, and for their variance in results to be compared for low to high heat flux. In Table 3 and Table 4, the term "spacer" refers to an air gap used in the test and the term "planar" refers to the configuration of the test used by Su *et al.* [91].

Table 3: TPP rating and TDU comparison using the no spacer - planar data

Time (seconds)	Heat flux (cal/cm^2/s)	TPP	TDU	TPP SD	TDU SD
Fabric A1					
36.0	0.20	7.31	4.30	0.39	1.62
9.0	0.72	6.45	5.77		
3.3	2.01	6.52	8.22		
Fabric A2					
40.0	0.20	8.12	4.77	0.45	1.78
11.5	0.72	8.24	7.37		
3.6	2.01	7.22	9.11		
Fabric A3					
35.0	0.20	7.11	4.18	0.45	1.40
9.0	0.72	6.45	5.77		
3.0	2.01	6.02	7.59		

Table 4: TPP rating and TDU comparison using the spacer - planar data

Time (seconds)	Heat flux (cal/cm^2/s)	TPP	TDU	TPP SD	TDU SD
Fabric A1					
71.0	0.20	14.41	8.47	1.06	3.49
16.5	0.72	11.82	10.58		
6.6	2.01	13.24	16.70		
Fabric A2					
71.0	0.20	14.41	8.47	0.89	4.10
17.5	0.72	12.54	11.22		
7.2	2.01	14.45	18.22		
Fabric A3					
67.0	0.20	13.60	7.99	0.74	3.54
16.5	0.72	11.82	10.58		
6.5	2.01	13.04	16.45		

The next alternative method for predicting burn injury in firefighters is the use of the Protective Clothing Performance Simulator [89]. This software tool has been developed for predicting the effectiveness of firefighter garments in protecting the skin from a burn injury. It was however not available at the time of this study due to export control regulations.

The firefighter working conditions that have been documented by others [77, 92-95] could be used to determine safe conditions for firefighters; however, they vary substantially between different sources. For example, Foster and Roberts [93] specifies 25 minutes for a 1 kW/m^2 heat flux exposure and Coletta *et al.* [94] specifies 5 minutes to 60 minutes for a 1.26 kW/m^2 heat flux exposure. Both sources specify a heat flux of approximately 1 kW/m^2, but their allowable exposure time is vastly different.

Stability of live fire training structure

The National Fire Protection Association [10] specifies that structures used for live fire training be protected in areas where flames come in contact with the structure and where the temperature may exceed 177 °C.

1.5.3 Selecting the appropriate TPP value

The term “TPP rating” refers to the rating that has been given to an item of clothing based on its performance in the TPP test. Here the term “TPP value” is also used. It too is calculated from Equation 16 but is used to define the heat flux exposure from the environment.

For flashover fires, NFPA 1971 specifies dividing the garment’s TPP rating in half to indicate the time at which second degree burns occur [86].

Behnke [96] specifies doubling a garment’s TPP rating for the anticipated TPP value. Doing this was proved at different heat flux levels [96]. The doubling of the garment’s TPP rating is explained to be a safety factor. The safety factor is to prevent burns from stored heat in clothing and for any variation in the fabric spacing on the wearer [96]. This means that clothing that has the minimum required TPP rating of 35, can only be subjected to a heat flux for a specific time period that would result in a 17.5 TPP value.

To determine the appropriate TPP value, a 17.5 and 35 TPP value is assessed. The time to achieve a critical heat flux is assessed at every 100 seconds into the simulation for a total of 1,300 seconds. Using the remaining available time and Equation 16, the critical heat flux can be calculated. Knowing the critical heat flux and exposure time allows for a comparison to be made with previously acknowledged firefighter conditions.

The critical heat flux calculated from a 20 second exposure and a 60 second exposure has also been included in the comparison. A 20 second exposure limit is typical of an emergency situation [94] and is similar to the situation being created in the NFPA 1971 TPP test [86]. For a 60 second exposure limit, firefighters would not be expected to perform search and rescue operations [77]. This is used in the comparison because rescue training is a typical training objective of live fire training structure use [10].

The firefighter working conditions for heat flux exposure and time duration, have been specified by Abbott and Schulman [92], Foster and Roberts [93], Coletta *et al.* [94], Donnelly *et al.* [77] and FEMA/USFA [95]. In Table 5 and Table 6, the highlighted cells show the comparison of the firefighter working conditions with the two TPP values.

The firefighter working conditions are conditions that can be tolerated and are not the time to a second-degree burn. Peacock *et al.* [97] identified the time between pain and a second-degree burn for firefighter turnout coats of various TPP ratings. In their study they do not provide the HRR of the fires they used. An average of

30 seconds between pain and second-degree burn is calculated from their loveseat fires, which can have a HRR of 3,012.4 kW [98]. An average of 10 seconds between pain and second-degree burn is calculated from their fully furnished room fires, which contained multiple items including a sofa. These fully furnished room fires are expected to have a HRR well over 3,000 kW due to a single sofa, of similar weight, being able to produce a HRR of 3,200 kW [99].

Table 5: Comparison of firefighter tenable limits and a 35 TPP value

TPP 35						
Exposure time (seconds)	**Critical heat flux ($cal/cm^2/s$)**	**Abbot**	**Foster**	**Coletta**	**NIST**	**USFA / FEMA**
1,300.0	1.13					
1,200.0	1.22					
1,100.0	1.33					
1,000.0	1.47					
900.0	1.63					
800.0	1.83					
700.0	2.09					
600.0	2.44					
500.0	2.93					
400.0	3.66					
300.0	4.88					
200.0	7.33					
100.0	14.65					
60.0	24.42					
20.0	73.27					

Table 6: Comparison of firefighter tenable limits and a 17.5 TPP value

TPP 17.5						
Exposure time (seconds)	**Critical heat flux ($cal/cm^2/s$)**	**Abbot**	**Foster**	**Coletta**	**NIST**	**USFA / FEMA**
1,300.0	0.56					
1,200.0	0.61					
1,100.0	0.67					
1,000.0	0.73					
900.0	0.81					
800.0	0.92					
700.0	1.05					
600.0	1.22					
500.0	1.47					
400.0	1.83					
300.0	2.44					
200.0	3.66					
100.0	7.33					
60.0	12.21					
20.0	36.63					

The 20 second exposure shows good comparison with both the 35 TPP value and the 17.5 TPP value. Further to this, Alarifi *et al.* [44] showed that firefighters could only withstand a 35 kW/m^2 heat flux for 20 seconds, which is only a good comparison for a 17.5 TPP value. It is clear from Table 3 and Table 4 that a 17.5 TPP rating provides a more adequate comparison to tolerable firefighter conditions.

1.5.4 Probability of injury

The FDS model predicts values that can then be used to determine if the critical values are exceeded for a given scenario [15]. If simulations are within the validation range provided by McGrattan *et al.* [100], FDS model uncertainty statistics can be used to determine the probability (P) with Equation 17.

$$P(x > x_c) = \frac{1}{2} erfc\left(\frac{x_c - \mu_a}{\sigma\sqrt{2}}\right) \quad (17)$$

The mean (μ_a) and standard deviation (σ) are calculated with Equation 18 and Equation 19.

$$\mu_a = \frac{M}{\delta} \quad (18)$$

$$\sigma = \tilde{\sigma}_M \frac{M}{\delta} \quad (19)$$

The bias factor (δ) and the relative standard deviation $(\tilde{\sigma}_M)$ as presented by McGrattan *et al.* [100], are shown in Table 7.

Table 7: Statistics for quantities used in the calculation of probability

Quantity	**Relative standard deviation $(\tilde{\sigma}_M)$**	**Bias factor (δ)**
Target temperature	0.17	1.00
Target heat flux	0.26	0.91
Surface temperature	0.15	1.02

There isn't a statistic for the number of firefighters injured for every live fire training incident. To determine an acceptable statistic, the probability of firefighters being injured when attending to a fire scene is investigated. In the controlled environment created in the live fire training structure, a firefighter should be less likely to sustain an injury than when attending an actual incident. Evarts and Molis [11] show that more firefighters are injured at an actual incident than during training. It has therefore been considered acceptable when the probability is less than that of a firefighter being injured at an actual fire.

Unfortunately, a statistic for firefighters being injured at a fire scene in South Africa is not known, so to compensate for this, international statistics have been investigated. The statistics must be specifically for the number of firefighters injured at a fire scene and the number of fires that occurred. Live fire training is for a fire incident, so using general-firefighter injury statistics will not be suitable as they contain injury statistics from non-fire incidents. The required information is available from the United States of America (USA), England and parts of Canada. In the USA, the statistics consist of the number of firefighter injuries; however, this was looked at more closely and found to be the number of firefighters injured [101].

In the USA, there is a 2.22 % probability of firefighters being injured at a fire scene [11]. In England, there is a 0.44 % probability of a firefighter being injured at a fire scene [12], [102]. In Canada, using their available 4 out of 6 jurisdictions, there is a 0.72 % probability of a firefighter being injured at a fire scene [103], [104]. These statistics are presented in Table 8, Table 9, and Table 10.

When using these probabilities for injuries at actual fire scenes, the probability of a training firefighter being injured must be reduced to below 0.44 % to be acceptable.

Table 8: Probability of a firefighter being injured at a fire scene in England

Year	Firefighters injured	Fires	Percentage
2009-10	1,096	241,462	0.45 %
2010-11	962	228,407	0.42 %
2011-12	966	223,937	0.43 %
2012-13	656	154,456	0.42 %
2013-14	733	171,343	0.43 %
2014-15	743	155,038	0.48 %
2015-16	693	162,249	0.43 %
2016-17	717	161,984	0.44 %
2017-18	741	167,291	0.44 %
Averaged probability			0.44 %

Table 9: Probability of a firefighter being injured at a fire scene in Canada

Year	Firefighters injured	Fires	Percentage
2010	329	42,524	0.77 %
2011	265	40,839	0.65 %
2012	298	42,871	0.70 %
2013	258	35,328	0.73 %
2014	257	34,677	0.74 %
Averaged probability			0.72 %

Table 10: Probability of a firefighter being injured at a fire scene in the USA

Year	Firefighters injured per 1,000 fire scenes	Percentage
2008	25.2	2.52 %
2009	24.1	2.41 %
2010	24.5	2.45 %
2011	22.0	2.20 %
2012	22.9	2.29 %
2013	24.0	2.40 %
2014	20.8	2.08 %
2015	21.6	2.16 %
2016	18.1	1.81 %
2017	18.6	1.86 %
Averaged probability		2.22 %

1.6 Scope of this research

The current facility being used by eThekwini Fire and Emergency Services to train firefighters is a repurposed structure used to simulate both residential and commercial fires. The concern exists that it has suffered damage from thermal stresses caused by repeated heating and cooling. The result of this is that even though core samples show minimal damage, there is potential for the concrete to undergo spalling. The result is the separation of concrete from the structural steel, allowing heat to affect the structural steel and subsequently cause a decrease in structural stability. To address this safety risk to trainee firefighters, it is therefore required that the structure be subjected to reduced fuel loads and thermal shock. The advice by Council structural engineers to eThekwini Fire & Emergency Services is to design and construct a purpose-built structure for live fire training.

The purpose of this research is to prevent any shortcomings from the existing eThekwini live fire training structure being repeated in the designs of future live fire training structures. This is accomplished by assessing the hazards that training firefighters may face in the existing live fire training structure.

The existing structure has no detailed measurements or recordings of the environment that is created in it by live fire training. This makes it difficult to assess for shortcomings, introducing an insupportable level of uncertainty on the existing structure. Not being able to define and/or quantify these possible shortcomings may lead to them being underestimated or overlooked when designing a new structure for live fire training, with subsequent firefighter safety concerns.

The objective of this study is to use CFD to numerically estimate the fire environment created during live fire training and point to fire related hazards for trainee firefighters in the existing live fire training structure.

FDS is considered the most widely used fire simulation tool [105]. It has been used before in studies on firefighter safety and firefighter training [43, 51]. It is therefore selected to be used in this study.

The existing live fire training structure consists of three (3) floors. The ground-floor consists of a large compartment with smaller compartments around its perimeter. There are both low-level and high-level openings for access/ventilation in the large compartment. It also includes a short flight of stairs to a high-level

access point into the compartment. The first floor consists of multiple smaller compartments and contains multiple access points. Access to this floor is from two external staircases. The second floor consists of a roof with wood trusses and contains no walls. Access to this floor is from one external staircase. There are no fires ignited on this floor. Of these three floors, the large compartment on the ground floor and the multi-compartment first floor are investigated in this study.

Figure 11:eThekwini live fire training structure

CHAPTER 2: METHODOLOGY

2.1 Materials

Thermophysical material properties are assigned to building elements of the existing live fire training structure with the best-informed material properties. These properties define the solid boundaries present in the FDS simulation.

Table 11: Building material properties

Material ID	**Specific heat [kJ/kg·K]**	**Conductivity [W/m·K]**	**Density [kg/m^3]**	**Reference**
Cement plaster	0.84	0.72	1,860	[106]
Brick	0.84	0.69	1,600	[107]
Concrete	0.88	1.1	2,100	[107]
Steel	0.46	45.8	7,850	[107]
Wood (pine)	2.85	0.14	640	[107]
Glass	0.84	0.76	2,700	[107]

The solid boundaries are defined by surfaces that include the composition of the materials used and the individual material thickness. A colour is also assigned to the individual surfaces to differentiate surfaces easily in the visualization produced in the simulation.

Table 12: Building composition

Surface ID	Material ID	Thickness (m)	FDS colour used
Brick wall – external First floor	Cement plaster – brick	0.015 – 0.23	Brown
Brick wall – external Ground floor	Cement plaster – brick – cement plaster	0.015 – 0.23 – 0.015	Brick
Brick wall – internal	Cement plaster – brick – cement plaster	0.015 – 0.11 – 0.015	Brick
Window	Glass	0.004	Cyan
Slab/column	Concrete	0.3	Gray
Window shutter	Wood	0.016	Goldenrod
Door	Steel	0.001	Silver
Fire	–	–	Red

The fuel that is commonly used in the existing facility is wood, however the current arrangement of wood is in an unorganized manner and the wood mass is not documented. The fuel used in the simulations is wood pallets, which has been identified as an appropriate fuel (refer to section 1.4 Design fire). The fuel properties required for FDS are listed in Table 13.

Table 13: Fuel properties

Fuel properties		Reference
Chemical formula	$CH_{1.7}O_{0.83}$	[108]
CO yield (kg/kg)	0.005	[109]
Soot yield (kg/kg)	0.015	[109]
Heat of combustion (MJ/kg)	12.5	[52]

Figure 12 and Figure 13 show the geometry of what has been modelled in FDS for the first-floor and for the ground floor.

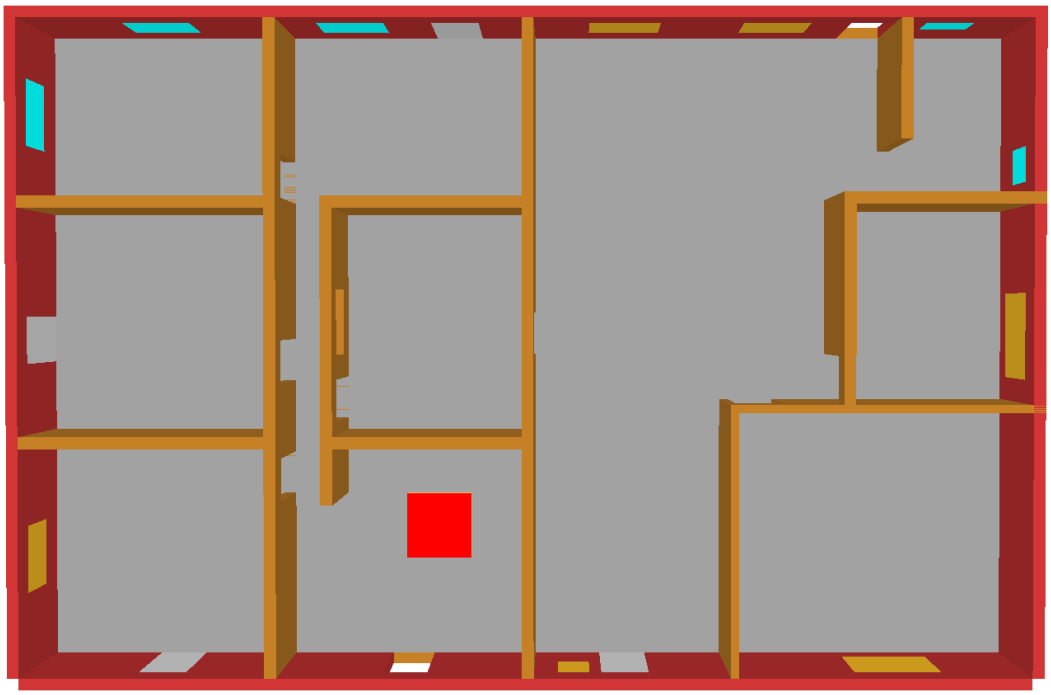

Figure 12: Top view of first floor modelled in FDS

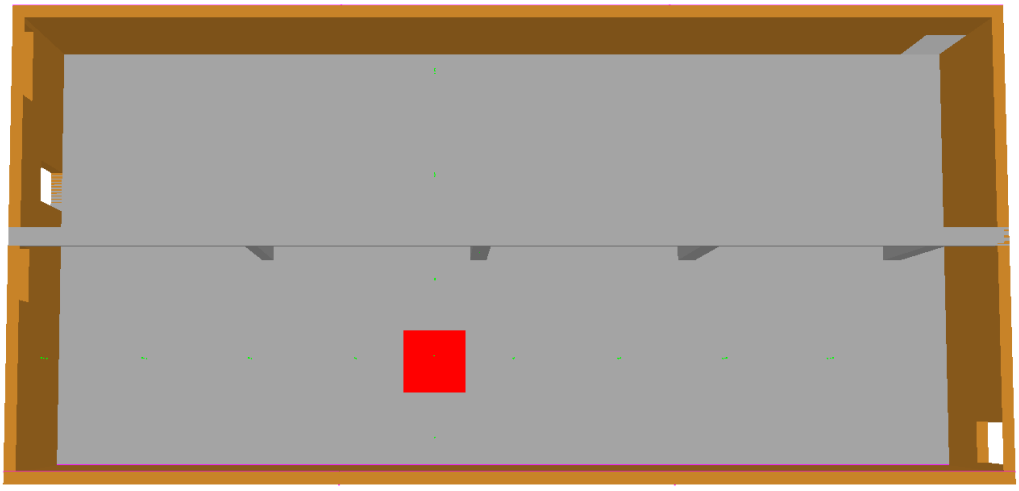

Figure 13: Top view of ground floor modelled in FDS

2.2 Heat release rate

The HRR that would result in a ventilation-controlled fire is avoided to prevent the occurrence of dangerous fire phenomena associated with ventilation-controlled fires (refer to section 1.4.1 Type of fuel). The HRR that can be sustained in the compartment before the fire becomes ventilation controlled is determined by modelling a t-squared fire with an appropriate growth coefficient. A short pallet stack is considered for the smaller burn room on the first floor and a tall pallet stack is considered for the bigger burn room on the ground floor.

The growth coefficient is selected according to the growth rate of the HRR. Using Figure 8 and Figure 9 (refer to section 1.4.3 Heat release rate), the growth coefficient can be found. An ultra-fast fire is shown for the tall pallet fires, thus requiring a growth coefficient of 0.01172 kW/s^2 [110]. A medium fire is shown for the short pallet fires, thus requiring a growth coefficient of 0.01172 kW/s^2 [110].

Figure 14 shows the deviation of the simulated HRR from the specified HRR on the first floor. The simulated HRR is shown to be deviating from the specified HRR between 1,000 kW and 1,500 kW. Using Table 2 and Equation 14 (refer to section 1.4.3 Heat release rate), it is calculated that a single stack of two pallets will produce a 1,000 kW fire and a single stack of three pallets will produce a 1,750 kW fire. It is therefore considered appropriate to use a stack of two pallets for the fire source on the first floor.

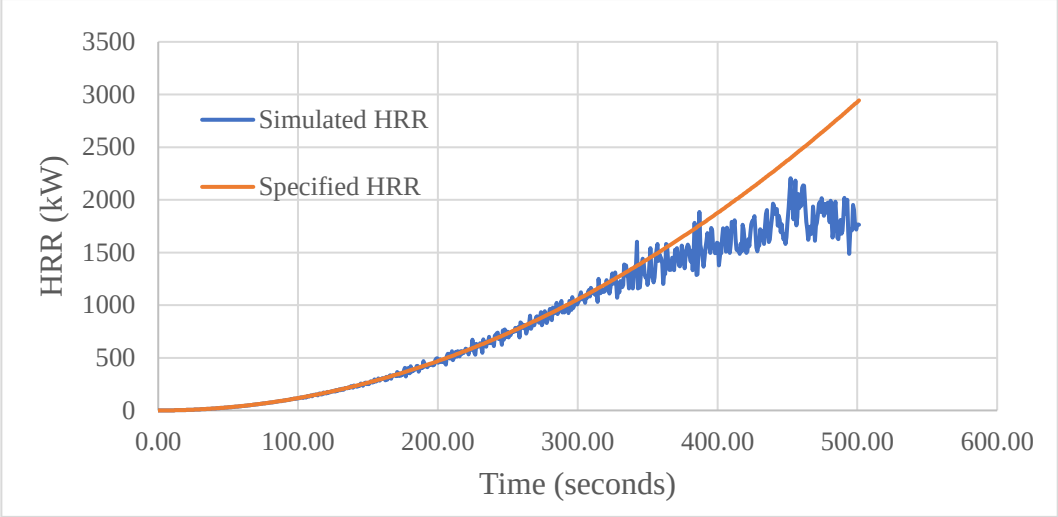

Figure 14: Comparison between simulated HRR and specified HRR on first floor

For the ground floor, the simulated HRR starts to deviate from the specified HRR between 3,000 kW and 4,000 kW. This is shown in Figure 13. Using Table 2 and Equation 14 (refer to section 1.4.3 Heat release rate) it is calculated that a single stack of seven pallets will provide a 3,250 kW fire. It is therefore considered appropriate to use a stack of seven pallets for the fire source on the ground floor.

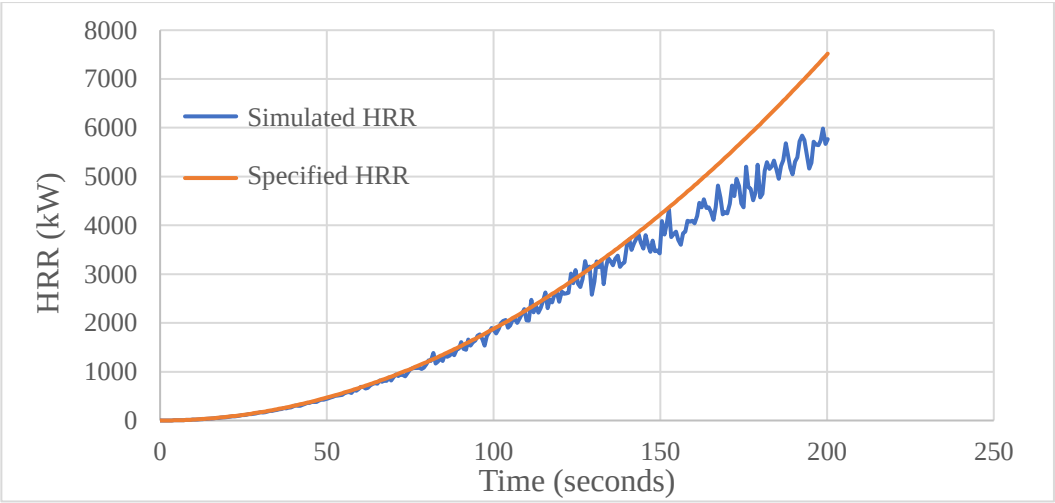

Figure 15: Comparison between simulated HRR and specified HRR on ground floor

By using the HRR fraction [24] taken from the medium and ultra-fast pallet fires in Figure 8 and Figure 9 (refer to section 1.4.3 Heat release rate) the HRR histories are estimated for both the ground floor and the first floor. The below medium HRR is for the first floor and the ultra-fast HRR is for the ground floor.

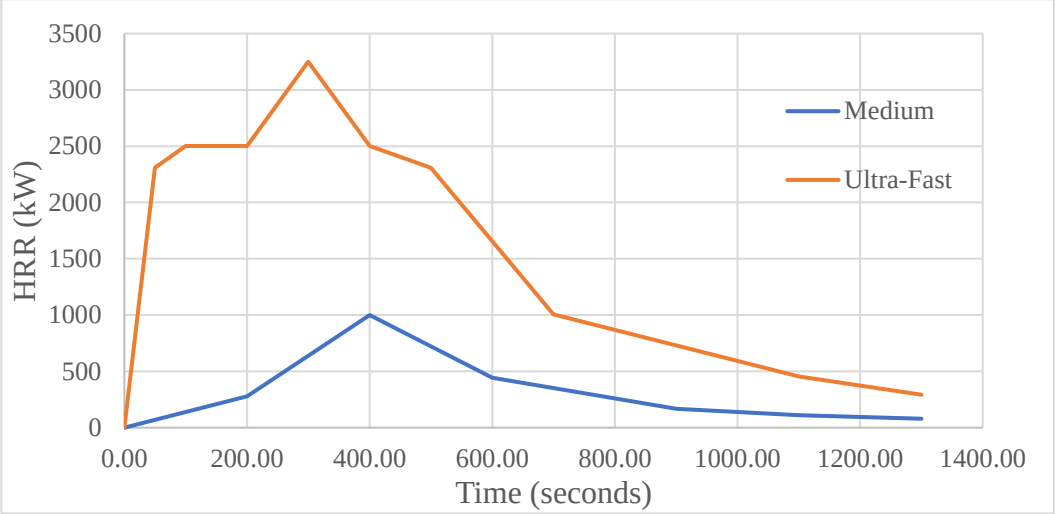

Figure 16: HRR for fires on ground floor and first floor

2.3 Emissivity change due to soot deposition

It is expected that soot will be deposited on the boundary surfaces and that those surfaces will have an emissivity equal to soot. To assess the coverage of soot in the existing live fire training structure, the soot modelling capabilities of FDS is used. Using the medium growth HRR in Figure 16, the coverage of the soot deposits on the first floor is found. The complex stoichiometry required for FDS to model soot deposit for a wood fire is provided by McGrattan *et al.* [24].

Figure 17 and Figure 18 are the results of the boundary soot deposit simulation. They show that after one fire, soot has been deposited on all exposed surfaces. The maximum range in these figures is set purposefully low in order to see the soot coverage in areas where there are low amounts of soot deposit. Soot deposits of 0.5 x 10^{-5} kg/m^2 is near the lower amounts of soot that is deposited to the boundary surfaces. Dividing this by the expected soot density of 1,800 kg/m^3 [111], equates to a soot coverage that is 0.00278 um thick. The expected soot particle diameter from burning wood is 0.05 um [112]. Thus, after eighteen fires the coverage of soot particles on the exposed surfaces is expected to be one particle thick in areas where there is low soot deposit. On surfaces with a high soot deposit of 3.0 x 10^{-5} kg/m^2, the expected one particle thickness can be reached after three fires.

It is possible to perform six live fire training evolutions in one day [14]. It is therefore considered appropriate to expect there having been at least eighteen fire evolutions performed in an existing live fire training structure. Thus, the soot emissivity of 0.95 is used for the boundary surfaces in the simulations [113].

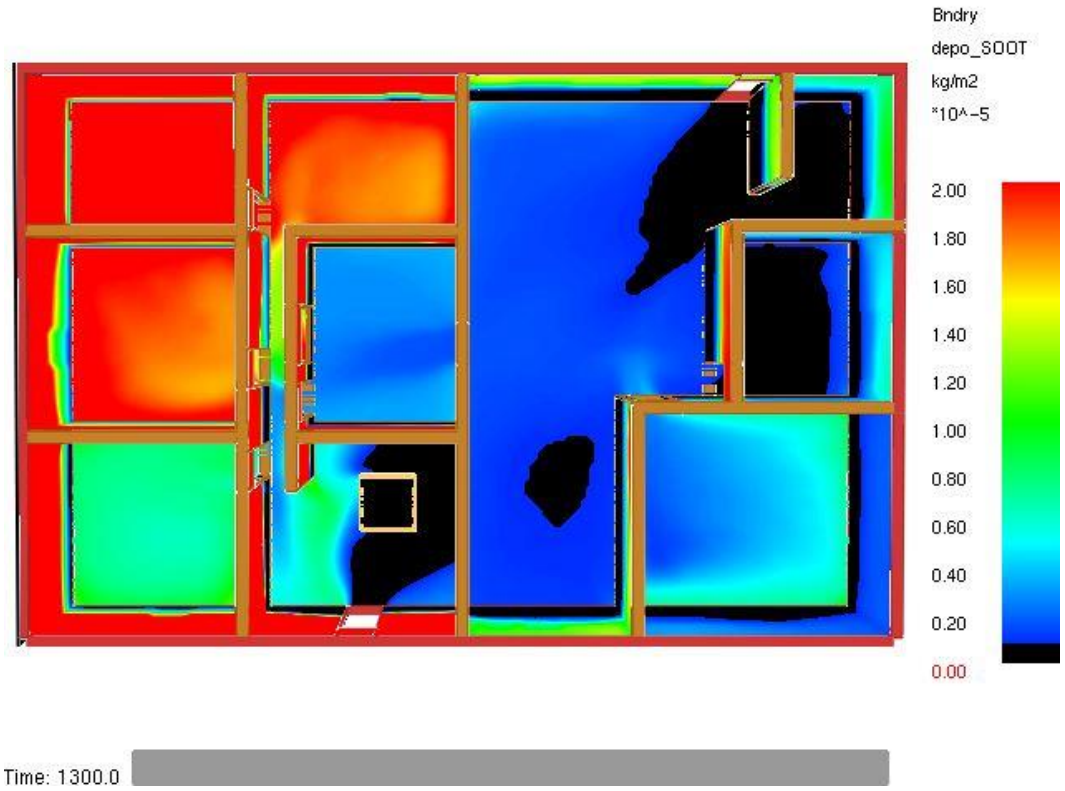

Figure 17: Top view of soot deposits on the first floor

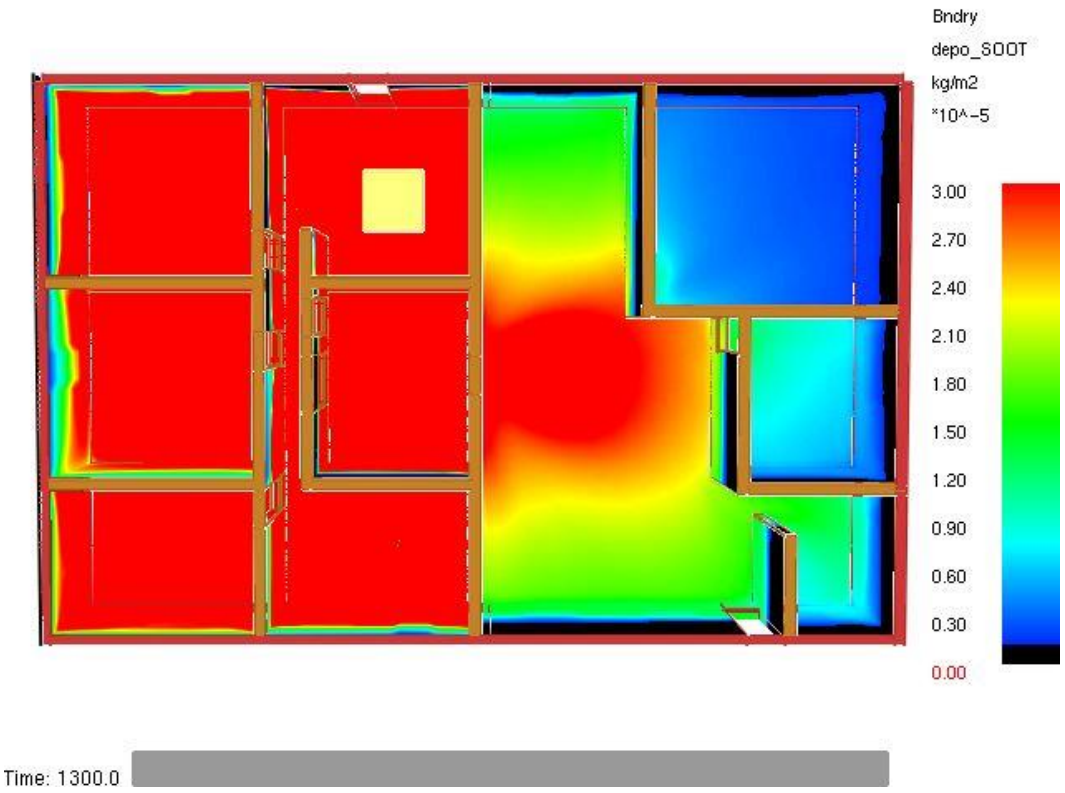

Figure 18: Bottom view of soot deposits on the first floor

2.4 Model validation

Model validation determines how well the physical phenomena is predicted by the mathematical model [100]. The model validation consists of using already validated test series that compare well to the models created in this study.

A validation range is created from the various non-dimensional parameters of multiple test series. Then the model's own non-dimensional parameters are calculated and must be shown to be within the validation range. The non-dimensional parameters are separated into experimental parameters and numerical parameters. The test series and calculation method of the non-dimensional parameters are found in the FDS Validation Guide [100]. A test series was excluded if the test was conducted out in the open and if the HRR used was very excessive when compared to that used in this study. This resulted in twenty out of thirty-six test series being selected to create the validation range.

2.4.1 Validation by experimental parameters

In the burn room on the first floor, the model was found to be within the validation range for all experimental non-dimensional parameters as shown in Table 14.

In the burn room on the ground floor, the model was found to be within the validation range for all experimental non-dimensional parameters except for one, the relative distance from the fire. This parameter is of importance when calculating the heat flux to a target [15]. Calculating target heat flux exposure is specifically

important for calculating firefighter safety (refer to section 1.5.2 Safety of firefighters during live fire training). Limiting the radial distance of the target to 7.6 m reduced the relative distance from the fire to be within the validation range as shown in Table 15. It follows, that targets on the ground floor cannot be further than 7.6 m from the centre of the fire.

Table 14: Model validation for experimental parameters on the first floor

Description	**Symbol**	**Validation range**		**Calculated quantity**
		Min	**Max**	
Fire Froude number	Q*	0.2	24.0	0.4
Flame height relate to ceiling height	L_f/H_c	0.1	1.7	0.9
Global equivalence ratio	ø	0.0	5.9	0.1
Compartment aspect ratio	W/H_c	0.1	2.3	1.5
	L/H_c	0.2	43.0	1.7
Relative distance along the ceiling	r_{cj}/H_c	0.0	6.0	1.2
Relative distance from the fire	r_{rad}/D	0.3	5.7	2.0

Table 15: Model validation for experimental parameters on the ground floor

Description	**Symbol**	**Validation range**		**Calculated quantity**
		Min	**Max**	
Fire Froude number	Q*	0.2	24.0	1.4
Flame height relate to ceiling height	L_f/H_c	0.1	1.7	1.5
Global equivalence ratio	ø	0.0	5.9	0.4
Compartment aspect ratio	W/H_c	0.1	2.3	2.3
	L/H_c	0.2	43.0	4.9
Relative distance along the ceiling	r_{cj}/H_c	0.0	6.0	3.8
Relative distance from the fire	r_{rad}/D	0.3	5.7	5.6

2.4.2 Validation by numerical parameters

In the burn room on the first floor, the model was found to be within the validation range for all numerical non-dimensional parameters as shown in Table 16. In Table 16, the grid cell length used 70 mm, the smallest cell length that can be used in the validation range.

In the burn room on the ground floor, the model was found to be within the validation range for all numerical non-dimensional parameters as shown in Table 17. In Table 17, the grid cell length used 110 mm, the smallest cell length that can be used in the validation range.

The plume resolution index is a particularly important numerical non-dimensional parameter. The greater the plume resolution index, the more the fire dynamics are resolved [100]. It is increased by using smaller grid cells in the simulation.

Table 16: Model validation for numerical parameters on the first floor

Description	**Symbol**	**Validation range**		**Calculated quantity**
		Min	**Max**	
Plume resolution index	D*/dx	1	15	13.7
Ceiling height relative to fire diameter	H_c/D^*	1.7	18.6	2.7

Table 17: Model validation for numerical parameters on the ground floor

Description	**Symbol**	**Validation Range**		**Calculated Quantity**
		Min	**Max**	
Plume resolution index	D*/dx	1	15	13.9
Ceiling height relative to fire diameter	H_c/D^*	1.7	18.6	2.3

2.4.3 Grid sensitivity study

A grid sensitivity study is performed for the ground floor and the first floor. It is possible for a fine grid to estimate results that are further from experimental results than results estimated from a coarser grid. This is seen to happen in the grid sensitivity study performed by Jahn, Rein and Torero [114]. To prevent this from occurring, a series of cell lengths are selected that result in a plume resolution index being within validation range of the non-dimensional numerical parameters.

There are ten cell lengths that are used in the grid sensitivity study for both the ground floor and first floor. The first cell length is selected as close as possible to the upper limit of the plume resolution index range, as mentioned in Table 16 and Table 17. The remaining nine cell lengths are selected by repeatedly increasing the cell length by 10 mm. Figure 17 and Figure 18 shows that the cells to be used in the grid sensitivity study are within the plume resolution index range. On the ground floor, the smallest cell length is bigger than the smallest cell length on the first floor. This is due to the fire having a considerably higher peak HRR, thus resulting in a higher plume resolution index.

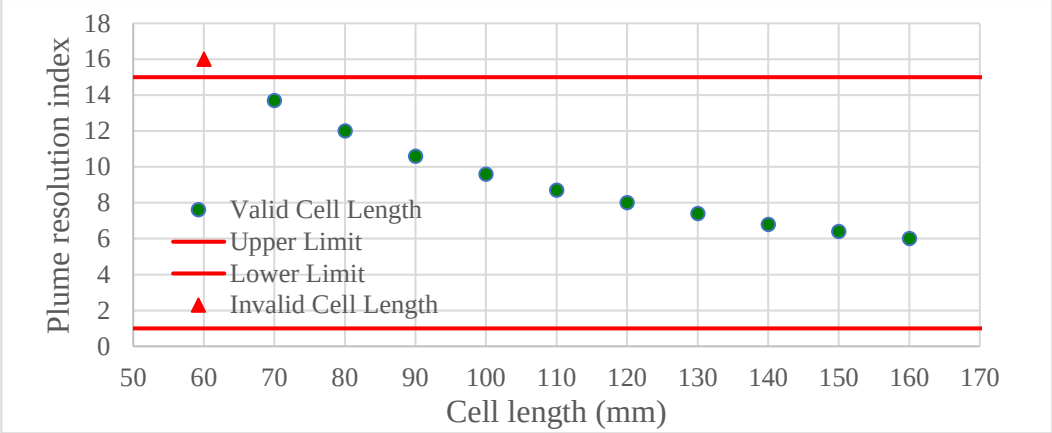

Figure 19: Plume resolution index vs cell length on the first floor

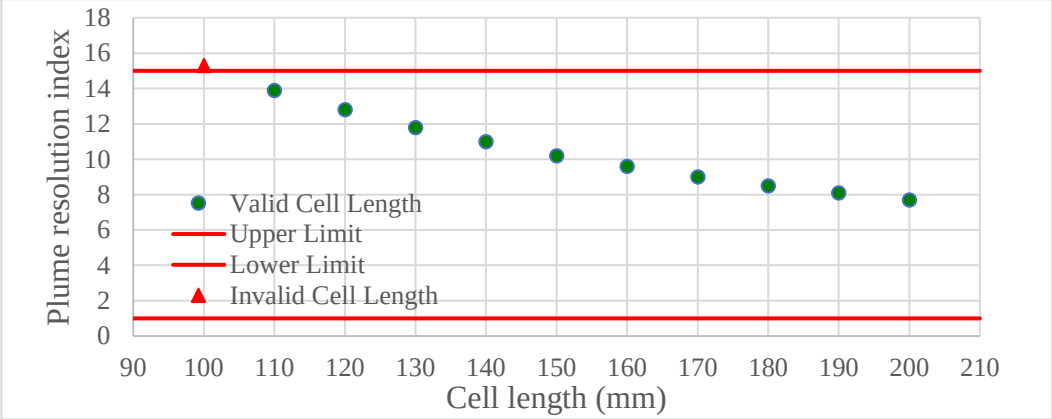

Figure 20: Plume resolution index vs cell length on the ground floor

The quantities used to compare the different cell lengths are important quantities that are to be measured in this study and have been selected for the grid sensitivity study. The graphs shown in Figure 21 to Figure 32 present the measurements taken at a time near the fire's peak HRR, 250 seconds for the ground-floor and 500 seconds for the first floor. A trendline is drawn on the graphs as the data points move between high and low values. Identifying the trend, helps to locate what the true value should be as the trend is clarified with accumulating data points.

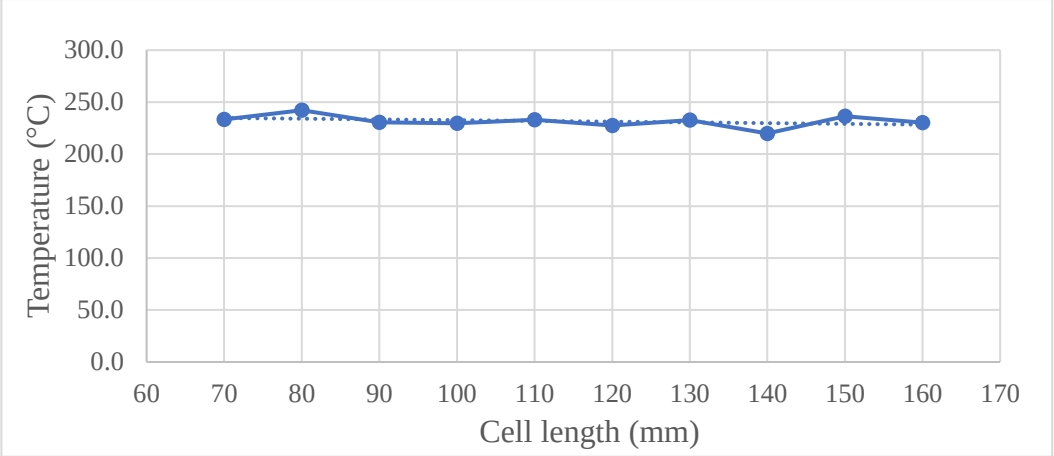

Figure 21: First floor – gas temperature vs cell length

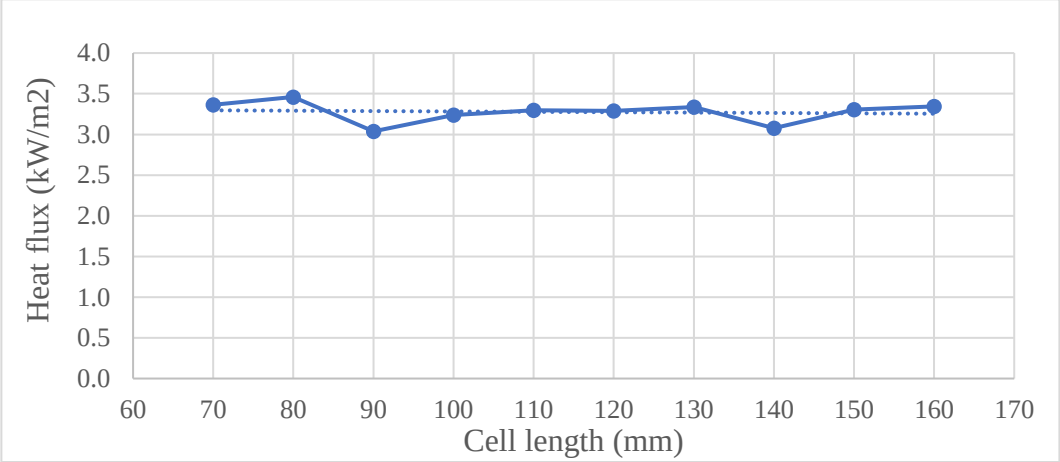

Figure 22: First floor – heat flux at wall surface vs cell length

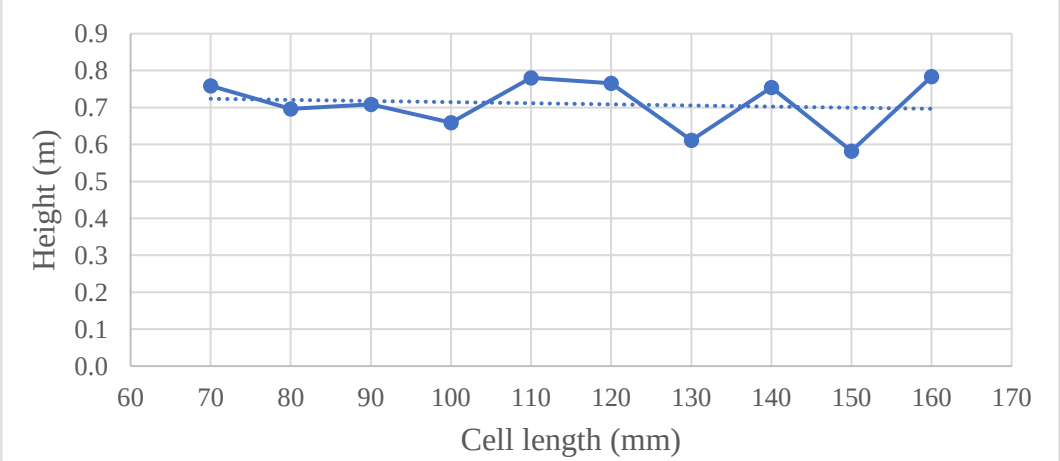

Figure 23: First floor – smoke layer height vs cell length

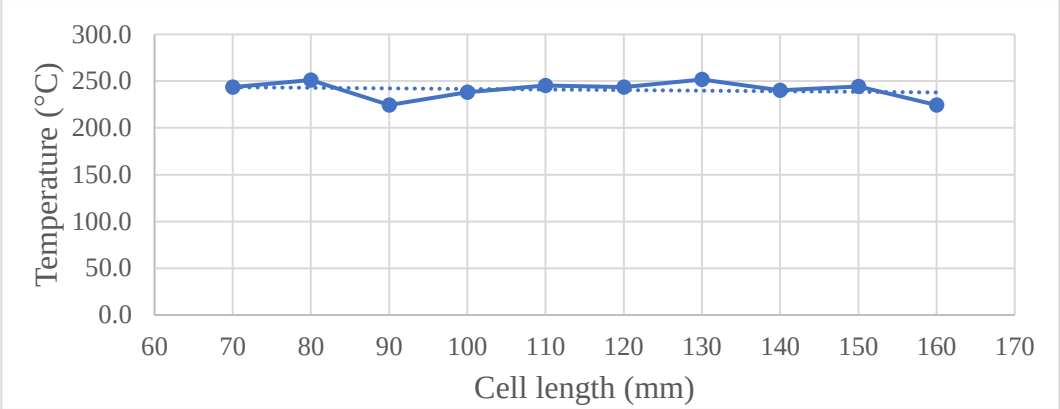

Figure 24: First floor – upper layer temperature vs cell length

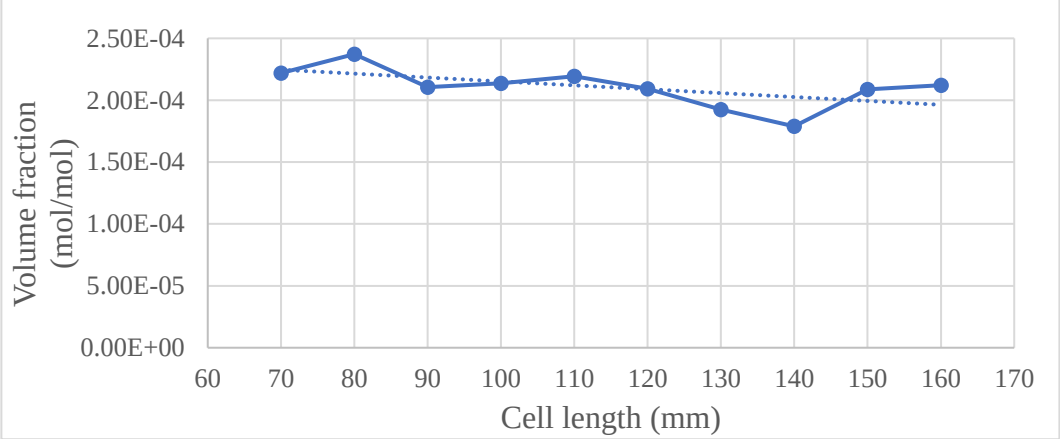

Figure 25: First floor – CO volume fraction vs cell length

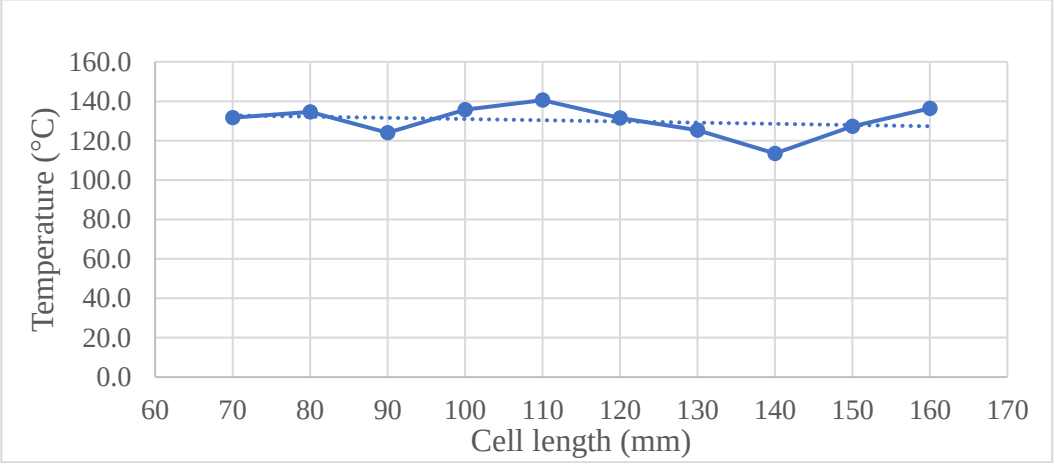

Figure 26: First floor – wall surface temperature vs cell length

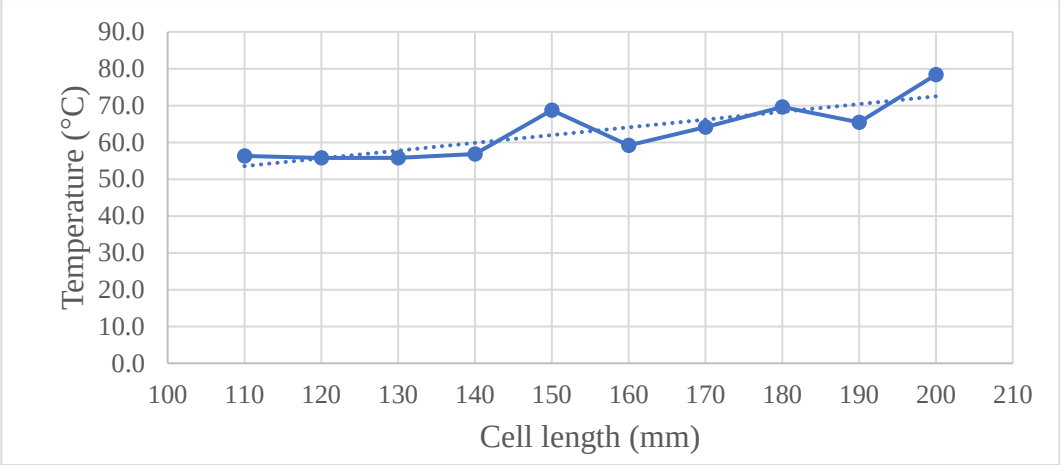

Figure 27: Ground floor – gas temperature vs cell length

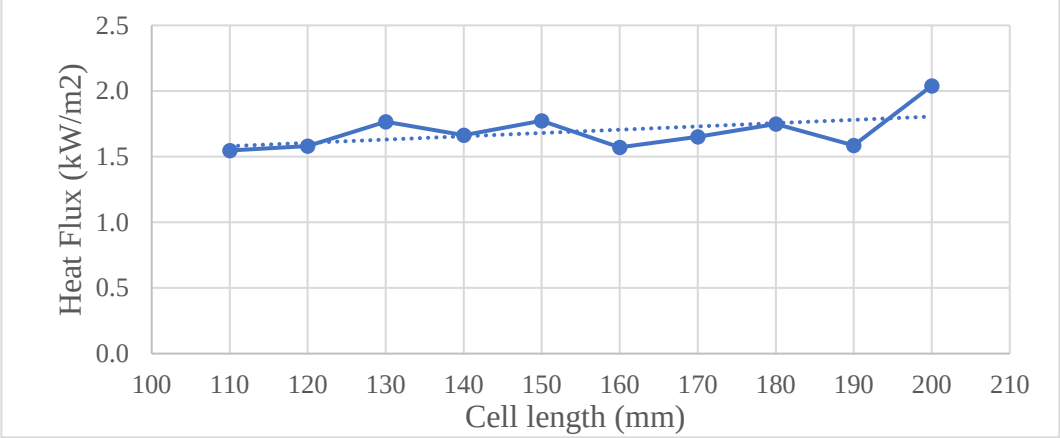

Figure 28: Ground floor – heat flux at wall surface vs cell length

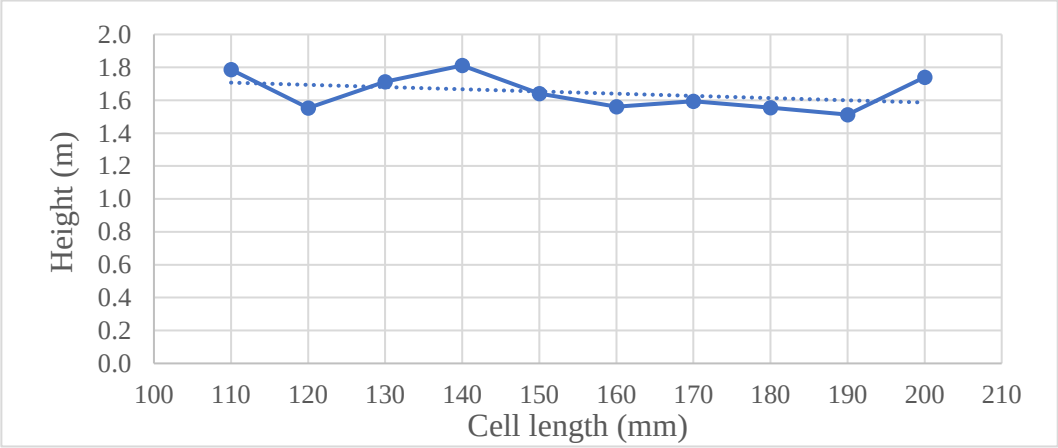

Figure 29: Ground floor – smoke layer height vs cell length

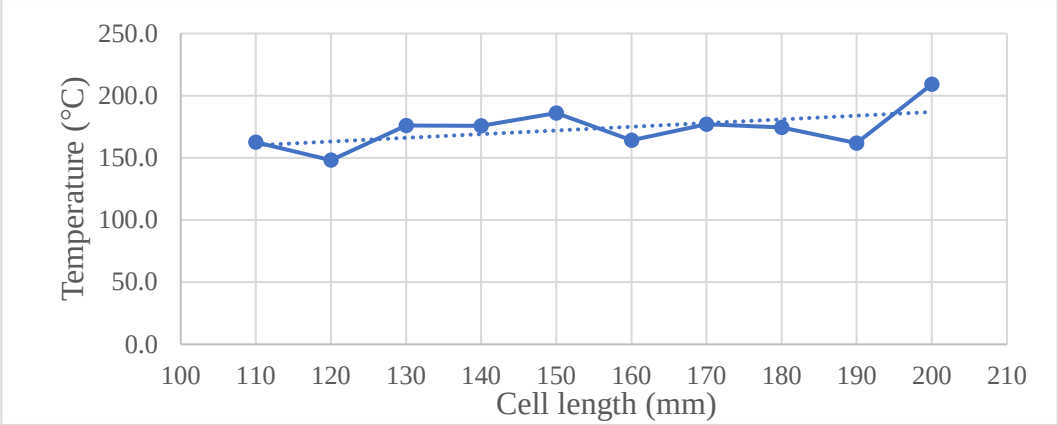

Figure 30: Ground floor – upper layer temperature vs cell length

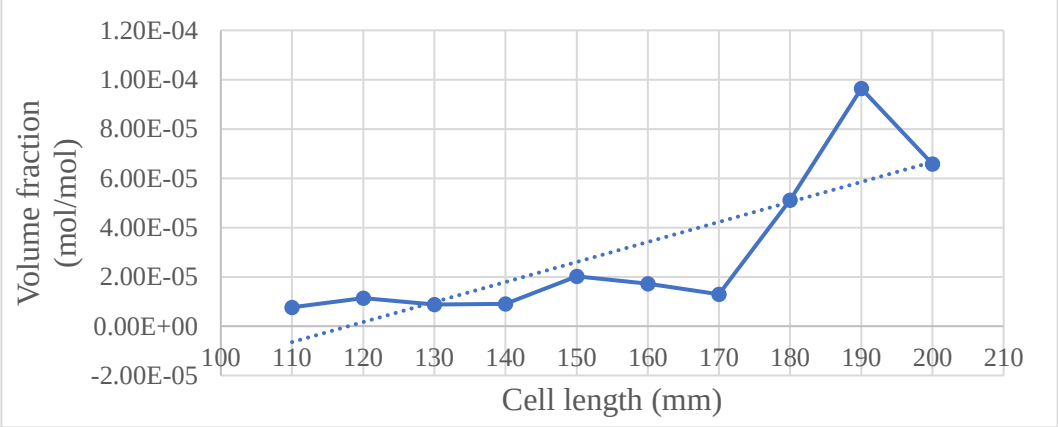

Figure 31: Ground floor – CO volume fraction vs cell length

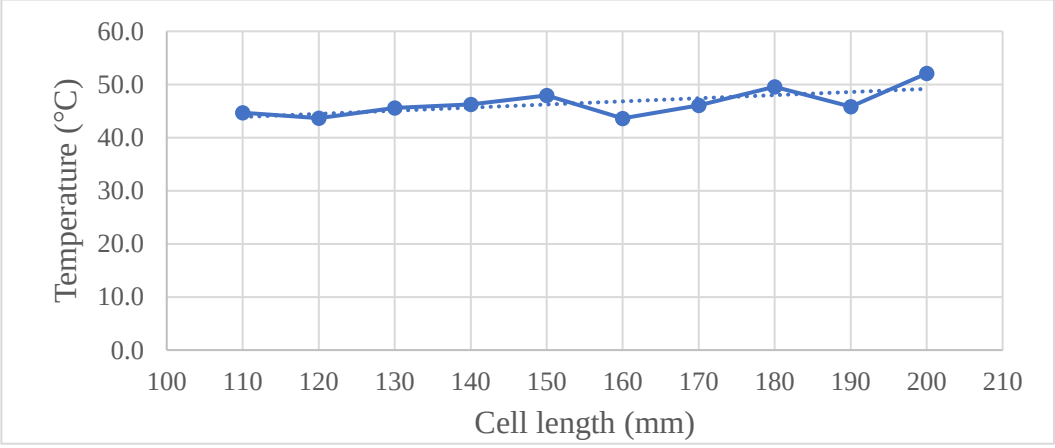

Figure 32: Ground floor – wall surface temperature vs cell length

In selecting the appropriate grid cell length, the time taken to complete the simulation is a common deciding factor. Should the available time to complete a simulation be restricted [115], the simulation will have to be restarted or a bigger grid cell length will have to be used that can allow the simulation to be completed in the available time.

When an FDS simulation is restarted, the output results are found to differ from the output results of an uninterrupted simulation. This was revealed by comparing results with and without any interruptions as shown in Table 18. The interrupted simulation was identical to the uninterrupted simulation, except it was restarted after every 100 seconds for a total simulation time of 580 seconds. The grid resolution used was 200 mm x 200 mm x 200 mm. The differences were then averaged from 100 seconds to 580 seconds of simulation time.

These differences were then compared to the differences that are experienced in results if the 120 mm x 120 mm x 120 mm grid is used instead of the 110 mm x 110 mm x 110 mm. The difference in grid size were also averaged from 100 seconds to 580 seconds of simulation time.

The results in Table 18 show that there is a larger effect on the simulation results if the grid cell length is increased. It is therefore better if the simulation is repeatedly restarted than using a coarser grid to try shortening the computation time.

Table 18: Effect of decreasing grid resolution vs effect of multiple simulation restarts

	Effect of increasing grid cell length		Effect of multiple simulation restarts	
Measured quantities	**Average difference**	**Maximum difference**	**Average difference**	**Maximum difference**
Gas temperature	5.60 %	22.95 %	3.77 %	16.43 %
Wall surface temperature	3.16 %	6.00 %	0.81 %	3.02 %
Heat flux at wall surface	5.65 %	20.53 %	3.85 %	19.57 %
Smoke layer height	6.12 %	30.55 %	4.21 %	20.81 %
Upper layer temperature	5.97 %	21.99 %	3.71 %	14.94 %
CO volume fraction	62.19 %	654.79 %	27.81 %	185.56 %

Based on the results, the best grid size to be used is 110 mm x 110 mm x 110 mm on the ground-floor and 70 mm x 70 mm x 70 mm on the first floor. Both grid sizes provide the best results possible and are within the validation range for the numerical parameters. The time taken to complete a simulation is not sufficient to warrant using a coarser grid should the available computation time be restricted.

2.5 Measuring output

Firefighters are required to keep low in fire situations [116]. Measuring devices are therefore positioned at 1.5 m above the ground. Measuring devices are also

positioned at 2.0 m above the ground to measure the effect on a firefighter standing up straight. This is due to the possibility of mistakes being made during live fire training (refer to section 1.5.2 Safety of firefighters during live fire training). Multiple mistakes are not considered and so devices measuring the effect of PPE being removed are only considered at 1.5 m above the ground.

On the first floor, measuring devices are positioned in every compartment as shown in Figure 33. In the burn room, the devices are spaced around the fire as well as at the entrances to the room. The devices are centered in the surrounding rooms except for Rooms G and H. Room G is long and narrow and Room H is considerably bigger than the other rooms. Data collected at multiple points was considered neccessary to better understand these areas.

On the ground floor there are measuring devices positioned 1.5 m away from the fire, with additional devices positioned further from the fire at 2.0 m intervals as shown in Figure 34. These devices are positioned within the 7.6 m distance required from the fire (refer to section 2.4.1 Validation by experimental parameters).

The devices measure heat flux, smoke layer height, upper layer temperature, and gas temperature. There are both vertical upward facing heat flux devices and horizontal facing heat flux devices so as to investigate were the majority of the heat flux is being received.

The wall temperature boundary quantity, is enabled in FDS to assess the temperature on the structure. There is also animated planes, known as slices, used

to view measured quantities in a two dimensional plane. To view the measured FED, slices used to view the measured volume fraction of carbon dioxide, carbon monoxide, and oxygen are enabled. These slices are positioned at 1.5 m above the ground.

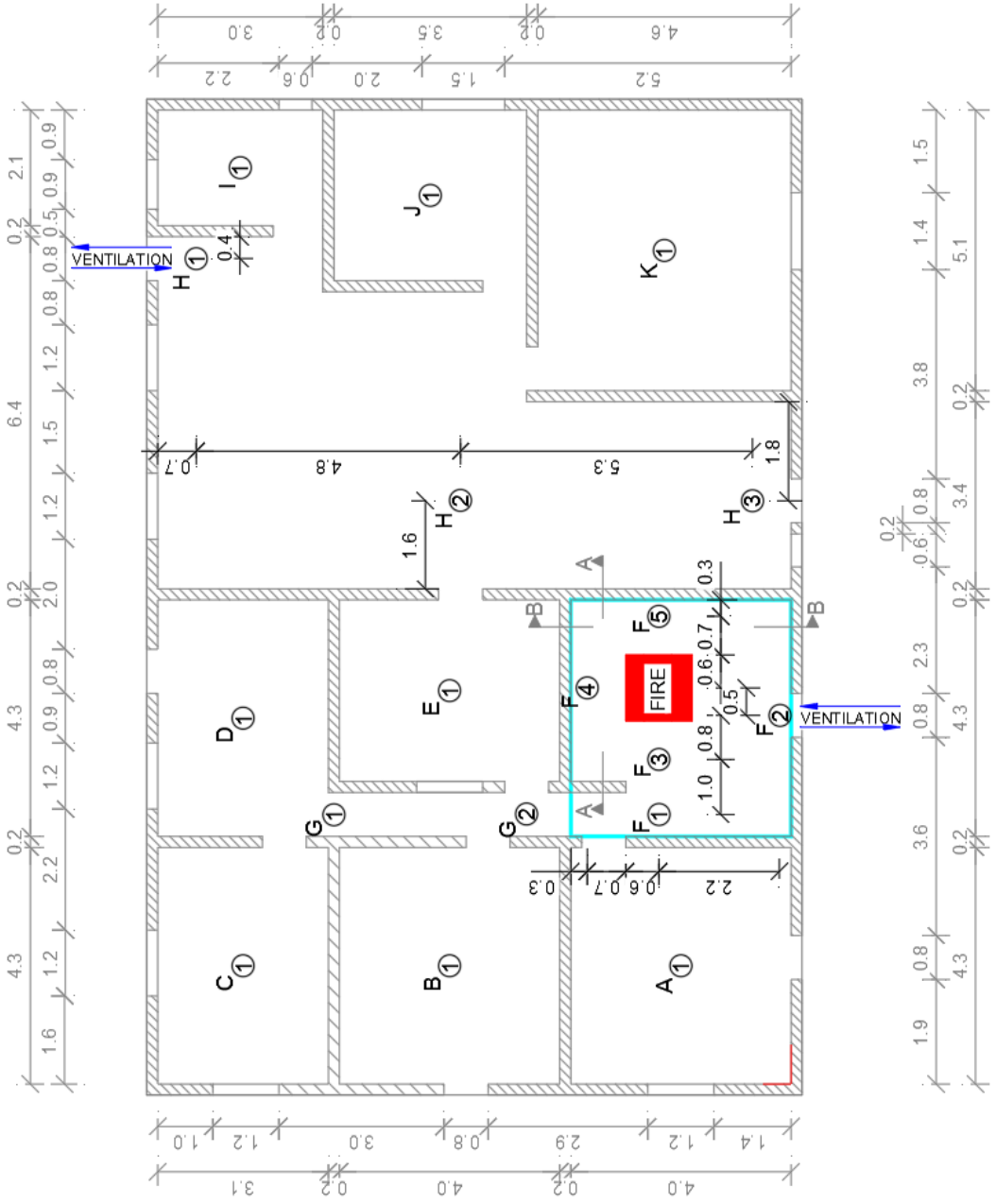

Figure 33: Position of devices on the first floor

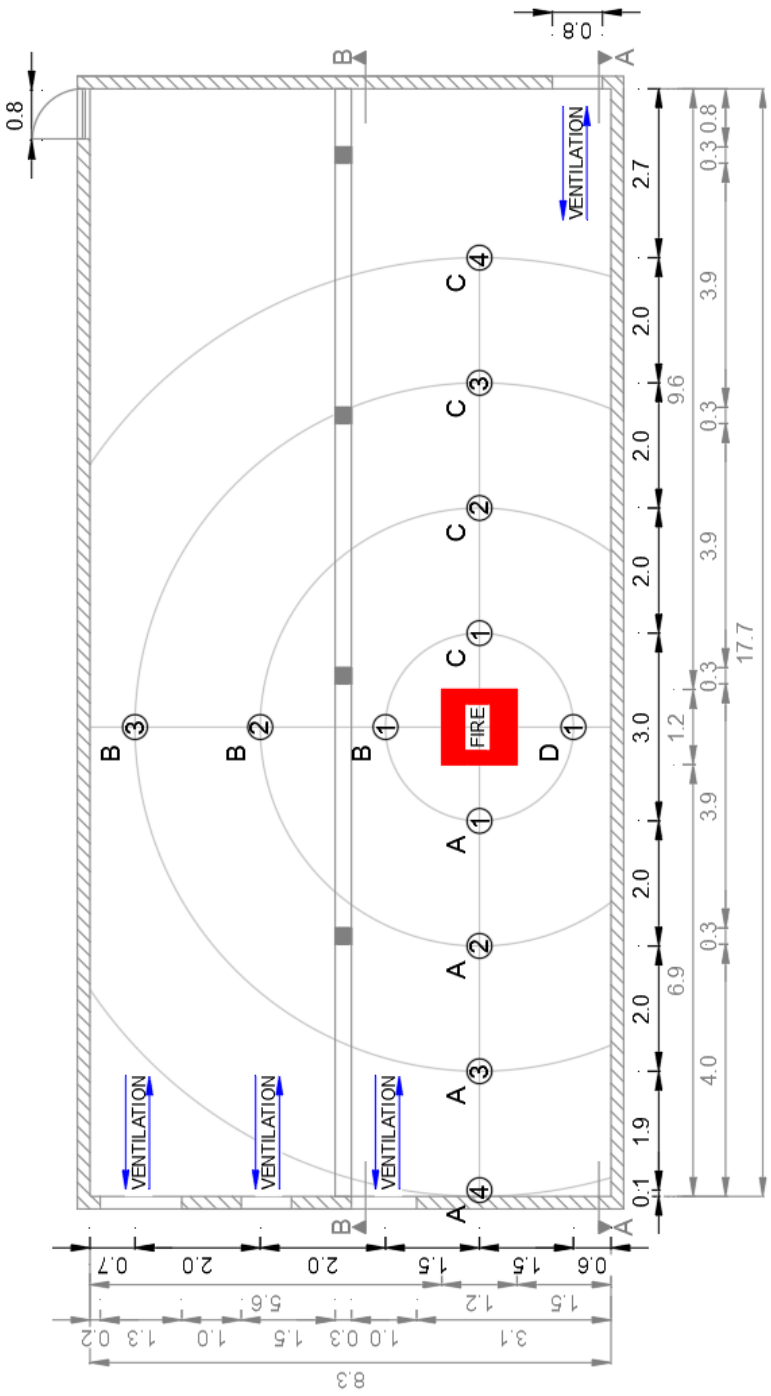

Figure 34: Position of devices on the ground floor

CHAPTER 3: RESULTS AND DISCUSSION

3.1 Results of the heat flux measured in the simulations

The heat flux measured for vertical and horizontal devices have been avaraged in order to identify which devices will be used. The devices selected are those that received the highest heat flux average. Measuring device positions are shown in Figure 33 and Figure 34 (refer to section 2.5 Measuring output).

Table 19 to Table 22 provides this information. The cells highlited in green identify whether a vertical or horizontal facing device is selected.

Table 19: First floor – average horizontal and vertical heat flux measured at 1.5 m above floor level

Horizontal	Vertical	Horizontal	Vertical	Horizontal	Vertical
Room A		**Room B**		**Room C**	
0.134	0.157	0.075	0.083	0.125	0.130
Room D		**Room E**		**Room F1**	
0.258	0.305	0.136	0.162	1.514	1.035
Room F2		**Room F3**		**Room F4**	
1.478	0.984	2.269	1.255	3.695	2.164
Room F5		**Room G1**		**Room G2**	
4.359	2.545	0.252	0.363	0.274	0.369
Room H1		**Room H2**		**Room H3**	
0.020	0.026	0.035	0.042	0.023	0.028
Room I		**Room J**		**Room K**	
0.015	0.019	0.011	0.013	0.006	0.007

Table 20: First floor – average horizontal and vertical heat flux measured at 2.0 m above floor level

Horizontal	Vertical	Horizontal	Vertical	Horizontal	Vertical
Room A		**Room B**		**Room C**	
0.158	0.145	0.085	0.073	0.135	0.115
Room D		**Room E**		**Room F1**	
0.313	0.271	0.163	0.145	1.660	0.983
Room F2		**Room F3**		**Room F4**	
1.606	0.984	2.127	1.153	3.148	2.115
Room F5		**Room G1**		**Room G2**	
3.647	2.453	0.391	0.401	0.462	0.472
Room H1		**Room H2**		**Room H3**	
0.028	0.025	0.044	0.042	0.032	0.026
Room I		**Room J**		**Room K**	
0.019	0.017	0.013	0.012	0.007	0.006

Table 21: Ground floor – average horizontal and vertical heat flux measured at 1.5 m above floor level

Horizontal	Vertical	Horizontal	Vertical	Horizontal	Vertical
Location A1		**Location A2**		**Location A3**	
10.007	7.808	3.176	2.814	1.313	1.600
Location A4		**Location B1**		**Location B2**	
0.920	1.010	9.295	6.673	2.709	1.755
Location B3		**Location C1**		**Location C2**	
0.932	0.794	7.781	4.366	2.097	1.573
Location C3		**Location C4**		**Location D1**	
0.816	1.047	0.575	0.906	8.684	5.465

Table 22: Ground floor – average horizontal and vertical heat flux measured at 2.0 m above floor level

Horizontal	Vertical	Horizontal	Vertical	Horizontal	Vertical
Location A1		**Location A2**		**Location A3**	
12.115	8.700	3.491	2.905	1.558	1.756
Location A4		**Location B1**		**Location B2**	
1.194	1.333	10.722	7.202	2.723	1.554
Location B3		**Location C1**		**Location C2**	
1.080	0.867	7.900	4.139	2.050	1.596
Location C3		**Location C4**		**Location D1**	
0.995	1.198	0.709	1.069	9.055	5.358

3.1.1 Results of the thermal protective performance of the firefighter's garments

Using the heat flux from the devices that recorded the highest average heat flux in Table 19 to Table 22, a spreadsheet is created to determine when a TPP value of 17.5 is reached (refer to section 1.5.3 Selecting the appropriate TPP value). It is also used to determine what the the probability is of the heat flux beging capable of exceeding the critical heatflux required to result in a TPP value being greater than 17.5.

A	B	C	D	E	F	G	H
s	kW/m2	cal/cm2/s	TPP Contribution per time interval	Accumulated TPP (0sec)	Probability (0sec)	Accumulated TPP (100sec)	Probability (100sec)
Time	RHFG A1	RHFG A1	RHFG A1	RHFG A1		RHFG A1	
70.203	10.108	0.241	0.314	13.961	79%		
71.503	10.994	0.263	0.341	14.302	85%		
72.800	10.849	0.259	0.336	14.638	84%		
74.109	10.886	0.260	0.340	14.979	84%		
75.402	11.876	0.284	0.367	15.346	89%		
76.700	12.857	0.307	0.398	15.744	93%		
78.008	12.208	0.292	0.381	16.125	91%		
79.303	12.062	0.288	0.373	16.499	90%		
80.606	11.191	0.267	0.348	16.847	86%		
81.906	11.324	0.270	0.352	17.198	87%		
83.206	10.855	0.259	0.337	17.535	84%		
84.509	11.232	0.268	0.350	17.885			
85.808	10.455	0.250	0.324	18.209			
87.107	11.419	0.273	0.354	18.564			
88.409	11.489	0.274	0.357	18.921			
89.700	10.850	0.259	0.335	19.256			
91.001	12.117	0.289	0.376	19.632			
92.303	12.793	0.306	0.398	20.030			
93.602	12.122	0.290	0.376	20.406			
94.909	12.961	0.310	0.405	20.811			
96.209	12.668	0.303	0.393	21.204			
97.502	12.672	0.303	0.391	21.595			
98.807	13.928	0.333	0.434	22.029			
100.101	12.891	0.308	0.398	22.428		0.000	
101.400	12.763	0.305	0.396	22.824		0.396	63%
102.702	12.465	0.298	0.388	23.212		0.784	60%
104.007	12.120	0.289	0.378	23.589		1.162	56%
105.306	11.955	0.286	0.371	23.960		1.532	54%
106.603	12.232	0.292	0.379	24.339		1.911	57%
107.908	13.456	0.321	0.420	24.759		2.331	70%
109.203	12.939	0.309	0.400	25.159		2.731	65%
110.509	13.154	0.314	0.411	25.569		3.141	67%

Figure 35: Spreadsheet used to determine the probability of critical heat flux being reached

Figure 35 is a screenshot from the spreadsheet used to process the results. Column B is the heat flux data collected from the selected measuring device in Table 19 to Table 22. This data is converted from kW/m^2 to $cal/cm^2/s$ as specified in Equation 16 (refer to section 1.5.2 Safety of firefighters during live fire training). For every time interval measured between time readings in column A, a TPP contribution is calculated and presented in column D. This TPP contribution is using the measured heat flux presented in column B. The TPP contirbution is then summed in column

E, starting from 0 seconds. The time taken for the accumulated TPP to reach 17.5 is then identified as the occupying time in a location and is presented in Table 23 - Table 28. The red highlighted cells in Table 23 - Table 28 is the time duration in which the 17.5 TPP value is reached in the simulation. The green highlited cells in Table 23 - Table 28 is the time duration were the 17.5 TPP value is not reached. Using this time duration, a critical heat flux is calculated that would result in a 17.5 TPP value in the same time period presented in Table 23 - Table 28. This critical heat flux is presented in Appendix A. The measured heat flux, used to determine the available occupying time, is used to determine the probability of whether it would actually be able to exceed the critical heat flux (refer to section 1.5.4 Probability of injury). This probability is presented in column F. The probability measured in column F is averaged and is recorded in Table 29 - Table 34. Column E and F are then repeated for every 100 seconds further into the simulation.

If a 0.00 % probability is calculated in Table 29 - Table 34, then it is unnecessary to recalculate the probability at the next 100 seconds. This is because there is only one growth and decay phase in the HRR histories shown in Figure 16 (refer to section 2.2 Heat release rate). This means that there is no growth in the HRR once it starts to decay and the critical heat flux only gets higher with a decreasing exposure time (refer to Appendix A). This means that there is no possibility for the probability to increase from 0.00 %.

An appropriate probability must be below 0.44% (refer to section 1.5.4 Probability of injury). Using Table 29 - Table 34 to identify locations with a probability greater than 0.44 %, the time available before a 0.44% probability is calculated. This is to

determine the time available at a location prior to there being sufficient probability in the achievement of the critical heat flux. To calculate this, the averaged highest probability is found that is below 0.44%, and then the corresponding available time is identified. The critical heat flux specified in Appendix A is not used here as the critical heat flux is required to be adjusted with each time step until the averaged highest probability is found that is below 0.44%. This available time is listed in Table 35 - Table 38.

Table 23: First floor – individual room occupying time using measuring devices at 1.5 m above the floor

Room entry time after ignition	**Individual room occupying time (seconds)**						
	A1	**B1**	**C1**	**D1**	**E1**	**G1**	**G2**
0 seconds	1,300.0	1,300.0	1,300.0	1,300.0	1,300.0	1,300.0	1,300.0
100 seconds	1,199.9	1,199.9	1,199.9	1,199.9	1,199.9	1,199.9	1,199.9
200 seconds	1,099.8	1,099.8	1,099.8	1,099.8	1,099.8	1,099.8	1,099.8
300 seconds	999.7	999.7	999.7	999.7	999.7	999.7	999.7
400 seconds	899.6	899.6	899.6	899.6	899.6	899.6	899.6
500 seconds	799.5	799.5	799.5	799.5	799.5	799.5	799.5
600 seconds	699.4	699.4	699.4	699.4	699.4	699.4	699.4
700 seconds	599.3	599.3	599.3	599.3	599.3	599.3	599.3
	H1	**H2**	**H3**	**I1**	**J1**	**K1**	
0 seconds	1,300.0	1,300.0	1,300.0	1,300.0	1,300.0	1,300.0	
100 seconds	1,199.9	1,199.9	1,199.9	1,199.9	1,199.9	1,199.9	
200 seconds	1,099.8	1,099.8	1,099.8	1,099.8	1,099.8	1,099.8	
300 seconds	999.7	999.7	999.7	999.7	999.7	999.7	
400 seconds	899.6	899.6	899.6	899.6	899.6	899.6	
500 seconds	799.5	799.5	799.5	799.5	799.5	799.5	
600 seconds	699.4	699.4	699.4	699.4	699.4	699.4	
700 seconds	599.3	599.3	599.3	599.3	599.3	599.3	

Table 24: First floor – location of occupying time in the burn room using measuring devices at 1.5 m above the floor

Location entry time after ignition	**Occupying time at location (seconds)**				
	F1	**F2**	**F3**	**F4**	**F5**
0 seconds	429.0	430.3	360.1	292.5	283.4
100 seconds	334.1	335.4	269.1	198.9	191.1
200 seconds	252.2	250.9	195.0	122.2	117.0
300 seconds	200.2	195.0	145.6	79.3	67.6
400 seconds	234.0	232.7	148.2	72.8	55.9
500 seconds	423.8	464.1	226.2	123.5	83.2
600 seconds	699.4	699.4	341.9	198.9	159.9
700 seconds	599.3	599.3	501.8	321.1	275.6
800 seconds	499.2	499.2	499.2	499.2	499.2
900 seconds	399.1	399.1	399.1	399.1	399.1
1,000 seconds	300.3	300.3	300.3	300.3	300.3
1,100 seconds	200.2	200.2	200.2	200.2	200.2
1,200 seconds	100.1	100.1	100.1	100.1	100.1

Table 25: First floor – individual room occupying time using measuring devices at 2.0 m above the floor

Room entry time after ignition	**Individual room occupying time (seconds)**						
	A2	**B2**	**C2**	**D2**	**E2**	**G4**	**G12**
0 seconds	1,300.0	1,300.0	1,300.0	1,300.0	1,300.0	1,300.0	1,300.0
100 seconds	1,199.9	1,199.9	1,199.9	1,199.9	1,199.9	1,199.9	1,199.9
200 seconds	1,099.8	1,099.8	1,099.8	1,099.8	1,099.8	1,099.8	1,099.8
300 seconds	999.7	999.7	999.7	999.7	999.7	999.7	999.7
400 seconds	899.6	899.6	899.6	899.6	899.6	899.6	899.6
500 seconds	799.5	799.5	799.5	799.5	799.5	799.5	799.5
600 seconds	699.4	699.4	699.4	699.4	699.4	699.4	699.4
700 seconds	599.3	599.3	599.3	599.3	599.3	599.3	599.3
	H2	**I2**	**J2**	**K2**	**L2**	**M2**	
0 seconds	1,300.0	1,300.0	1,300.0	1,300.0	1,300.0	1,300.0	
100 seconds	1,199.9	1,199.9	1,199.9	1,199.9	1,199.9	1,199.9	
200 seconds	1,099.8	1,099.8	1,099.8	1,099.8	1,099.8	1,099.8	
300 seconds	999.7	999.7	999.7	999.7	999.7	999.7	
400 seconds	899.6	899.6	899.6	899.6	899.6	899.6	
500 seconds	799.5	799.5	799.5	799.5	799.5	799.5	
600 seconds	699.4	699.4	699.4	699.4	699.4	699.4	
700 seconds	599.3	599.3	599.3	599.3	599.3	599.3	

Table 26: First floor – location of occupying time in the burn room using measuring devices at 2.0 m above the floor

Location entry time after ignition	**Occupying time at location (seconds)**				
	F1	**F2**	**F3**	**F4**	**F5**
0 seconds	413.4	416.0	377.0	325.0	317.2
100 seconds	317.2	319.8	280.8	228.8	221.0
200 seconds	230.1	234.0	197.6	141.7	133.9
300 seconds	167.7	172.9	139.1	83.2	72.8
400 seconds	183.3	195.0	139.1	70.2	54.6
500 seconds	371.8	404.3	244.4	157.3	113.1
600 seconds	699.4	699.4	421.2	310.7	266.5
700 seconds	599.3	599.3	599.3	552.5	508.3
800 seconds	499.2	499.2	499.2	499.2	499.2
900 seconds	399.1	399.1	399.1	399.1	399.1
1,000 seconds	300.3	300.3	300.3	300.3	300.3
1,100 seconds	200.2	200.2	200.2	200.2	200.2
1,200 seconds	100.1	100.1	100.1	100.1	100.1

Table 27: Ground floor – location of occupying time using measuring devices at 1.5 m above the floor

Location entry time after ignition	**Occupying time at location (seconds)**					
	A1	**A2**	**A3**	**A4**	**B1**	**B2**
0 seconds	83.2	209.3	336.7	479.7	85.8	243.1
100 seconds	57.2	161.2	262.6	412.1	62.4	196.3
200 seconds	53.3	135.2	236.6	405.6	59.8	172.9
300 seconds	49.4	133.9	243.1	529.1	53.3	166.4
400 seconds	53.3	146.9	323.7	899.6	57.2	174.2
500 seconds	55.9	178.1	556.4	799.5	61.1	213.2
600 seconds	61.1	261.3	699.4	699.4	68.9	292.5
700 seconds	75.4	345.8	599.3	599.3	83.2	386.1
800 seconds	85.8	435.5	499.2	499.2	92.3	499.2
900 seconds	98.8	399.1	399.1	399.1	104.0	399.1
1,000 seconds	122.2	300.3	300.3	300.3	124.8	300.3
1,100 seconds	148.2	200.2	200.2	200.2	152.1	200.2
1,200 seconds	100.1	100.1	100.1	100.1	100.1	100.1
	B3	**C1**	**C2**	**C3**	**C4**	**D1**
0 seconds	560.3	81.9	270.4	492.7	570.7	76.7
100 seconds	505.7	70.2	253.5	442.0	522.6	62.4
200 seconds	516.1	74.1	256.1	460.2	577.2	66.3
300 seconds	625.3	70.2	260.0	555.1	715.0	61.1
400 seconds	899.6	75.4	287.3	774.8	899.6	67.6
500 seconds	799.5	81.9	341.9	799.5	799.5	72.8
600 seconds	699.4	85.8	405.6	699.4	699.4	76.7
700 seconds	599.3	102.7	479.7	599.3	599.3	92.3
800 seconds	499.2	110.5	499.2	499.2	499.2	98.8
900 seconds	399.1	120.9	399.1	399.1	399.1	109.2
1,000 seconds	300.3	139.1	300.3	300.3	300.3	127.4
1,100 seconds	200.2	165.1	200.2	200.2	200.2	149.5
1,200 seconds	100.1	100.1	100.1	100.1	100.1	100.1

Table 28: Ground floor – location of occupying time using measuring devices at 2.0 m above the floor

Location entry time after ignition	**Occupying time at location (seconds)**					
	A1	**A2**	**A3**	**A4**	**B1**	**B2**
0 seconds	75.4	192.4	317.2	371.8	76.7	239.2
100 seconds	45.5	141.7	243.1	300.3	50.7	192.4
200 seconds	40.3	118.3	215.8	279.5	49.4	166.4
300 seconds	37.7	115.7	219.7	304.2	41.6	161.2
400 seconds	40.3	127.4	273.0	494.0	45.5	169.0
500 seconds	42.9	152.1	461.5	799.5	48.1	208.0
600 seconds	48.1	236.6	699.4	699.4	57.2	291.2
700 seconds	65.0	334.1	599.3	599.3	76.7	404.3
800 seconds	76.7	449.8	499.2	499.2	84.5	499.2
900 seconds	92.3	399.1	399.1	399.1	100.1	399.1
1,000 seconds	123.5	300.3	300.3	300.3	127.4	300.3
1,100 seconds	162.5	200.2	200.2	200.2	167.7	200.2
1,200 seconds	100.1	100.1	100.1	100.1	100.1	100.1
	B3	**C1**	**C2**	**C3**	**C4**	**D1**
0 seconds	491.4	74.1	263.9	432.9	482.3	68.9
100 seconds	438.1	66.3	253.5	378.3	423.8	55.9
200 seconds	431.6	74.1	257.4	377.0	432.9	62.4
300 seconds	494.0	68.9	262.6	427.7	517.4	57.2
400 seconds	670.8	74.1	295.1	595.4	733.2	62.4
500 seconds	799.5	79.3	357.5	799.5	799.5	66.3
600 seconds	699.4	85.8	434.2	699.4	699.4	72.8
700 seconds	599.3	104.0	529.1	599.3	599.3	92.3
800 seconds	499.2	111.8	499.2	499.2	499.2	98.8
900 seconds	399.1	126.1	399.1	399.1	399.1	113.1
1,000 seconds	300.3	149.5	300.3	300.3	300.3	136.5
1,100 seconds	200.2	189.8	200.2	200.2	200.2	171.6
1,200 seconds	100.1	100.1	100.1	100.1	100.1	100.1

Table 29: First floor – individual room critical heat flux probability using measuring devices at 1.5 m above the floor

Room entry time after ignition	**Individual room probability of critical heat flux being reached in the occupying time**						
	A1	**B1**	**C1**	**D1**	**E1**	**G1**	**G2**
0 seconds	0.17%	0.00%	0.00%	17.85%	0.22%	24.57%	24.95%
100 seconds	0.05%	0.00%	0.00%	16.00%	0.06%	23.42%	23.75%
200 seconds	0.01%	0.00%	0.00%	13.73%	0.01%	21.95%	22.24%
300 seconds	0.00%	0.00%	0.00%	10.97%	0.00%	20.00%	20.24%
400 seconds	0.00%	0.00%	0.00%	6.41%	0.00%	12.97%	13.37%
500 seconds	0.00%	0.00%	0.00%	0.75%	0.00%	2.97%	3.18%
600 seconds	0.00%	0.00%	0.00%	0.00%	0.00%	0.01%	0.03%
700 seconds	0.00%	0.00%	0.00%	0.00%	0.00%	0.00%	0.00%
	H1	**H2**	**H3**	**I1**	**J1**	**K1**	
0 seconds	0.00%	0.00%	0.00%	0.00%	0.00%	0.00%	
100 seconds	0.00%	0.00%	0.00%	0.00%	0.00%	0.00%	
200 seconds	0.00%	0.00%	0.00%	0.00%	0.00%	0.00%	
300 seconds	0.00%	0.00%	0.00%	0.00%	0.00%	0.00%	
400 seconds	0.00%	0.00%	0.00%	0.00%	0.00%	0.00%	
500 seconds	0.00%	0.00%	0.00%	0.00%	0.00%	0.00%	
600 seconds	0.00%	0.00%	0.00%	0.00%	0.00%	0.00%	
700 seconds	0.00%	0.00%	0.00%	0.00%	0.00%	0.00%	

Table 30: First floor – location of critical heat flux probability in the burn room using measuring devices at 1.5m above the floor

Location entry time after ignition	**Location probability of critical heat flux being reached in the occupying time**				
	F1	**F2**	**F3**	**F4**	**F5**
0 seconds	43.28%	41.23%	44.80%	39.31%	41.32%
100 seconds	47.26%	45.70%	47.99%	41.15%	45.76%
200 seconds	52.08%	51.50%	53.14%	51.41%	52.67%
300 seconds	59.32%	59.25%	60.13%	57.09%	55.63%
400 seconds	54.50%	53.16%	61.22%	58.96%	58.54%
500 seconds	49.47%	47.69%	55.80%	56.94%	54.68%
600 seconds	40.49%	37.07%	54.60%	58.42%	58.24%
700 seconds	22.46%	19.14%	49.22%	49.51%	49.07%
800 seconds	4.05%	2.53%	30.35%	44.24%	45.11%
900 seconds	0.00%	0.00%	4.69%	13.60%	14.55%
1,000 seconds	0.00%	0.00%	0.01%	0.22%	0.22%
1,100 seconds	0.00%	0.00%	0.00%	0.00%	0.00%
1,200 seconds	0.00%	0.00%	0.00%	0.00%	0.00%

Table 31: First floor – individual room critical heat flux probability using measuring devices at 2.0m above the floor

Room entry time after ignition	**Individual room probability of critical heat flux being reached in the occupying time**						
	A2	**B2**	**C2**	**D2**	**E2**	**G4**	**G12**
0 seconds	0.23%	0.00%	0.01%	19.15%	0.36%	27.72%	33.32%
100 seconds	0.07%	0.00%	0.00%	17.43%	0.12%	26.87%	32.90%
200 seconds	0.01%	0.00%	0.00%	15.28%	0.03%	25.74%	32.16%
300 seconds	0.00%	0.00%	0.00%	12.62%	0.00%	24.04%	30.28%
400 seconds	0.00%	0.00%	0.00%	7.63%	0.00%	16.04%	21.09%
500 seconds	0.00%	0.00%	0.00%	1.04%	0.00%	4.67%	8.40%
600 seconds	0.00%	0.00%	0.00%	0.00%	0.00%	0.04%	0.37%
700 seconds	0.00%	0.00%	0.00%	0.00%	0.00%	0.00%	0.00%
	H2	**I2**	**J2**	**K2**	**L2**	**M2**	
0 seconds	0.00%	0.00%	0.00%	0.00%	0.00%	0.00%	
100 seconds	0.00%	0.00%	0.00%	0.00%	0.00%	0.00%	
200 seconds	0.00%	0.00%	0.00%	0.00%	0.00%	0.00%	
300 seconds	0.00%	0.00%	0.00%	0.00%	0.00%	0.00%	
400 seconds	0.00%	0.00%	0.00%	0.00%	0.00%	0.00%	
500 seconds	0.00%	0.00%	0.00%	0.00%	0.00%	0.00%	
600 seconds	0.00%	0.00%	0.00%	0.00%	0.00%	0.00%	
700 seconds	0.00%	0.00%	0.00%	0.00%	0.00%	0.00%	

Table 32: First floor – location of critical heat flux probability in the burn room using measuring devices at 2.0m above the floor

Location entry time after ignition	**Probability of critical heat flux being reached in the occupying time at location**				
	F1	**F2**	**F3**	**F4**	**F5**
0 seconds	40.29%	39.56%	41.24%	35.15%	36.40%
100 seconds	44.51%	44.18%	45.22%	41.06%	42.01%
200 seconds	49.20%	50.21%	50.16%	49.58%	47.69%
300 seconds	57.25%	58.60%	58.89%	52.60%	52.52%
400 seconds	55.86%	55.13%	59.70%	55.22%	56.75%
500 seconds	48.26%	47.56%	52.81%	51.58%	51.19%
600 seconds	42.05%	40.14%	50.46%	53.08%	53.56%
700 seconds	23.65%	21.66%	41.74%	43.73%	43.31%
800 seconds	4.55%	3.53%	17.35%	21.78%	23.56%
900 seconds	0.00%	0.00%	0.75%	1.53%	1.92%
1,000 seconds	0.00%	0.00%	0.00%	0.00%	0.00%
1,100 seconds	0.00%	0.00%	0.00%	0.00%	0.00%
1,200 seconds	0.00%	0.00%	0.00%	0.00%	0.00%

Table 33: Ground floor – location of critical heat flux probability using measuring devices at 1.5m above the floor

Location entry time after ignition	**Probability of critical heat flux being reached in the occupying time at location**					
	A1	**A2**	**A3**	**A4**	**B1**	**B2**
0 seconds	59.84%	60.03%	57.30%	60.30%	59.63%	61.89%
100 seconds	62.44%	62.32%	57.51%	59.38%	63.14%	60.72%
200 seconds	61.52%	61.03%	61.87%	60.05%	61.47%	61.97%
300 seconds	63.16%	62.51%	61.96%	52.03%	63.98%	63.15%
400 seconds	63.56%	63.51%	55.11%	38.04%	61.69%	62.56%
500 seconds	62.07%	59.39%	41.73%	25.08%	63.16%	58.95%
600 seconds	60.81%	56.59%	32.83%	9.83%	62.86%	56.54%
700 seconds	62.03%	58.52%	12.69%	0.34%	62.12%	56.39%
800 seconds	59.70%	55.66%	1.03%	0.00%	62.79%	52.05%
900 seconds	63.13%	30.32%	0.00%	0.00%	62.86%	20.22%
1,000 seconds	62.53%	2.22%	0.00%	0.00%	62.04%	0.59%
1,100 seconds	62.23%	0.00%	0.00%	0.00%	62.09%	0.00%
1,200 seconds	2.56%	0.00%	0.00%	0.00%	2.49%	0.00%
	B3	**C1**	**C2**	**C3**	**C4**	**D1**
0 seconds	60.55%	58.09%	62.01%	64.81%	64.46%	59.40%
100 seconds	59.63%	61.26%	62.19%	62.53%	61.58%	61.17%
200 seconds	59.08%	61.92%	62.44%	60.65%	57.62%	62.77%
300 seconds	52.00%	63.37%	62.82%	53.13%	48.30%	63.43%
400 seconds	42.47%	63.33%	60.94%	44.25%	39.38%	63.90%
500 seconds	29.25%	62.51%	58.19%	32.73%	25.29%	62.48%
600 seconds	13.57%	61.54%	59.31%	15.42%	9.60%	62.06%
700 seconds	1.76%	63.37%	58.82%	1.83%	0.43%	63.46%
800 seconds	0.01%	62.93%	46.55%	0.01%	0.00%	62.50%
900 seconds	0.00%	62.52%	14.79%	0.00%	0.00%	63.34%
1,000 seconds	0.00%	61.43%	0.38%	0.00%	0.00%	62.15%
1,100 seconds	0.00%	62.06%	0.00%	0.00%	0.00%	61.82%
1,200 seconds	0.00%	0.82%	0.00%	0.00%	0.00%	2.31%

Table 34: Ground floor – location of critical heat flux probability using measuring devices at 2.0m above the floor

Location entry time after ignition	**Probability of critical heat flux being reached in the occupying time at location**					
	A1	**A2**	**A3**	**A4**	**B1**	**B2**
0 seconds	59.24%	59.77%	57.77%	57.56%	57.24%	62.36%
100 seconds	61.39%	61.38%	57.56%	57.18%	60.31%	60.39%
200 seconds	61.61%	61.32%	61.57%	60.61%	61.18%	60.97%
300 seconds	62.61%	62.44%	61.51%	58.33%	60.68%	62.25%
400 seconds	63.29%	62.61%	57.46%	46.82%	61.03%	61.97%
500 seconds	62.94%	59.52%	43.61%	36.21%	59.82%	58.70%
600 seconds	61.55%	55.55%	39.39%	19.76%	60.50%	55.87%
700 seconds	61.52%	57.53%	18.66%	3.60%	63.06%	54.66%
800 seconds	59.91%	53.38%	2.70%	0.04%	61.87%	44.36%
900 seconds	61.67%	26.67%	0.01%	0.00%	61.47%	15.29%
1,000 seconds	61.18%	1.57%	0.00%	0.00%	61.45%	0.27%
1,100 seconds	60.97%	0.00%	0.00%	0.00%	60.76%	0.00%
1,200 seconds	0.55%	0.00%	0.00%	0.00%	0.68%	0.00%
	B3	**C1**	**C2**	**C3**	**C4**	**D1**
0 seconds	60.95%	56.28%	61.65%	64.47%	64.32%	57.04%
100 seconds	60.61%	61.56%	62.65%	62.18%	62.04%	63.14%
200 seconds	61.73%	63.15%	62.60%	62.12%	61.23%	61.38%
300 seconds	56.47%	63.33%	62.60%	57.57%	54.48%	61.88%
400 seconds	47.61%	63.47%	60.47%	46.98%	44.59%	61.76%
500 seconds	37.82%	62.31%	57.01%	40.67%	33.96%	62.19%
600 seconds	21.20%	61.84%	58.52%	22.79%	16.74%	62.59%
700 seconds	5.04%	63.17%	56.78%	5.13%	2.27%	63.43%
800 seconds	0.12%	63.19%	37.34%	0.14%	0.02%	62.67%
900 seconds	0.00%	62.88%	9.43%	0.00%	0.00%	63.40%
1,000 seconds	0.00%	61.19%	0.13%	0.00%	0.00%	60.94%
1,100 seconds	0.00%	61.08%	0.00%	0.00%	0.00%	61.26%
1,200 seconds	0.00%	0.08%	0.00%	0.00%	0.00%	0.25%

Table 35: First floor – location of available time using measuring devices at 1.5m above the floor

Location entry time after ignition	**Time available before a 0.44% probability at location (seconds)**			
	D1	**G1**	**G2**	**F1**
0 seconds	535.6	458.9	447.2	260.0
100 seconds	618.8	455.0	439.4	195.0
200 seconds	618.8	455.0	439.4	143.0
300 seconds	618.8	455.0	369.2	100.1
400 seconds	622.7	460.2	445.9	94.9
500 seconds	635.7	507.0	592.8	135.2
600 seconds	699.4	699.4	699.4	213.2
700 seconds	599.3	599.3	599.3	275.6
800 seconds	499.2	499.2	499.2	378.3
900 seconds	399.1	399.1	399.1	399.1
1,000 seconds	300.3	300.3	300.3	300.3
1,100 seconds	200.2	200.2	200.2	200.2
1,200 seconds	100.1	100.1	100.1	100.1
	F2	**F3**	**F4**	**F5**
0 seconds	269.1	218.4	180.7	172.9
100 seconds	200.2	156.0	124.8	109.2
200 seconds	140.4	111.8	57.2	54.6
300 seconds	98.8	79.3	36.4	29.9
400 seconds	91.0	71.5	29.9	24.7
500 seconds	135.2	93.6	45.5	28.6
600 seconds	226.2	137.8	83.2	67.6
700 seconds	295.1	172.9	111.8	80.6
800 seconds	408.2	234.0	165.1	144.3
900 seconds	399.1	314.6	249.6	248.3
1,000 seconds	300.3	300.3	300.3	300.3
1,100 seconds	200.2	200.2	200.2	200.2
1,200 seconds	100.1	100.1	100.1	100.1

Table 36: First floor – location of available time using measuring devices at 2.0 m above the floor

Location entry time after ignition	**Time available before a 0.44% probability at location (seconds)**			
	D1	**G1**	**G2**	**F1**
0 seconds	588.9	412.1	386.1	258.7
100 seconds	588.9	378.3	321.1	189.8
200 seconds	588.9	377.0	299.0	124.8
300 seconds	588.9	377.0	299.0	87.1
400 seconds	592.8	383.5	302.9	75.4
500 seconds	725.4	534.3	449.8	117.0
600 seconds	699.4	699.4	699.4	201.5
700 seconds	599.3	599.3	599.3	267.8
800 seconds	499.2	499.2	499.2	371.8
900 seconds	399.1	399.1	399.1	399.1
1,000 seconds	300.3	300.3	300.3	300.3
1,100 seconds	200.2	200.2	200.2	200.2
1,200 seconds	100.1	100.1	100.1	100.1
	F2	**F3**	**F4**	**F5**
0 seconds	262.6	232.7	219.7	209.3
100 seconds	189.8	167.7	135.2	128.7
200 seconds	133.9	115.7	57.2	65.0
300 seconds	89.7	75.4	39.0	29.9
400 seconds	79.3	65.0	28.6	20.8
500 seconds	120.9	92.3	52.0	33.8
600 seconds	214.5	153.4	113.1	93.6
700 seconds	279.5	196.3	157.3	133.9
800 seconds	388.7	271.7	236.6	221.0
900 seconds	399.1	382.2	356.2	348.4
1,000 seconds	300.3	300.3	300.3	300.3
1,100 seconds	200.2	200.2	200.2	200.2
1,200 seconds	100.1	100.1	100.1	100.1

Table 37: Ground floor – location of available time using measuring devices at 1.5m above the floor

Location entry time after ignition	**Time available before a 0.44% probability at location (seconds)**					
	A1	**A2**	**A3**	**A4**	**B1**	**B2**
0 seconds	41.6	107.9	182.0	247.0	41.6	122.2
100 seconds	29.9	88.4	149.5	202.8	32.5	110.5
200 seconds	27.3	75.4	119.6	187.2	31.2	92.3
300 seconds	26.0	66.3	117.0	189.8	27.3	85.8
400 seconds	27.3	75.4	135.2	224.9	29.9	88.4
500 seconds	28.6	81.9	152.1	258.7	31.2	96.2
600 seconds	28.6	107.9	232.7	386.1	32.5	119.6
700 seconds	35.1	153.4	374.4	599.3	42.9	161.2
800 seconds	42.9	179.4	462.8	499.2	45.5	192.4
900 seconds	49.4	210.6	399.1	399.1	52.0	228.8
1,000 seconds	58.5	258.7	300.3	300.3	61.1	292.5
1,100 seconds	72.8	200.2	200.2	200.2	75.4	200.2
1,200 seconds	85.8	100.1	100.1	100.1	85.8	100.1
	B3	**C1**	**C2**	**C3**	**C4**	**D1**
0 seconds	286.0	41.6	114.4	258.7	292.5	37.7
100 seconds	248.3	36.4	132.6	231.4	260.0	32.5
200 seconds	237.9	39.0	132.6	222.3	254.8	33.8
300 seconds	237.9	36.4	132.6	222.3	256.1	31.2
400 seconds	253.5	39.0	139.1	244.4	283.4	33.8
500 seconds	282.1	41.6	150.8	270.4	317.2	37.7
600 seconds	361.4	41.6	175.5	365.3	422.5	37.7
700 seconds	508.3	53.3	217.1	523.9	599.3	46.8
800 seconds	499.2	58.5	236.6	499.2	499.2	52.0
900 seconds	399.1	63.7	265.2	399.1	399.1	57.2
1,000 seconds	300.3	67.6	300.3	300.3	300.3	62.4
1,100 seconds	200.2	81.9	200.2	200.2	200.2	74.1
1,200 seconds	100.1	94.9	100.1	100.1	100.1	88.4

Table 38: Ground floor – location of available time using measuring devices at 2.0 m above the floor

Location entry time after ignition	**Time available before a 0.44% probability at location (seconds)**					
	A1	**A2**	**A3**	**A4**	**B1**	**B2**
0 seconds	36.4	101.4	165.1	193.7	37.7	119.6
100 seconds	23.4	78.0	137.8	163.8	26.0	109.2
200 seconds	20.8	65.0	111.8	133.9	26.0	89.7
300 seconds	18.2	57.2	107.9	132.6	20.8	83.2
400 seconds	19.5	66.3	123.5	162.5	23.4	85.8
500 seconds	22.1	70.2	137.8	192.4	23.4	93.6
600 seconds	23.4	96.2	210.6	289.9	27.3	115.7
700 seconds	29.9	143.0	336.7	473.2	39.0	159.9
800 seconds	37.7	172.9	416.0	499.2	41.6	195.0
900 seconds	45.5	208.0	399.1	399.1	49.4	237.9
1,000 seconds	57.2	265.2	300.3	300.3	58.5	300.3
1,100 seconds	76.7	200.2	200.2	200.2	78.0	200.2
1,200 seconds	85.8	100.1	100.1	100.1	96.2	100.1
	B3	**C1**	**C2**	**C3**	**C4**	**D1**
0 seconds	262.6	37.7	107.9	226.2	253.5	35.1
100 seconds	226.2	32.5	130.0	205.4	223.6	28.6
200 seconds	214.5	39.0	133.9	189.8	210.6	31.2
300 seconds	215.8	35.1	133.9	189.8	211.9	29.9
400 seconds	228.8	37.7	141.7	209.3	235.3	32.5
500 seconds	253.5	39.0	153.4	231.4	262.6	33.8
600 seconds	322.4	41.6	182.0	314.6	351.0	36.4
700 seconds	443.3	54.6	230.1	458.9	509.6	46.8
800 seconds	499.2	58.5	252.2	499.2	499.2	52.0
900 seconds	399.1	65.0	283.4	399.1	399.1	57.2
1,000 seconds	300.3	70.2	300.3	300.3	300.3	63.7
1,100 seconds	200.2	89.7	200.2	200.2	200.2	80.6
1,200 seconds	100.1	100.1	100.1	100.1	100.1	100.1

3.1.2 Results of heat flux exposure if PPE is removed

Using the heat flux from the devices that recorded the highest average heat flux in Table 19 to Table 22, the heat flux exposure over time has been provided for the first floor and ground floor. Using Equation 17 with Table 7, the heat flux that will result in the critical heat flux being exceeded with sufficient probability is included in the below graphs (refer to section 1.5.4 Probability of injury).

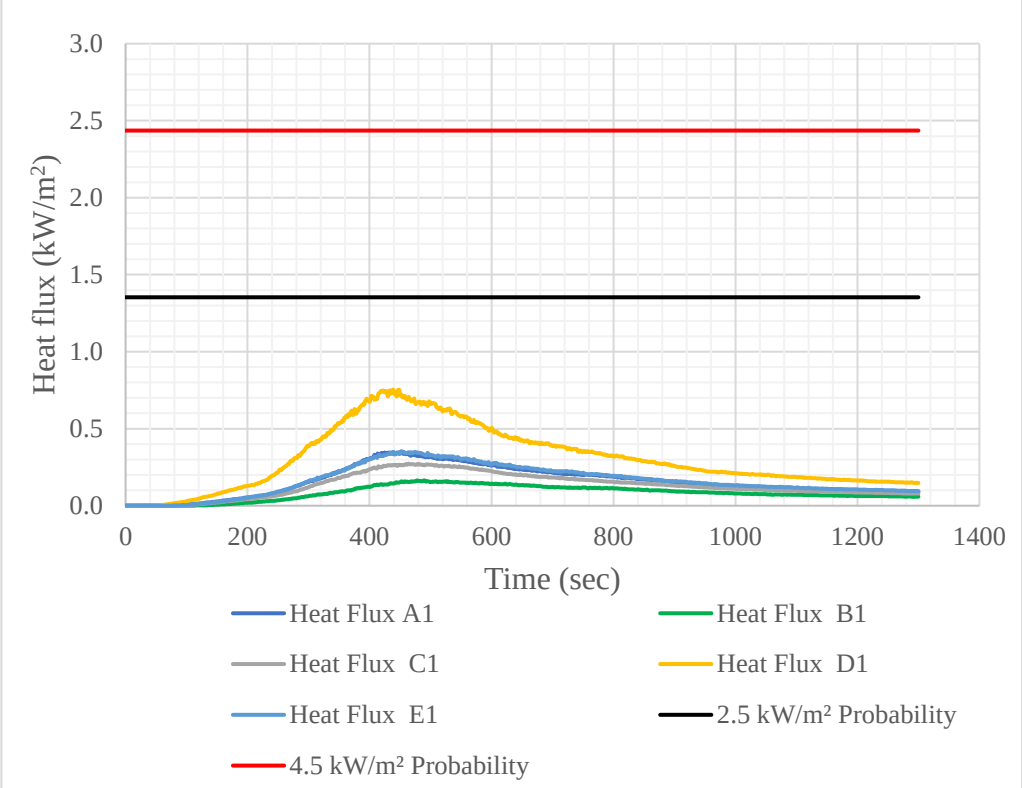

Figure 36: First floor – heat flux exposure in Rooms A-E

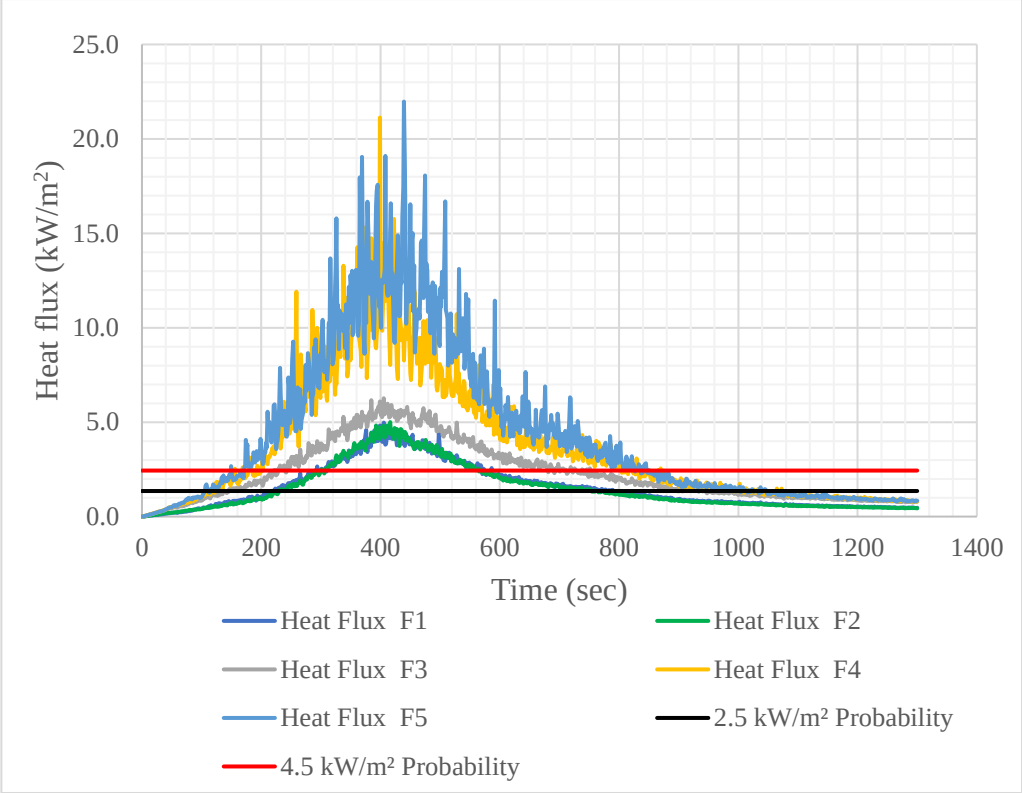

Figure 37: First floor – heat flux exposure in Room F (burn room)

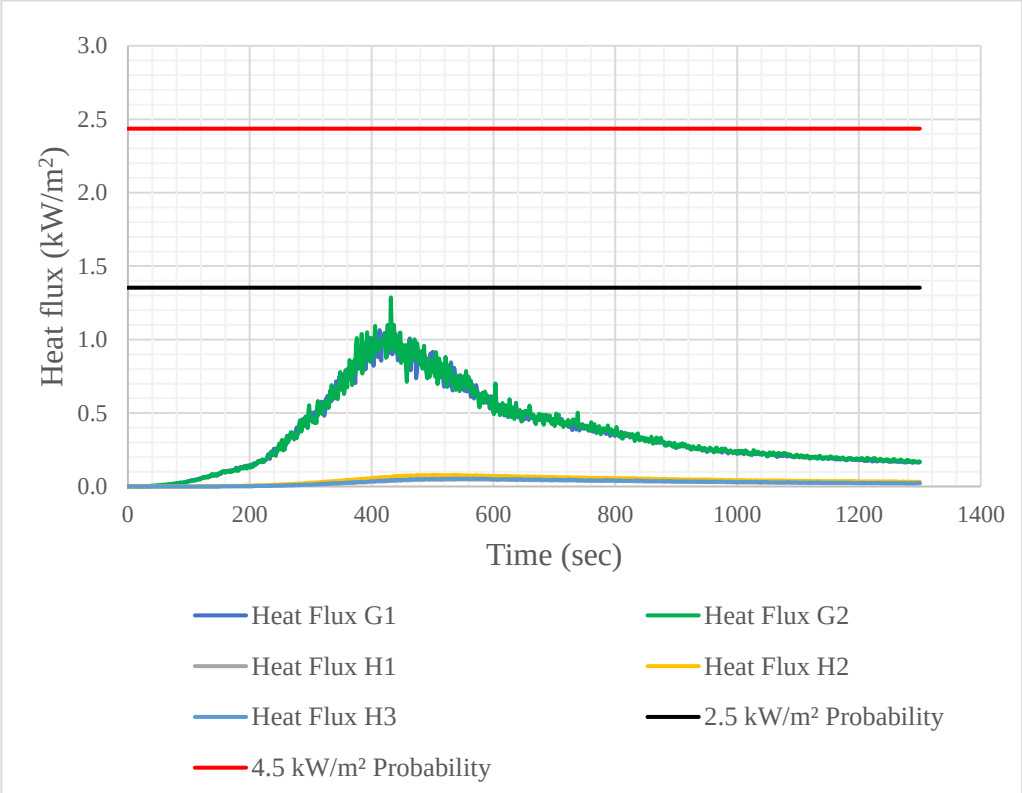

Figure 38: First floor – heat flux exposure in Rooms G-H

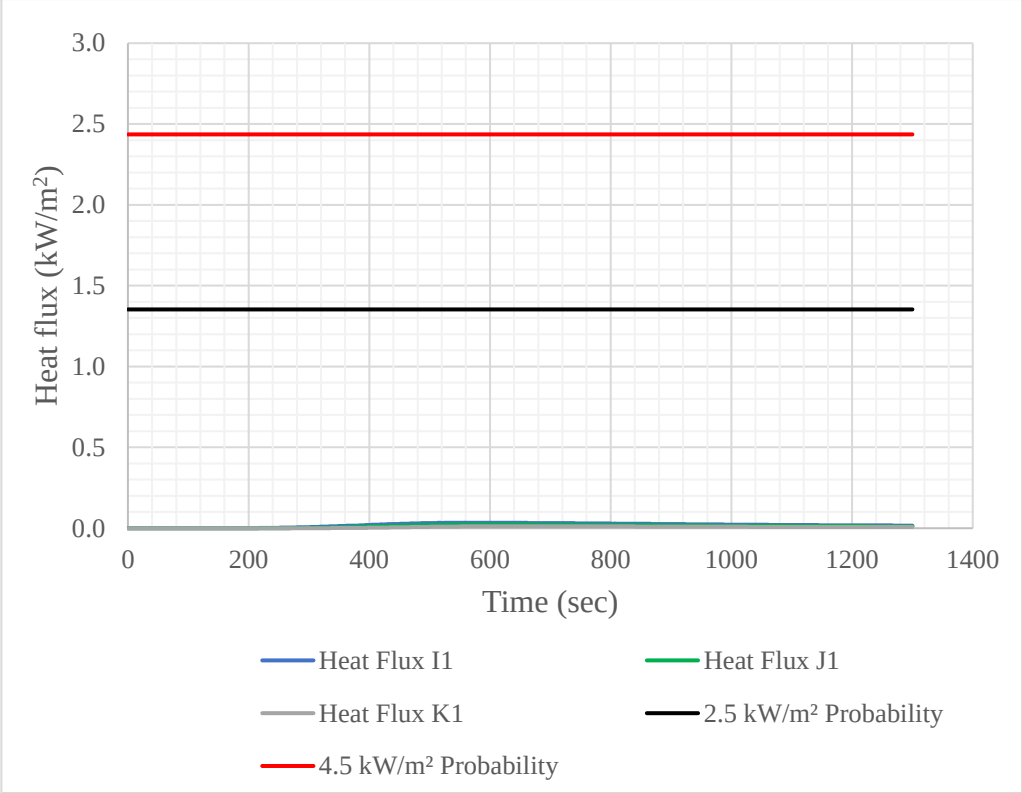

Figure 39: First floor – heat flux exposure in Rooms I-K

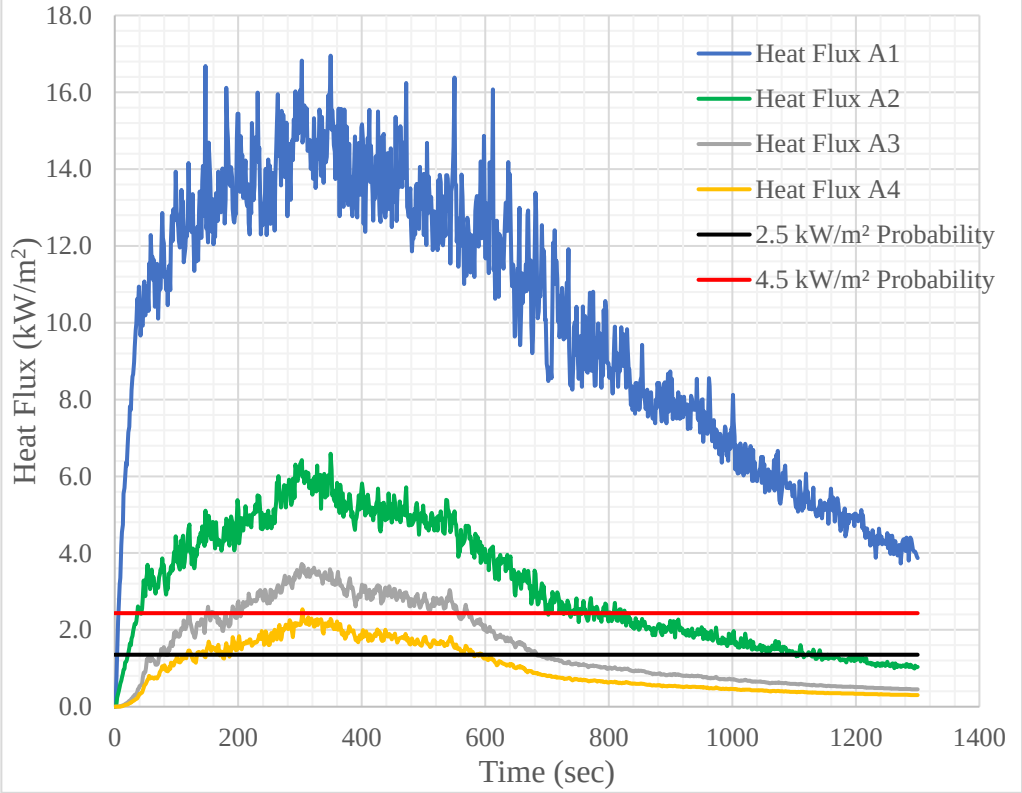

Figure 40: Ground floor – heat flux exposure in Location A

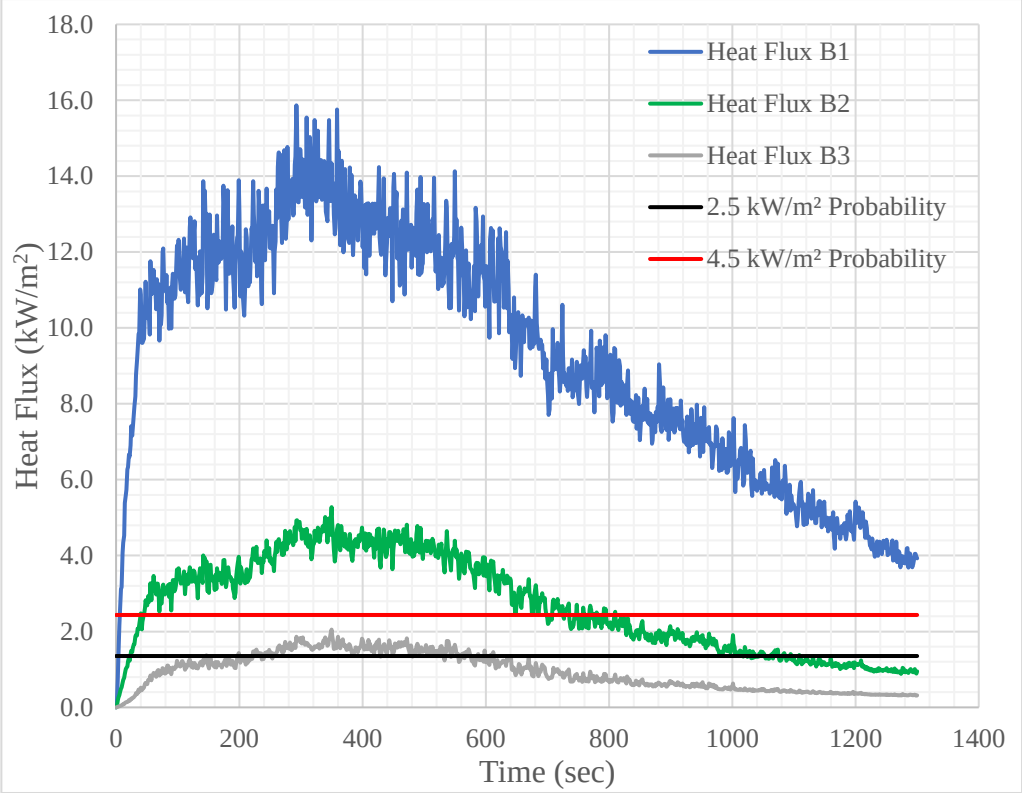

Figure 41: Ground floor – heat flux exposure in Location B

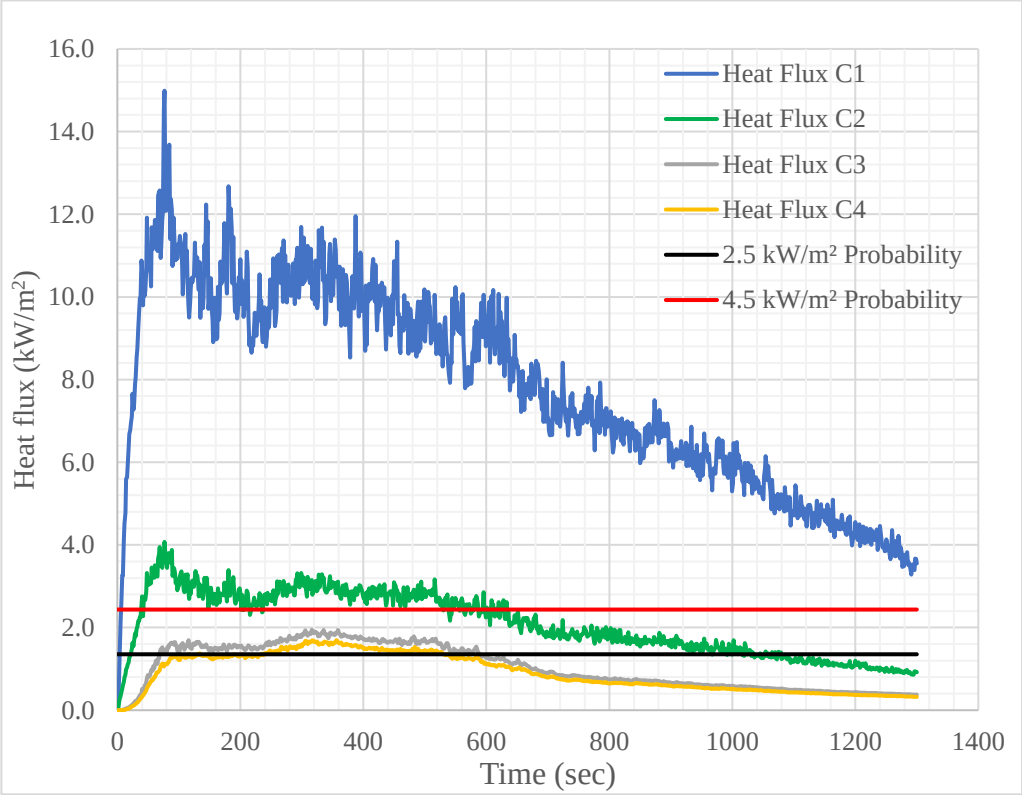

Figure 42: Ground floor – heat flux exposure in Location C

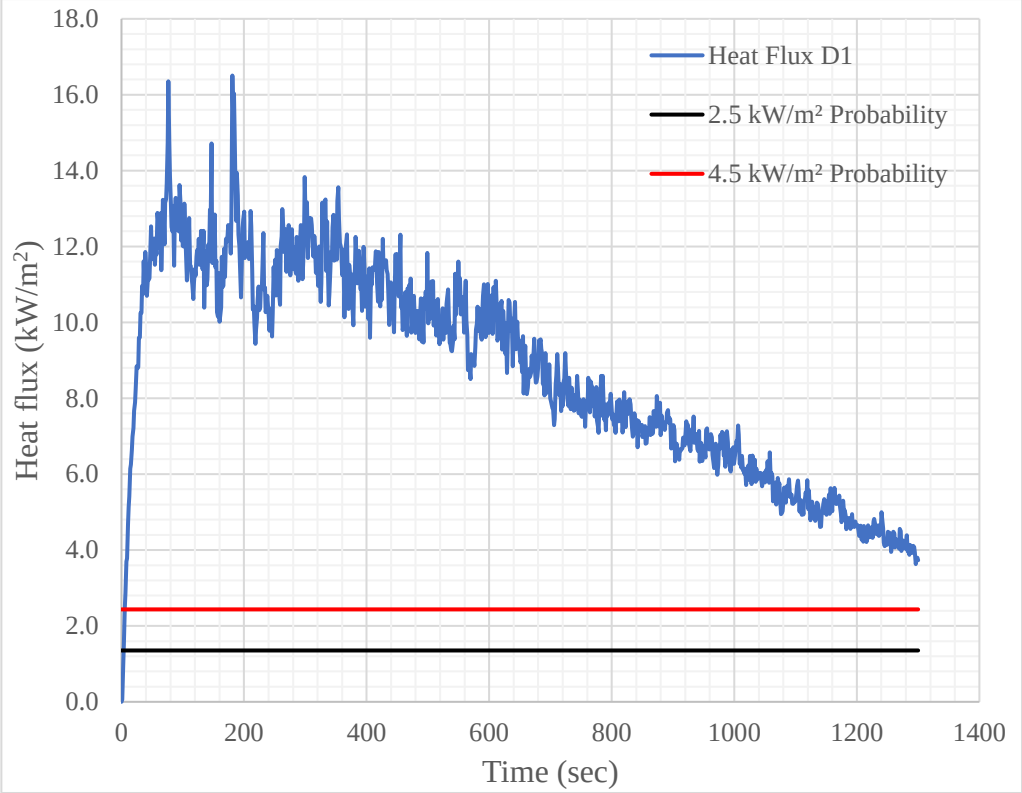

Figure 43: Ground floor – heat flux exposure in Location D

3.2 Results for gas temperature

The gas temperature has been measured on the first floor and on the ground floor. At 1.5 m above the ground, the temperature results are shown for PPE that has been removed and for PPE that has not been removed (refer to section 2.5 Measuring output). At 2.0 m above the ground, the temperature results are for a firefighter standing up straight with PPE (refer to section 2.5 Measuring output). Using Equation 17 with Table 7, the temperature that will result in the critical temperature being exceeded with sufficient probability is included in the below graphs (refer to section 1.5.4 Probability of injury). Measuring device positions are shown in Figure 33 and Figure 34 (refer to section 2.5 Measuring output).

3.2.1 Results for gas temperature at 1.5 m above ground

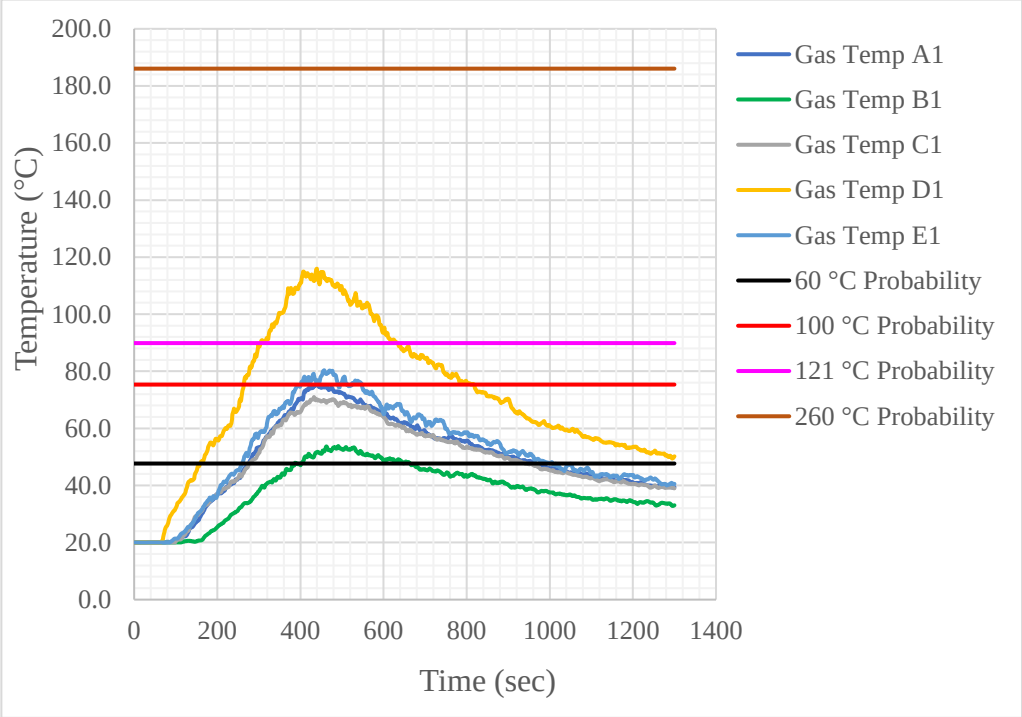

Figure 44: First floor – temperature at 1.5 m in Rooms A-E

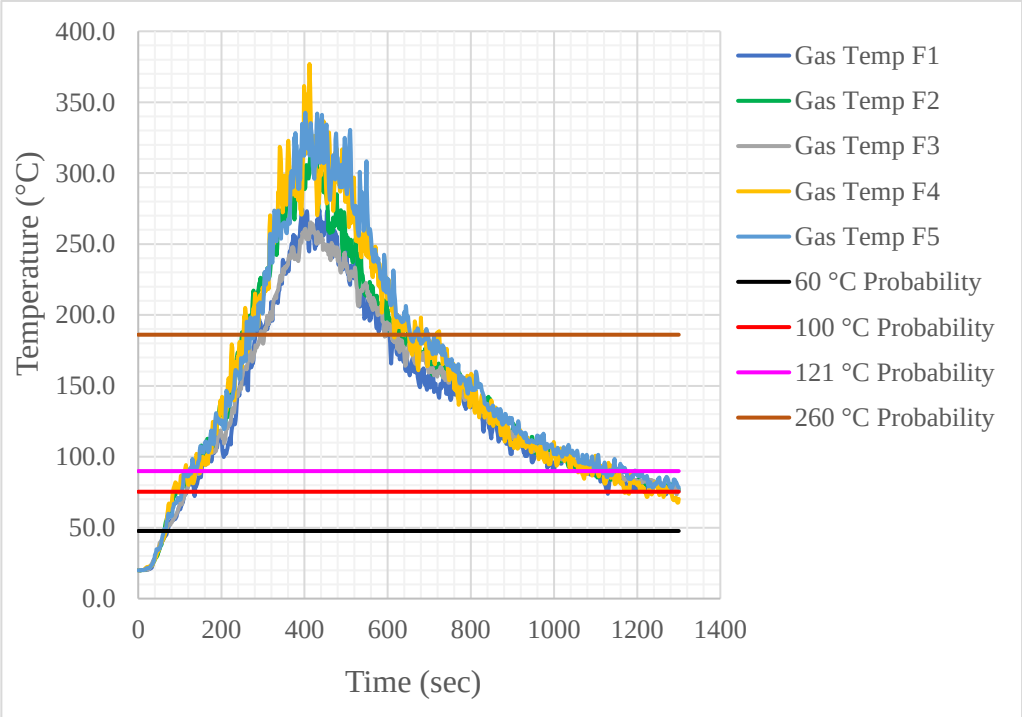

Figure 45: First floor – temperature at 1.5 m in Room F (burn room)

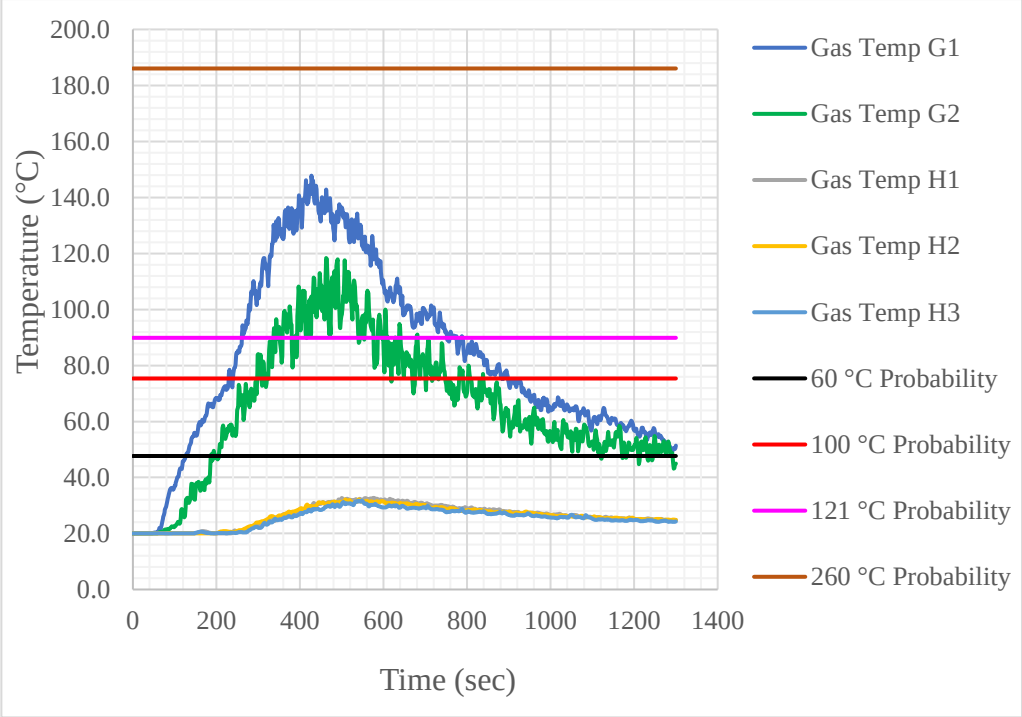

Figure 46: First floor – temperature at 1.5 m in Rooms G-H

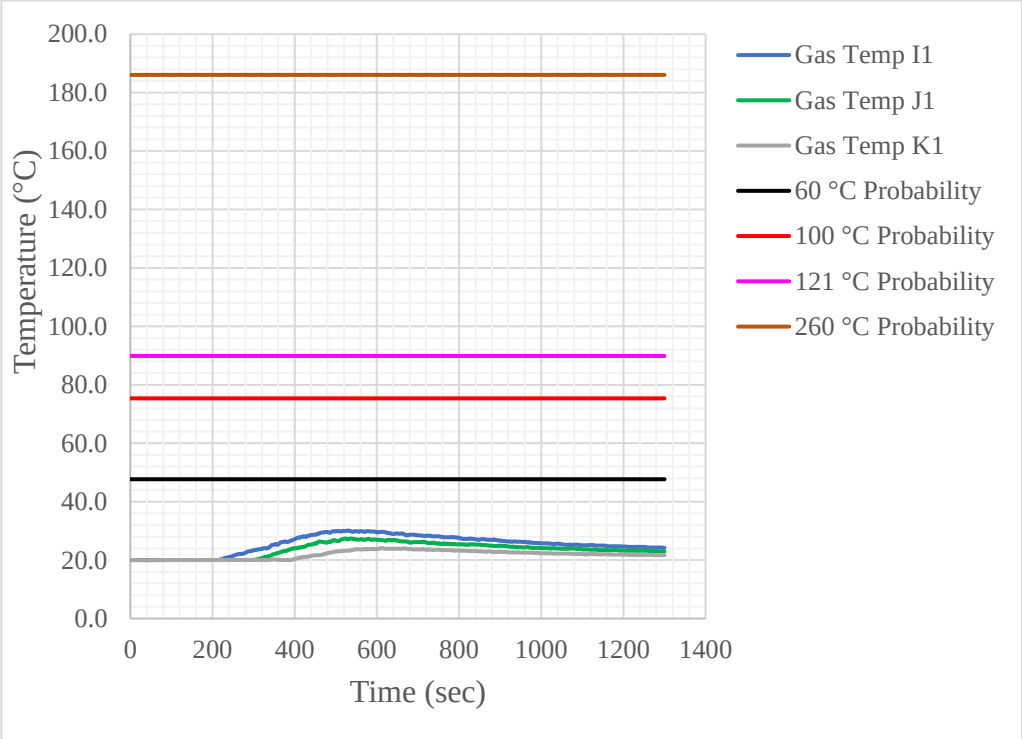

Figure 47: First floor – temperature at 1.5 m in Rooms I-K

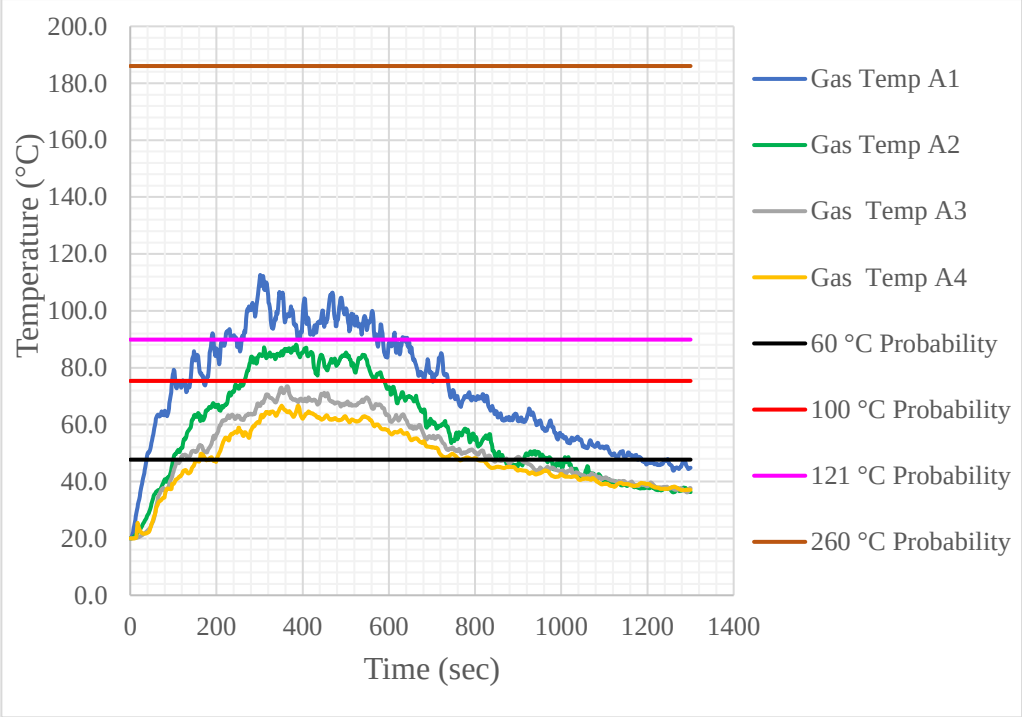

Figure 48: Ground floor – temperature at 1.5 m in Location A

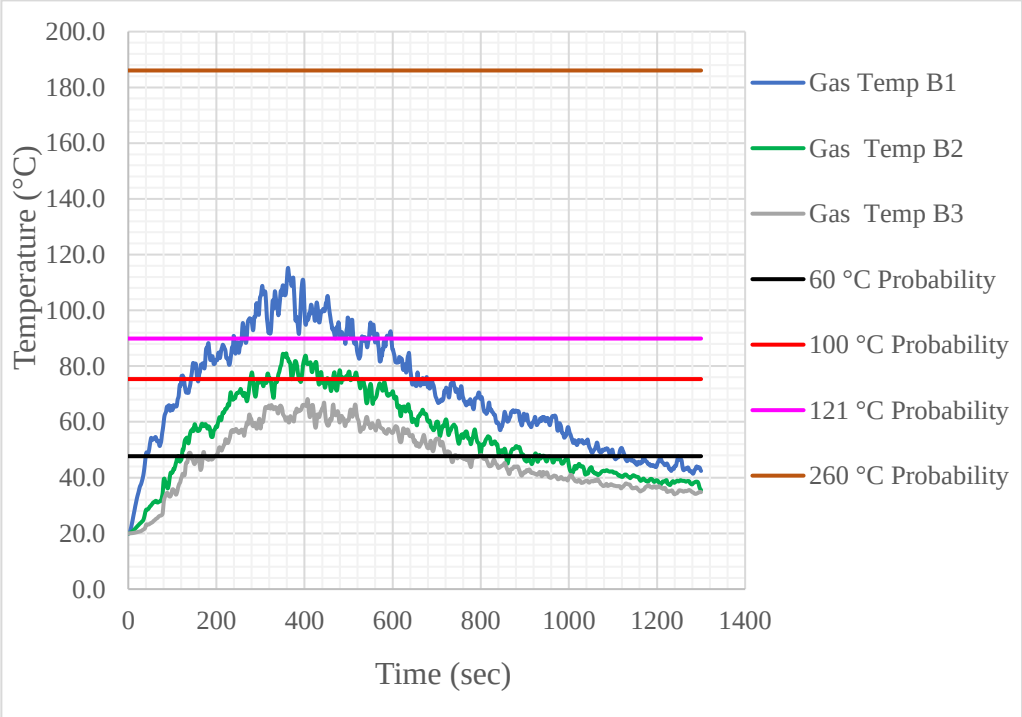

Figure 49: Ground floor – temperature at 1.5 m in Location B

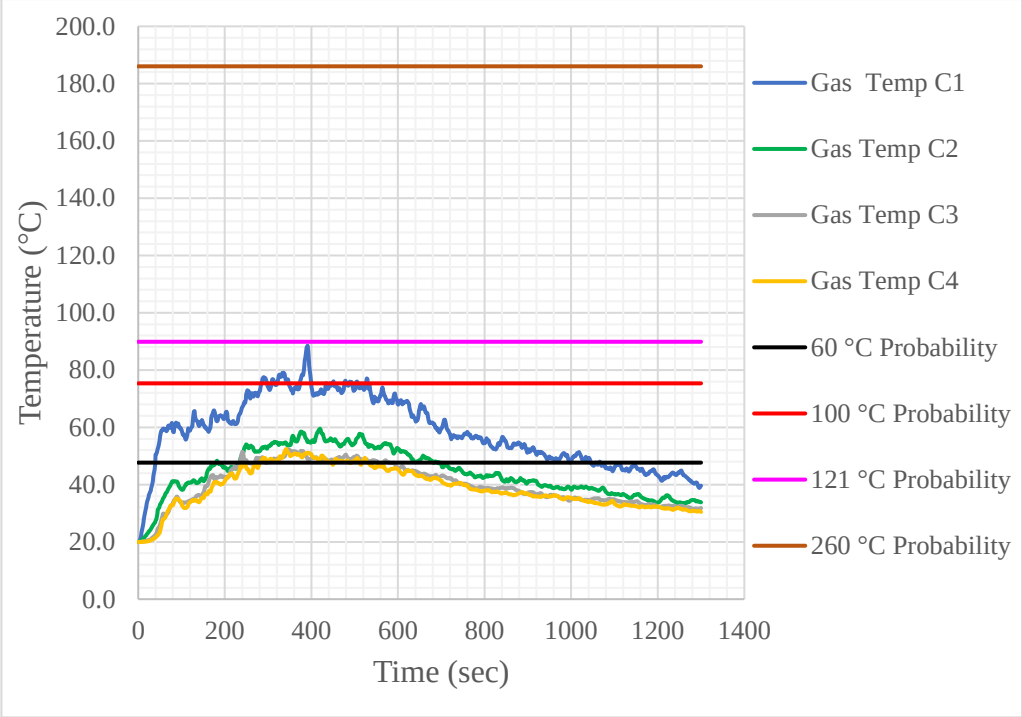

Figure 50: Ground floor – temperature at 1.5 m in Location C

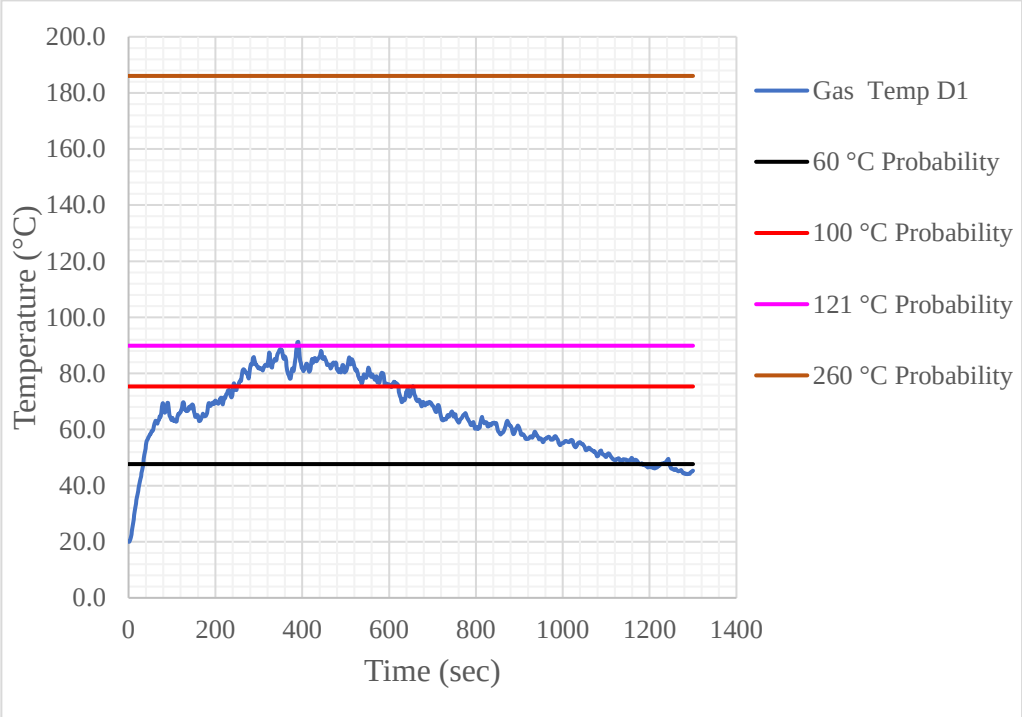

Figure 51: Ground floor – temperature at 1.5 m in Location D

3.2.2 Results for gas temperature at 2.0 m above ground

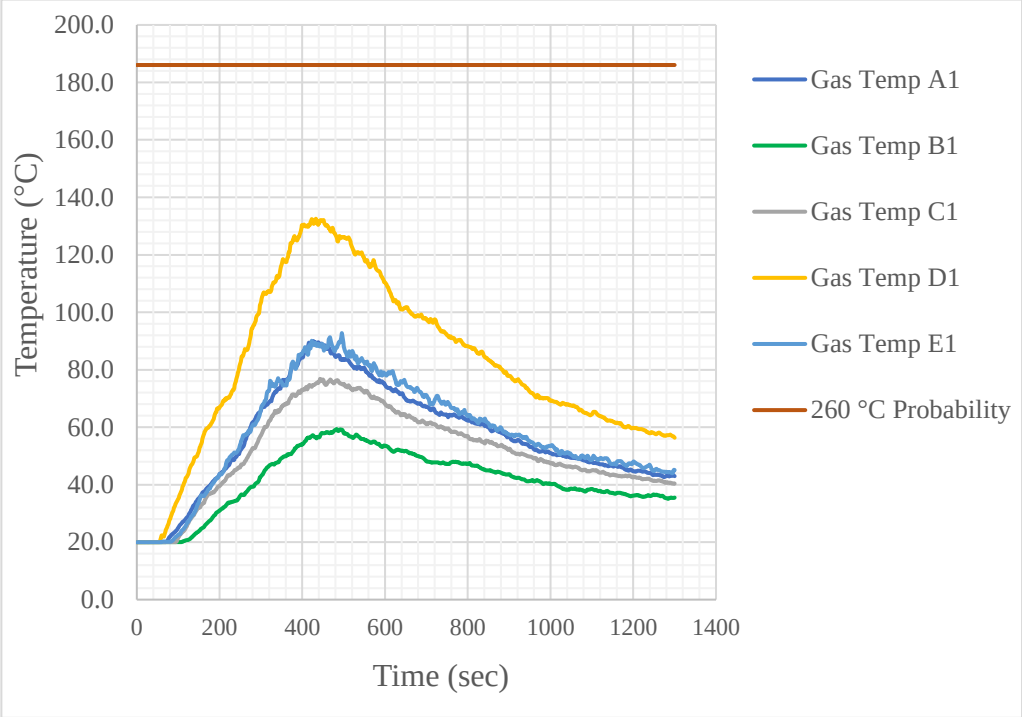

Figure 52: First floor – temperature at 2.0 m in Rooms A-E

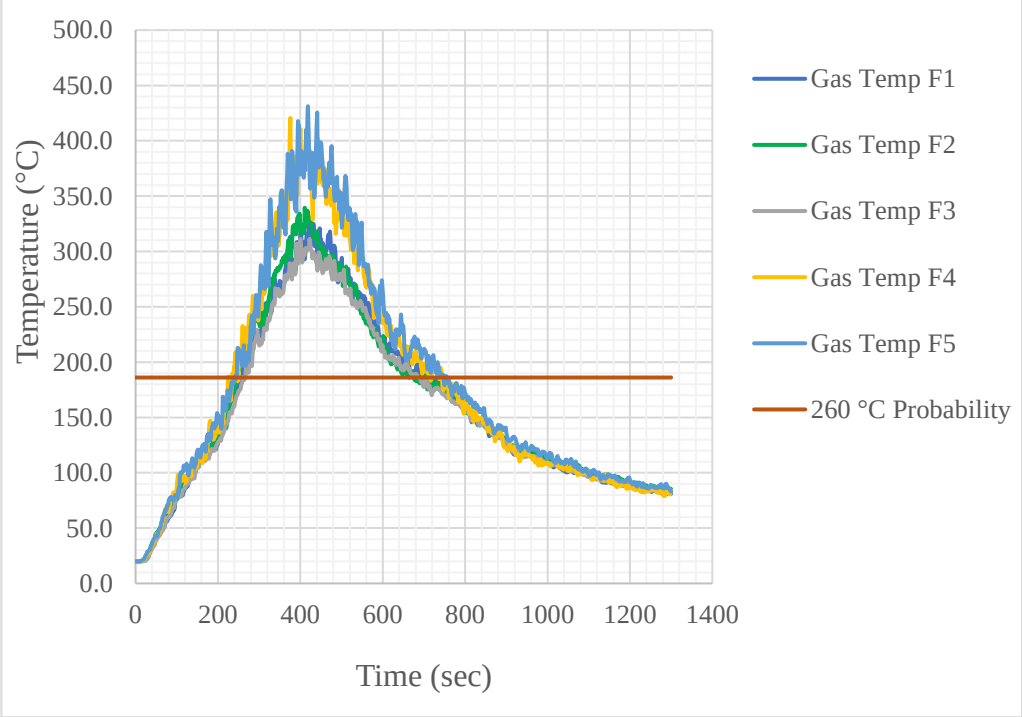

Figure 53: First floor – temperature at 2.0 m in Room F (burn room)

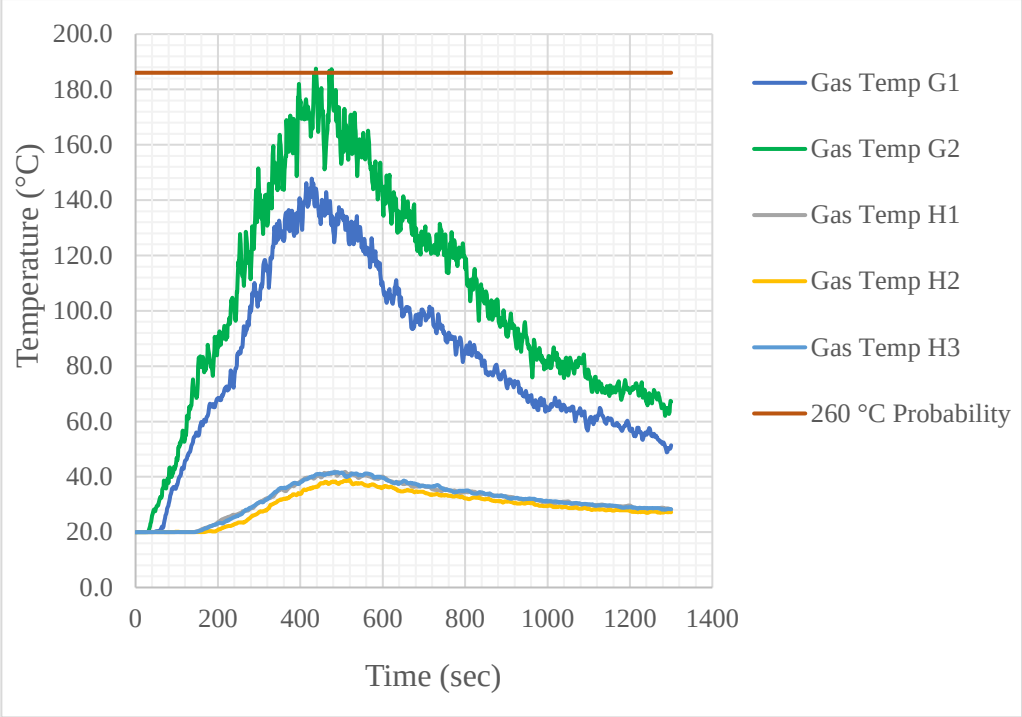

Figure 54: First floor – temperature at 2.0 m in Rooms G-H

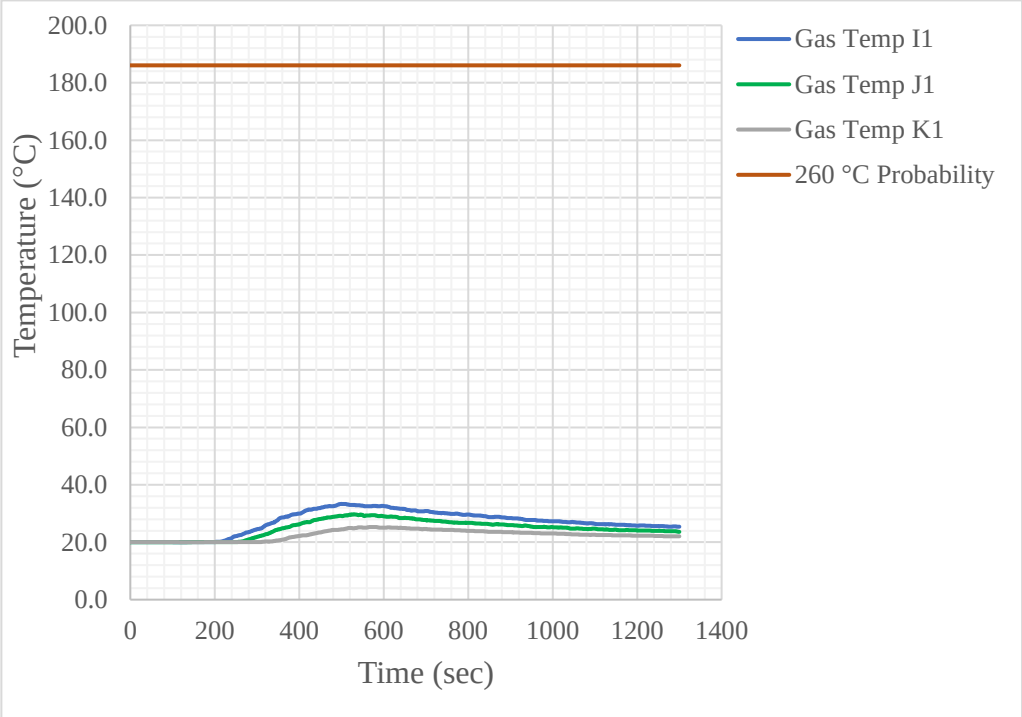

Figure 55: First floor – temperature at 2.0 m in Rooms I-K

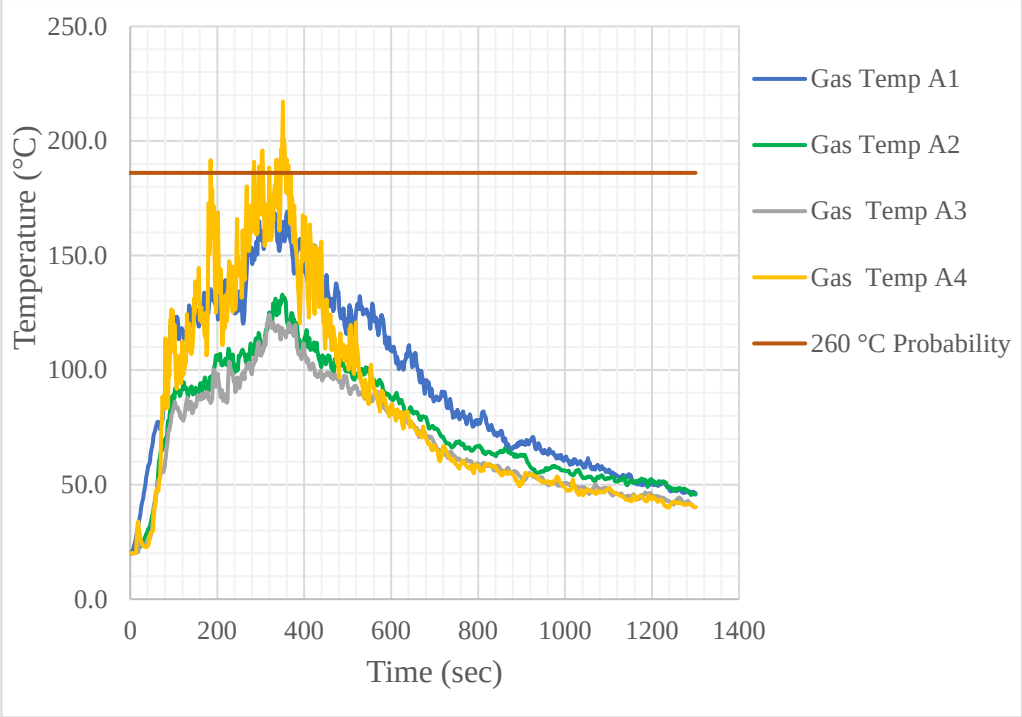

Figure 56: Ground floor – temperature at 2.0 m in Location A

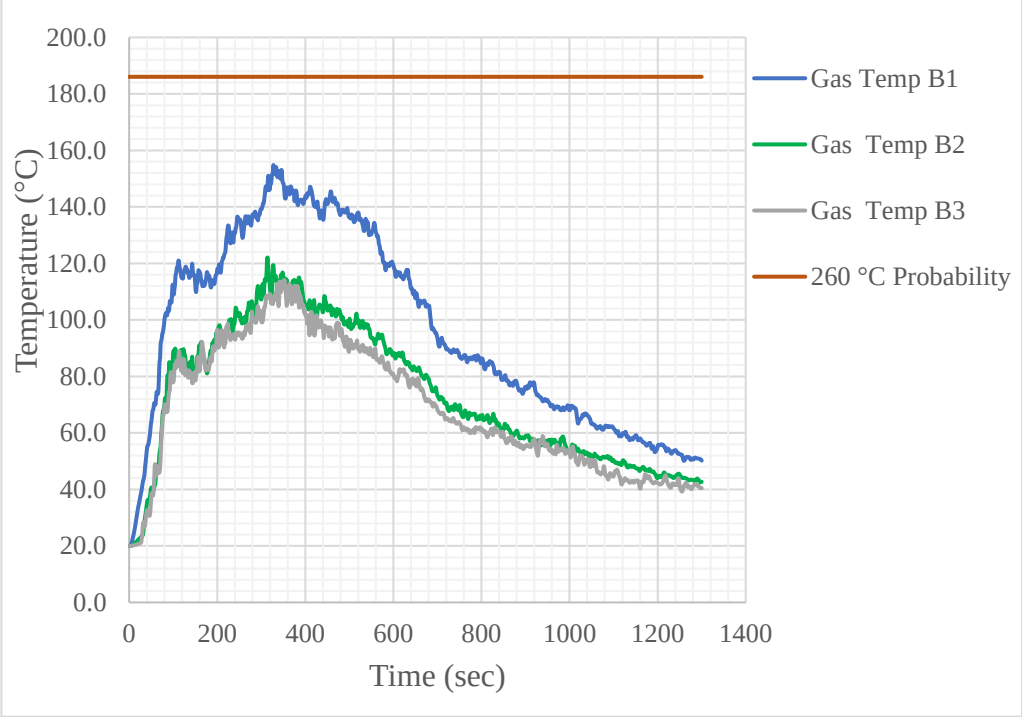

Figure 57: Ground floor – temperature at 2.0 m in Location B

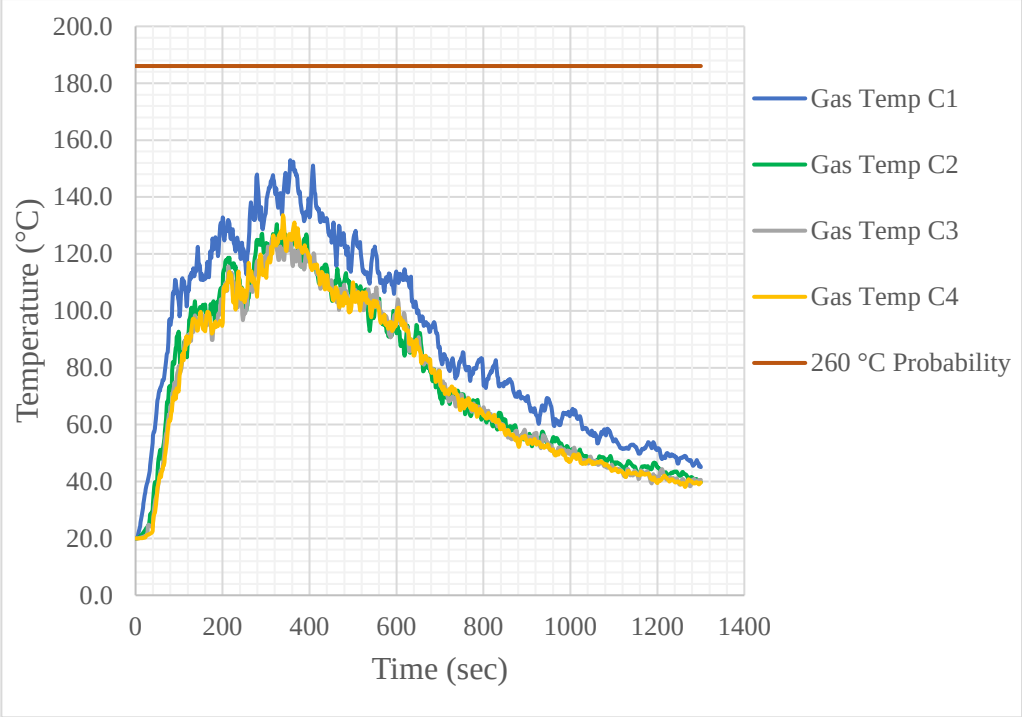

Figure 58: Ground floor – temperature at 2.0 m in Location C

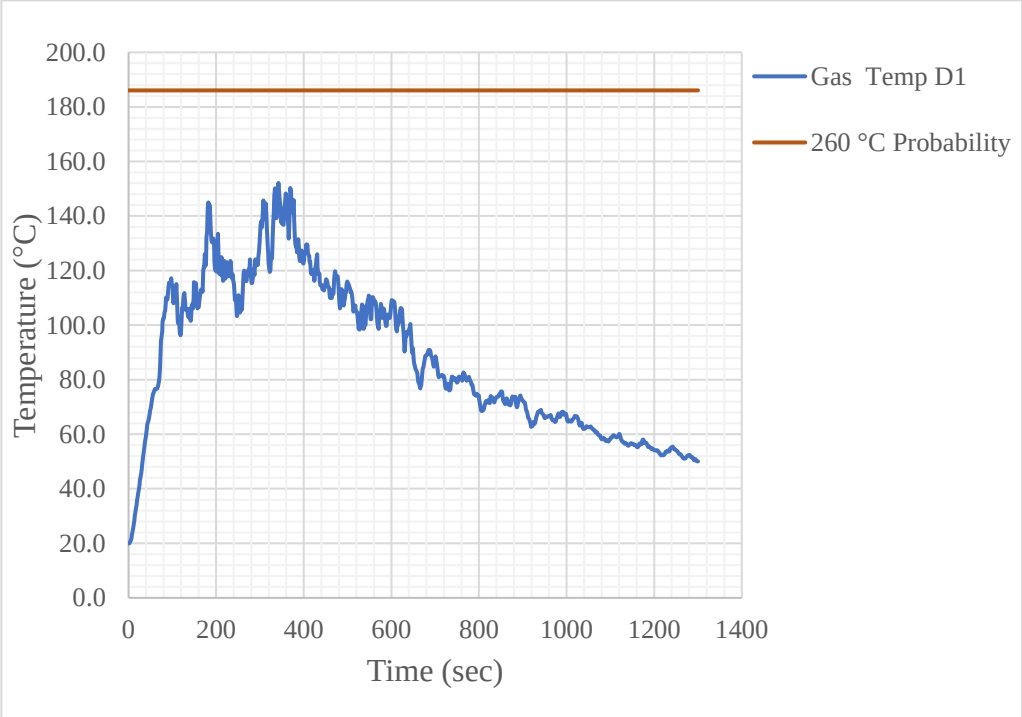

Figure 59: Ground floor – temperature at 2.0 m in Location D

3.3 Results of toxicity

The FED has been measured on the first floor and on the ground floor. At 1.5 m above the ground, the FED results are shown for PPE that has been removed (refer to section 2.5 Measuring output).

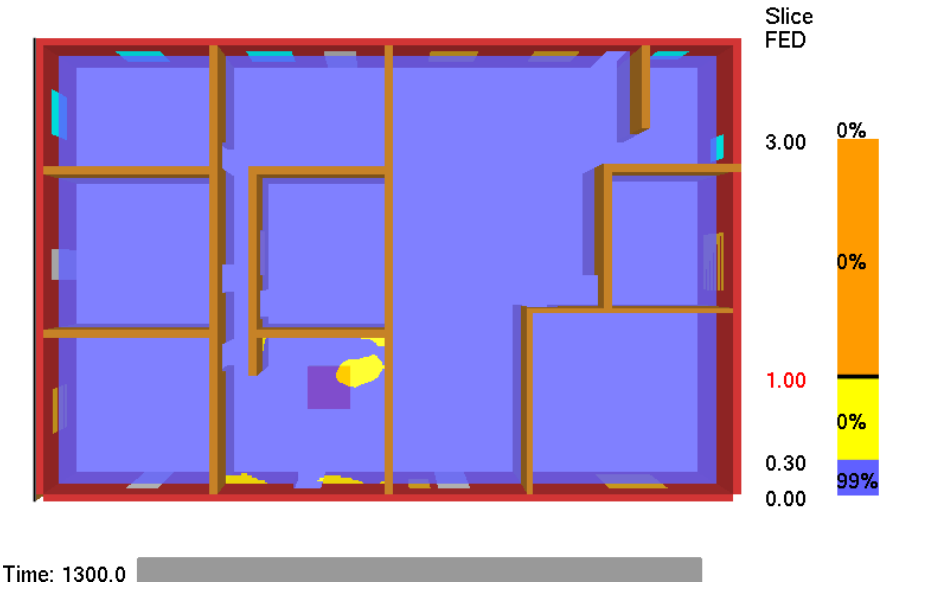

Figure 60: First floor – FED at 1.5 m

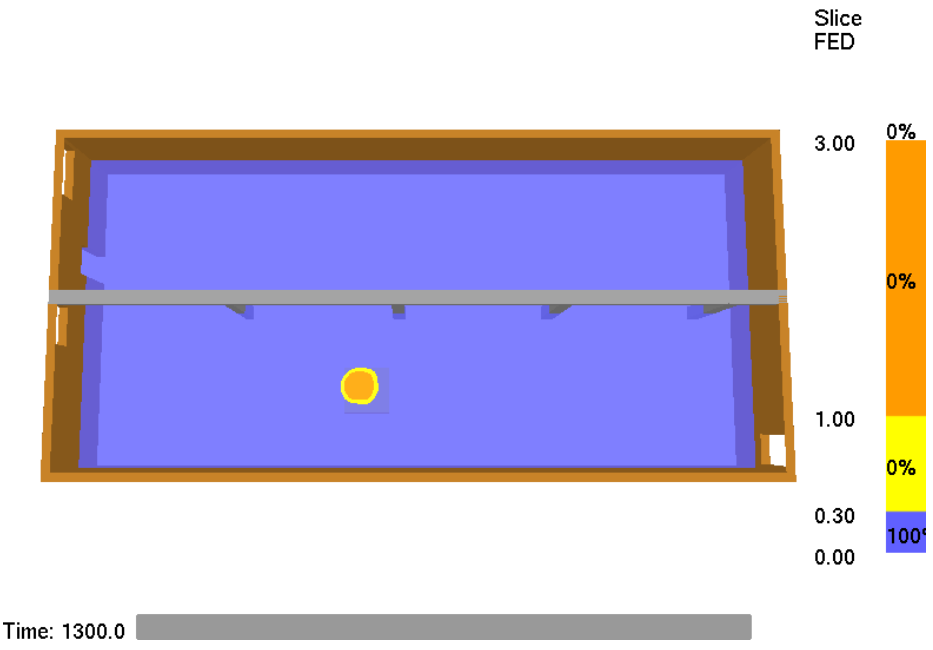

Figure 61: Ground floor – FED at 1.5 m

3.4 Results for the surface temperature of the structure

Surface temperatures on the structure have been investigated and those surfaces with peak temperatures in excess of 177 °C have been recorded with the use of the animated boundary surface temperature measurements. These animated boundary surfaces have been taken out of FDS and rescaled in CAD so that the 177 °C area can be measured. The probability of the temperatures on the colour bar being able to exceed 177 °C have also been included. The measurements of the lengths shown below is in meters and have been round up to the nearest 100 mm. The location of the below sections is provided in Figure 33 and Figure 34 (refer to section 2.5 Measuring output).

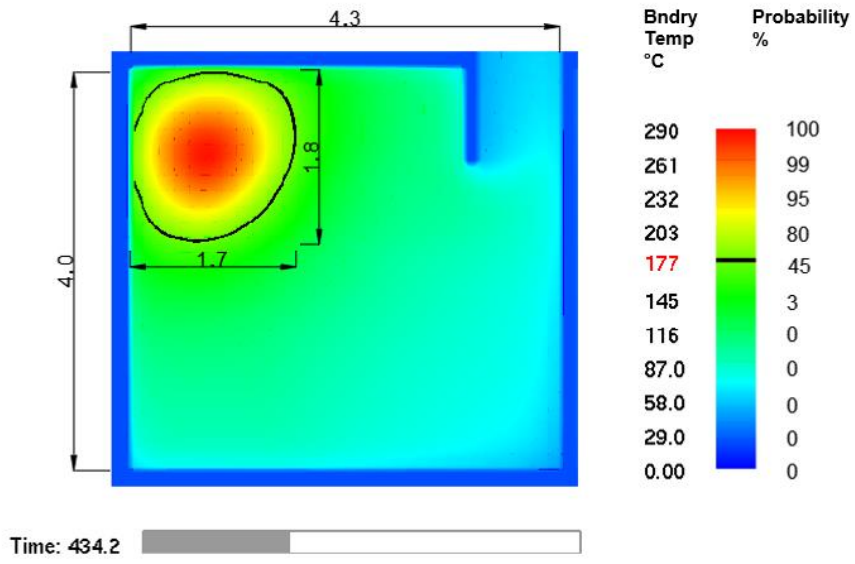

Figure 62: First floor – peak surface temperature of ceiling

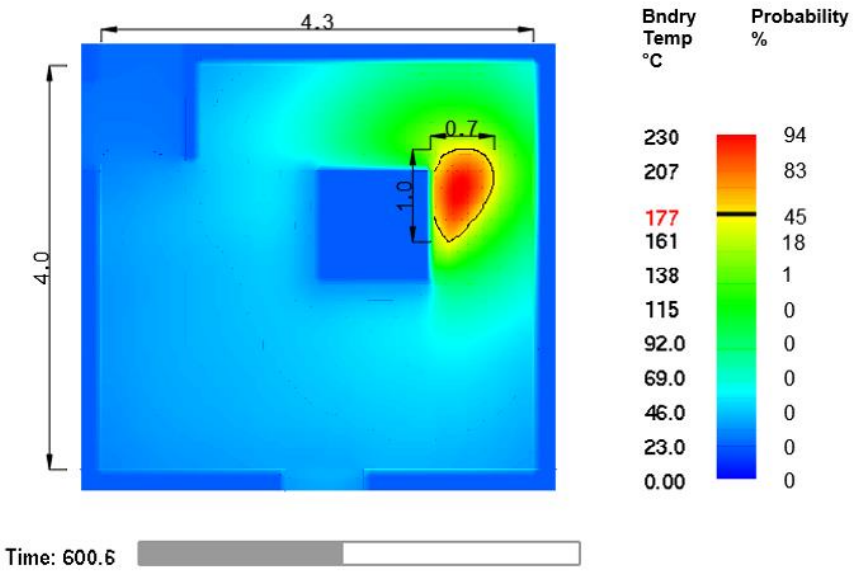

Figure 63: First floor – peak surface temperature of floor

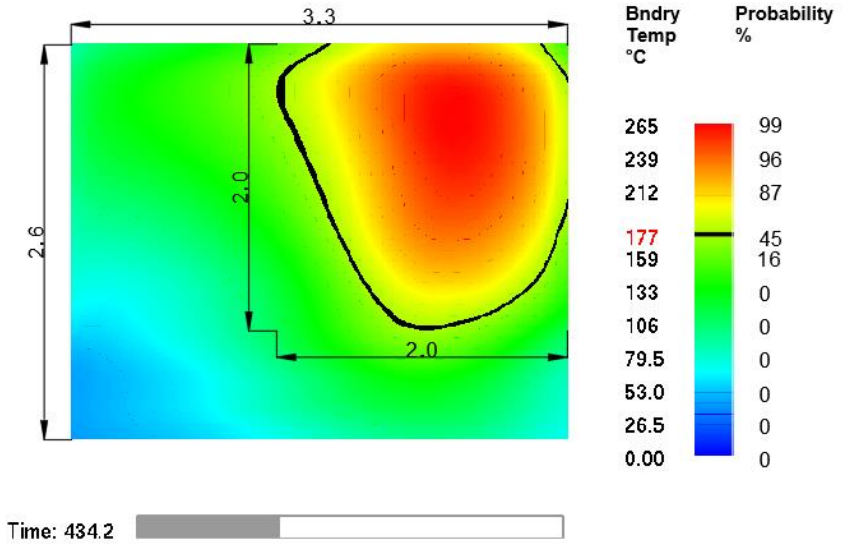

Figure 64: First floor – peak surface temperature of wall (section A-A)

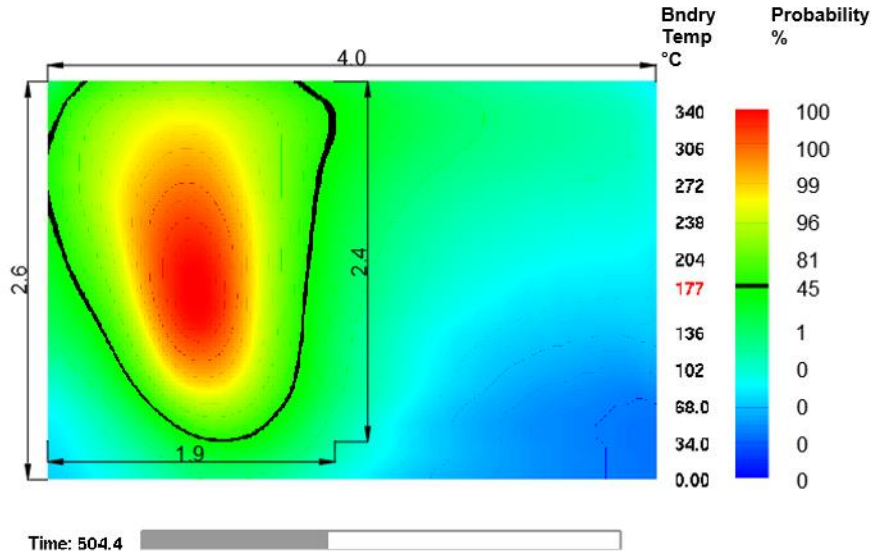

Figure 65: First floor – peak surface temperature of wall (section B-B)

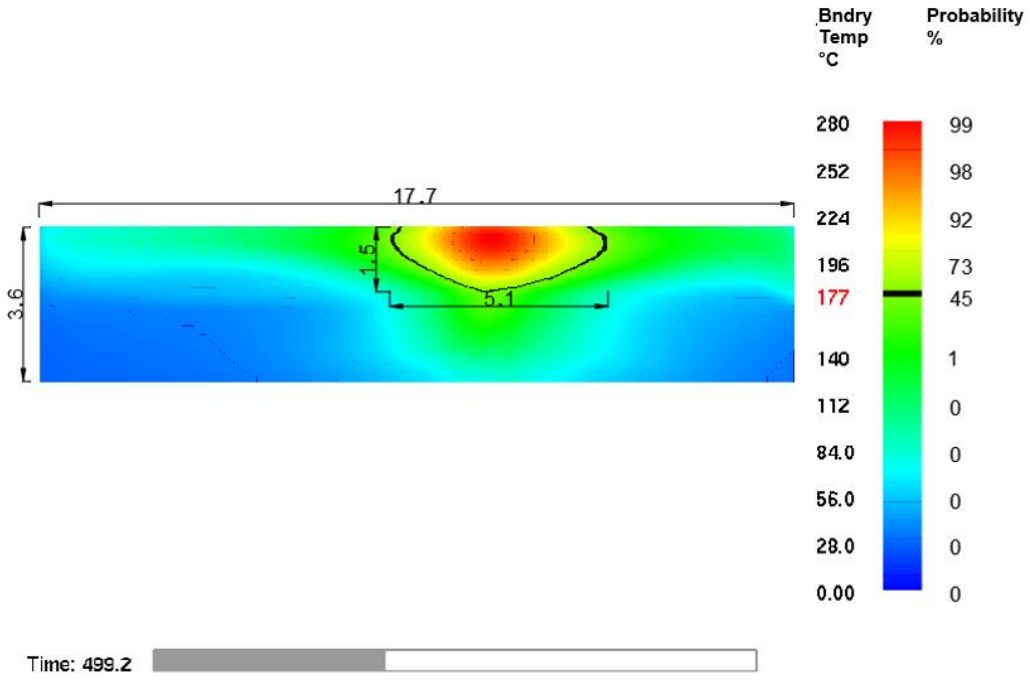

Figure 66: Ground floor – peak surface temperature of wall (section A-A)

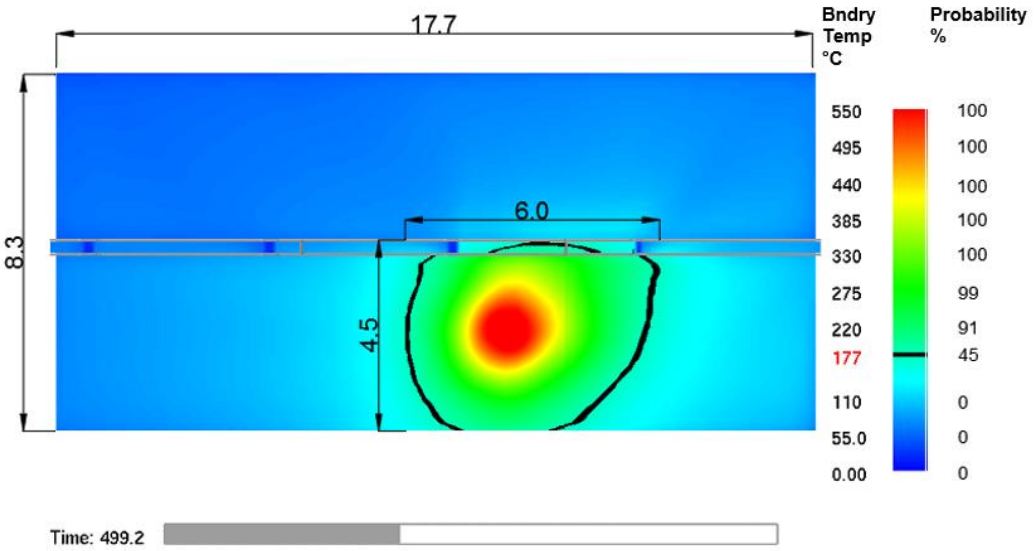

Figure 67: Ground floor – peak surface temperature of ceiling

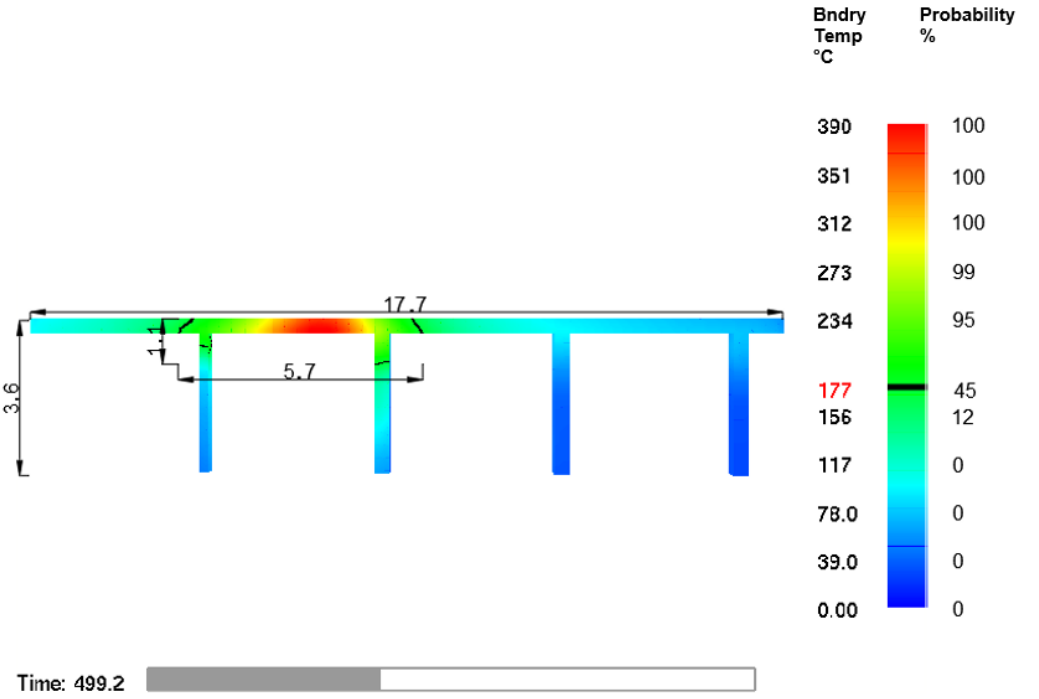

Figure 68: Ground floor – peak surface temperature of the columns (section B-B)

3.5 Discussion of fire related hazards for trainee firefighters on the first floor

3.5.1 Outcome if no mistakes are made during live fire training

It was found that in the burn room, most of the thermal radiation is received horizontally, directly from the fire source (refer to Table 19). In the rooms surrounding the burn room, most of the thermal radiation is received from the hot gas layer forming along the underside of the ceiling.

At 1.5 m above floor level, the amount of thermal radiation received in the rooms surrounding the burn room on the first floor is minor. There is no recorded measurement exceeding a TPP of 17.5 for the firefighter's clothing (refer to Table 23). There is a sufficient probability in Room D and Room G to receive a TPP above 17.5 for the first 600 seconds after the fire's ignition (refer to Table 29), therefore the time spent in Room G and Room D must be limited as per Table 35.

The amount of thermal radiation received in the burn room is found to be considerably more than in the surrounding rooms. In Table 30 it is noted that there is sufficient probability to limit the time spent at the entrances into the burn room for the first 900 seconds. If the firefighter moves further into the burn room the time must be limited during the first 1,000 seconds after the fire's ignition. The limited time should be limited as per Table 35.

There is sufficient probability to limit the available time to below 60 seconds in the burn room (refer to Table 35). These areas are therefore not suitable for search and rescue training (refer to section 1.5.3 Selecting the appropriate TPP value).

The gas temperatures in the rooms surrounding the burn room is below the critical gas temperature (refer to Figure 44, Figure 46, and Figure 47). The probability of the recorded temperatures being sufficient to exceed the critical gas temperature is not present for the entire duration of the simulation. In the burn room there is sufficient gas temperatures recorded to require the burn room to be avoided from 200 seconds to 750 seconds after the fire's ignition (refer to Figure 45).

3.5.2 Outcome if mistakes are made during training

Standing up straight

At 2.0 m above the floor level in the burn room, the highest average thermal radiation was measured in the horizontal orientation (refer to Table 20). For the rooms surrounding the burn room, except Room G, the devices on the horizontal axis measured a higher average thermal radiation than those on the vertical axis.

At 2.0 m above floor level, the amount of thermal radiation received in the rooms surrounding the burn room on the first floor was minor. There is no recorded measurement exceeding a 17.5 TPP value (refer to Table 25); however, there is sufficient probability in Room D and Room G to receive a TPP value above 17.5 for the first 600 seconds after the fire's ignition (refer to Table 31). This will

therefore require the time spent in Room G and Room D to be limited as per Table 36.

In the burn room there is sufficient probability to limit the time spent at the entrances into the burn room for the first 900 seconds as per Table 32. If the firefighter moves further into the burn room the time must be limited during the first 1,000 seconds after the fire's ignition. The time should be limited as per Table 36.

There is sufficient probability, at 2.0 m above floor level, to limit the available time to below 60 seconds in the burn room (refer to Table 36). These areas are not suitable for search and rescue training (refer to section 1.5.3 Selecting the appropriate TPP value).

At 2.0 m above the floor, there is sufficient probability for the 260°C critical gas temperature to be exceeded in Room G, location 2. This location should be avoided between 400 seconds and 500 seconds after the fire's ignition (refer to Figure 46). In the burn room there is sufficient probability for it to be avoided between 200 seconds and 800 seconds (refer to Figure 45).

No PPE

Firefighters without their BA are able to receive burns to the respiratory tract in all of the rooms except for Rooms H, I, J, and K (refer to Figure 44 - Figure 47). Firefighters without their BA mask in Rooms B and C may be able to escape burns

to the respiratory tract as these rooms are below the probability for a gas temperature of 100 °C. In the remaining rooms, the gas temperature is in excess of 100 °C (refer to Figure 44 - Figure 47). This means that burns to the repository tract can be expected after breathing in the gas.

Firefighters without their BA, are not expected to succumb to the fire's toxic combustion by-products (refer to Figure 60).

Should an item of protective clothing be removed, and skin is exposed, then burns can be expected in rooms D, F, and G due to there being sufficient probability for the critical gas temperature to be exceeded (refer to Figure 44 - Figure 47). Burns to exposed skin from heat flux exposure are only expected in the burn room (refer to Figure 36 - Figure 39).

3.5.3 Stability of live fire training structure

To maintain the stability of the structure and maximize the life of the structure, it has been found that there are four surfaces that require additional thermal protection against elevated temperatures (refer to Figure 62-Figure 65). These areas received temperatures in excess of 177 °C. The additional protection required for the floor requires protection up to 0.7 m from the edge of the fire source. It is thought necessary to protect 0.7 m right around and under the fire source, even though Figure 63 shows just to one side of the fire source needing protection. This is because the fire source is simulated as a vent placed on top of an inert obstruction. This inert obstruction blocks some of the thermal radiation, which would normally

transmit to the ground on which the fire is located. This should be considered when interpreting Figure 63 and is why the floor protection should be extended fully around the fire source.

3.6 Discussion of fire related hazards for trainee firefighters on the ground floor

3.6.1 Outcome if no mistakes are made during live fire training

The appropriate orientation of the heat flux measuring devices have been investigated (refer to Table 21). For Groups A and C, it was found that most of the heat flux is received directly from the fire source, between 3.5 m and 5.5 m from the fire's centre. From 5.5 m to 7.5 m, most of the heat flux received in Groups A and C is from the hot gas layer. The whole of Group B and D received more heat flux from the fire source than from the hot gas layer. This information was then used to determine which results are to be used.

Right around the fire, at 1.5 m from the fire's centre, there is sufficient probability to receive a TPP value above 17.5 for the whole of the simulation (refer to Table 33) . Also, from 3.5 m away from the fire, all of the locations around the fire are capable of receiving a TPP value above 17.5. Later in the simulation, the probability of exceeding a TPP value over 17.5 is insufficient in these locations. The time spent at locations where there is sufficient probability to receive a TPP value above 17.5, will have to be limited according to Table 37.

There is sufficient probability to limit the available time to below 60 seconds in locations close to the fire (refer to Table 37). These area will therefore not be suitbale for search and rescue training (refer to section 1.5.3 Selecting the appropriate TPP value).

At 1.5 m above the floor, the gas temperatures on the ground floor is below the critical gas temperature (refer to Figure 48 - Figure 51). There is an insufficient probability for the recorded temperatures to exceed the critical gas temperature for the entire duration of the simulation.

3.6.2 Outcome if mistakes are made during training

Standing up straight

The appropriate orientation of the heat flux measuring devices have been investigated (refer to Table 22). It was found that the device orientation used at 1.5 m on the ground floor, is also appropriate for the device orientation at 2.0 m.

At 2.0 m above the floor, there is sufficient probability to receive a TPP value above 17.5 at 1.5 m from the fire's centre for the whole of the simulation (refer to Table 33). From 3.5 m away from the fire, all of the locations around the fire are capable of receiving a TPP value above 17.5. Later in the simulation, the probability of exceeding a TPP value over 17.5 is insufficient in these locations. The time spent

at locations where there is sufficient probability to receive a TPP value above 17.5, will have to be limited according to Table 38.

There is sufficient probability to limit the available time to below 60 seconds in locations close to the fire (refer to Table 38). These areas will therefore not be suitable for search and rescue training (refer to section 1.5.3 Selecting the appropriate TPP value).

At 2.0 m above the floor, and for most of the temperature recorded locations, there is insufficient probability for the temperatures to exceed the critical gas temperature for the entire duration of the simulation (refer to Figure 56 - Figure 59). Location A1 is the only location with sufficient probability to exceed the critical gas temperature.

Location A4 is the next highest temperature location. The reason why location A4 recorded a higher temperature than locations A2 and A3 is because of the close proximity of location A4 to a wall. The hot gas layer at the ceiling is hotter than the gas lower down and it moves faster. When it comes in contact with the compartment's wall, it moves down along the wall, through the cooler gas layer below. This creates a cooler gap in the gas temperature readings between A1 and A4. This can be seen in Figure 69.

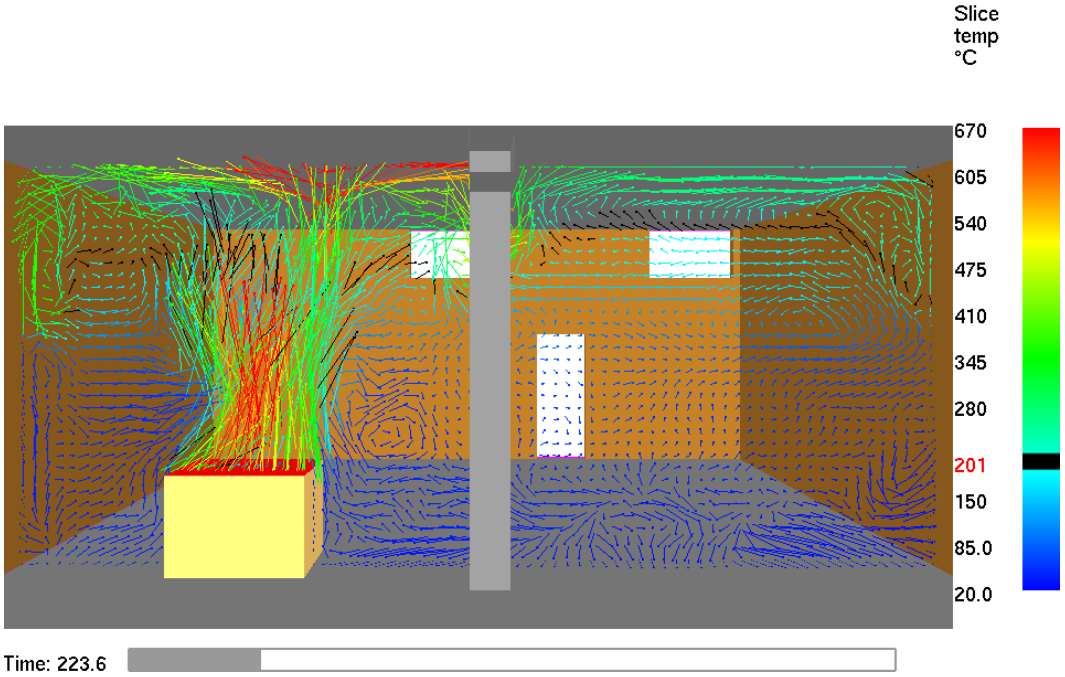

Figure 69: Vertical heat vector slice through the fire on the ground floor

No PPE

Group A has the highest gas temperatures recorded for its locations compared to Groups B, C and D. The wall behind group A, has the only low-level ventilation opening on this floor, providing the fire with oxygen. In the same wall, the high-level openings exhaust smoke and heat. This creates the route for the heat to flow to and escape. This also means that Group C on the opposite side of group A has the lowest gas temperatures recorded for its locations. This is illustrated in Figure 70, identifying where the hottest gas temperatures are at 1.5 m above floor level.

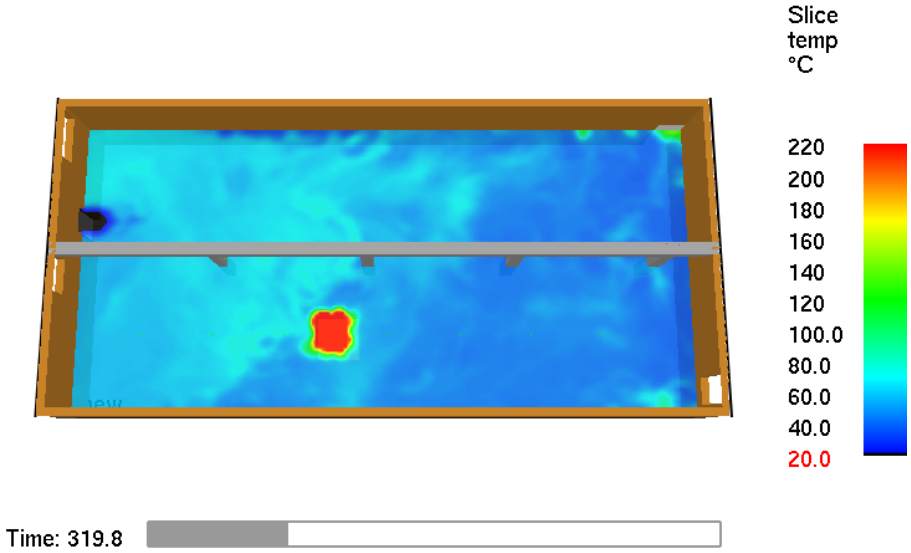

Figure 70: Temperature slice at 1.5 m on ground-floor

Burns to the respiratory tract are possible throughout the validated space (refer to Figure 48 - Figure 51). Firefighters without their BA mask in locations A3, A4, B3, C3 and C4, may be able to escape burns to the respiratory tract as these locations are below the probability for a gas temperature of 100 °C.

Firefighters without their BA are not expected to succumb to the fire's toxic combustion by-products (refer to Figure 61).

Should an item of protective clothing be removed, and skin is exposed, then burns can be expected in locations A1, B1, and D1. This is due to there being sufficient probability for the critical gas temperature to be exceeded (refer to Figure 48-Figure 51). Burns to exposed skin from heat flux exposure is possible in all locations (refer to Figure 40-Figure 43). Second degree burns can be avoided in locations B3, C3, and C4 if the firefighter escapes on receipt of pain.

3.6.3 Stability of live fire training structure

To maintain the stability of the structure and maximize the life of the structure it has been found that wall near the fire, the ceiling, the beam and the two columns closest to the fire need thermal protection (refer to Figure 66-Figure 68). These areas received temperatures in excess of 177 °C. The columns should be protected not just on the front face shown in Figure 68, but also on the sides of column.

As with the first floor, the floor around the fire should also receive thermal protection. The floor area to be protected is estimated to be the same size of the area to be protected on the ceiling. This should be considered as a conservative option. Mayfield and Hopkin [117] show that a significant portion of heat released from a pallet fire is convective heat. About 40 % is being convected at a HRR of 3,250 kW. With so much heat being convected away from the floor, it is considered that the remaining two methods of heat transfer, radiation and conduction, will not be successful in causing a larger affected area than that shown for the ceiling.

CHAPTER 4: CONCLUSIONS

The CFD based fire simulation model, FDS, has been successfully used for the purpose of measuring the fire environment in eThekwini's live fire training structure. The results from the FDS simulations have been used to identify fire related hazards for training firefighters using the live fire training structure, therefore satisfying the objective of this study.

For assessing heat flux exposure, firefighter garments were investigated. It was found that the TPP test used to rate firefighter garments, could be used to assess the safe time available to firefighters. It was considered more appropriate for estimating the time to second degree burns through protective clothing than the use of TDU. The use of the 17.5 TPP value was found to be appropriate for assessing the safety provided to firefighters from their garments. This, and a critical gas temperature of 260 °C for preventing damage to PPE and injury, could be found after further processing the results provided by FDS.

Past deaths in live fire training structures was reviewed. It was found that it was necessary to estimate firefighter tenability should mistakes be made. The mistakes included in the assessment of the results include the removing of protective garments, breathing in gases produced by the fire environment, and standing up straight when in fire conditions.

The results provided by the FDS simulations is an estimation of what actual results would be during live fire training. To assess the probability of the critical values

being exceeded, the likelihood which firefighters are injured at fire incidents was investigated. It was found that an appropriate probability would have to be below 0.44 %. This is to ensure that firefighters are less likely to be injured during live fire training than when attending to an actual fire scene.

The results show that trainee firefighters will face temperature and heat flux exposure hazards that must be avoided. These hazards are dependent on location of the firefighter, the time spent in the location and the time entering the location after the fire is ignited. The burn room on the first floor is significantly more hazardous than the surrounding compartments. The time spent in the burn room and the adjoining rooms, G and D, will have to be limited or only entered later after the fire's ignition. The ground floor, consisting of a single room, has similar results to the burn room on the first floor. The time must be limited, or the room must only be entered later after the fire's ignition. The severity of the hazards on both floors is also increased if mistakes are made during live fire training.

Avoiding these hazards will have to be incorporated into firefighter training. This can be done by utilizing the safe available time when planning training exercises for different locations found in the structure.

The rooms surrounding the burn room on the first floor provide the safest rooms in the existing structure. These rooms should be considered for training firefighters new to live fire training. This is due to these rooms predicting low hazards to training firefighters that might make a mistake.

The existing structure is required to use reduced fuel loads during firefighter training because the structure has been damaged from repeated heating and cooling. The results show that surfaces of the structure should have been thermally protected in areas close to the fire. The usability of the existing structure could have been prolonged if these surfaces were suitably thermally protected.

To reduce these hazards, the fire size can be reduced. The fire size was limited to prevent it becoming ventilation controlled. This ensured that the design of the structure is sufficient to provide enough oxygen for the fire. If the fire size is reduced, then the amount of oxygen required to the fire is reduced. This can allow the reduction in the burn room volume and ventilation requirements to the burn room.

CHAPTER 5: RECOMMENDATIONS AND FUTURE WORK

The literature shows that much has been done to understand the hazards that training firefighters may face in eThekwini's existing live fire training structure. However, it is acknowledged that some aspects of this study may require future work.

During this study, the following has been identified as areas that require further research to better the study:

1. The acceptable probability used to assess the training firefighter hazards was based on international firefighter injury statistics (refer to section 1.5.4 Probability of injury). It is recommended that research is done on developing South African firefighter injury statistics. This is to better comprehend the probability of critical values being exceeded when interpreting FDS simulations on South African firefighter hazards. This research should contain annual information on the number of firefighter injuries, cause of injury, and activity of firefighter at time of injury.

2. On the ground floor, the distance of measuring devices from the fire had to be limited to ensure validation (refer to section 2.4.1 Validation by experimental parameters). It is recommended that further validated test

series be conducted for devices to be located further from the fire in the burn room.

3. Access to the Protective Clothing Performance Simulator was prevented (refer to section 1.5.2 Safety of firefighters during live fire training). It is recommended that the use of the TPP value method used in this study, be compared to the Protective Clothing Performance Simulator. This is to determine the best method for assessing the impact of heat flux exposure on a firefighter's safe available time.

4. Moisture content has been noted to affect the HRR and it was acknowledged that the moisture content of wood pallets in the eThekwini area will have a higher moisture content than those that are typically tested (refer to section 1.4.3 Heat release rate). It is recommended that pallet fire tests be conducted in the eThekwini area in order to provide HRR histories that are better representatives for pallet fires simulated in the eThekwini area.

5. Both the first floor and the ground floor had set ventilation openings, shown in Figure 33 and Figure 34 (refer to section 2.5 Measuring output). Ventilation openings may vary throughout the duration of live fire training. This can be due to firefighters moving through ventilation openings, opening access points to enter the structure, and by tactically opening the structure to ventilate. This may change the HRR produced by the fire and impact the safe available time extended to firefighters. This impact is recommended to be investigated in future research.

REFERENCES

1. Zikanov, O., *Essential computational fluid dynamics*. 2010, Hoboken, New Jersey: John Wiley & Sons.

2. Liu, Y. and S. Cassady *A modified critical velocity for road tunnel fire smoke management with dedicated smoke extraction configuration*. Case Studies in Fire Safety, 2014. **2**, 16-27 DOI: http://dx.doi.org/10.1016/j.csfs.2014.09.001.

3. Hasib, R., et al. *Simulation of an experimental compartment fire by CFD*. Building and Environment, 2007. **42**, 3149-3160 DOI: http://dx.doi.org/10.1016/j.buildenv.2006.08.002.

4. United States Nuclear Regulatory Commission, *Verification and validation of selected fire models for nuclear power plant applications*. 2016, U.S. Nuclear Regulatory Commission Office of Nuclear Regulatory Research: Washington, DC.

5. Clarke, C. and M.J. Zak, *Fatalities to law enforcement officers and firefighters, 1992-97*, in *environments*. 1999, U.S. Bureau of Labor Statistics: Washington, DC. p. 5.

6. Raimundo, A.M. and A.R. Figueiredo, *Personal protective clothing and safety of firefighters near a high intensity fire front.* Fire Safety Journal, 2009. **44**(4): p. 514-521.

7. National Fallen Firefighters Foundation, *Report of the National Fire Service Research Agenda Symposium*. 2005, National Fallen Firefighters Foundation: Emmitsburg, MD.

8. National Fallen Firefighters Foundation, *Report of the 2nd National Fire Service Research Agenda Symposium*. 2011, National Fallen Firefighters Foundation: Emmitsburg, MD.

9. National Fallen Firefighters Foundation, *2015 National Fire Service Research Agenda*. 2016, National Fallen Firefighters Foundation: Arlington, VA.

10. National Fire Protection Association, *Standard on facilities for fire training and associated props*. 2019, National Fire Protection Association: Quincy, MA.

11. Evarts, B. and J.L. Molis, *United states firefighter injuries-2017*. 2018, National Fire Protection Association: Quincy, MA.

12. *Injuries sustained by firefighters and firefighter fatalities by Fire and Rescue Authority,*. 2017; Available from: https://data.gov.uk/dataset/f7ccba2d-f679-46e1-8d6d-de7bee690d40/fire-statistics-fatalities-and-casualties.

13. National Fire Protection Association, *Standard on live fire training evolutions*. 2018, National Fire Protection Association: Quincy, MA.

14. Madrzykowski, D., *Fatal Training Fires: Fire Analysis for the Fire Service*. 2007, National Institute of Standards and Technology Gaithersburg, MD.

15. United States Nuclear Regulatory Commission, *Nuclear Power Plant Fire Modeling Analysis Guidelines*. 2012, U.S. Nuclear Regulatory Commission Office of Nuclear Regulatory Research: Washington, DC.

16. National Fire Protection Association, *Standard for fire fighter professional qualifications*. 2019, National Fire Protection Association: Quincy, MA.

17. Yeoh, G.-H. and K.K. Yuen, *Computational fluid dynamics in fire engineering: theory, modelling and practice*. 2009, Jordan Hill, Oxford: Butterworth-Heinemann.

18. Ferziger, J.H. and M. Peric, *Computational methods for fluid dynamics*. Third ed. 2002, New York: Springer-Verlag

19. Panton, R.L., *Incompressible flow*. Fourth ed. 2013, Hoboken, New Jersey: John Wiley & Sons.

20. Pletcher, R.H., J.C. Tannehill, and D. Anderson, *Computational fluid mechanics and heat transfer*. Second ed. 1997, Washington, DC: Taylor & Francis.

21. Tu, J., G.-H. Yeoh, and C. Liu, *Computational fluid dynamics: a practical approach*. Second ed. 2012, Waltham, MA: Butterworth-Heinemann.

22. Blazek, J., *Computational Fluid Dynamics : Principles and Applications*. Second ed. 2005, Oxford, United Kingdom: Elsevier Science & Technology.

23. McGrattan, K., et al., *Fire Dynamics Simulator; Technical Reference Guide, Volume 1: Mathematical Model*. 2017, National Institute of Standards and Technology: Gaithersburg, MD.

24. McGrattan, K., et al., *Fire Dynamic Simulator User's Guide*. 2017, National Institute of Standards and Technology and VTT Technical Research Centre of Finland: Gaithersburg, MD.

25. Forney, G.P., *Smokeview, A Tool for Visualizing Fire Dynamics Simulation Data Volume I: User's Guide*. 2017, National Institute of Standards and Technology: Gaithersburg, Maryland.

26. McGrattan, K., et al., *Fire Dynamic Simulator, Technical Reference Guide, Volume 4: Configuration Management*. 2017, National Institute of Standards and Technology: Gaithersburg, MD.

27. McDermott, R.J. *A velocity divergence constraint for large-eddy simulation of low-Mach flows*. Journal of Computational Physics, 2014. **274**, 413-431 DOI: https://doi.org/10.1016/j.jcp.2014.06.019.

28. Baum, H.R. and R.G. Rehm, *The equations of motion for thermally driven, buoyant flows.* Journal of Research of the Notional Bureau of Standards, 1978. **83**(3): p. 297-308.

29. Xiao, B. *Comparison of numerical and experimental results of fire induced doorway flows*. Fire technology, 2012. **48**, 595-614.

30. McGrattan, K.B., H.R. Baum, and R.G. Rehm *Large eddy simulations of smoke movement*. Fire Safety Journal, 1998. **30**, 161-178 DOI: https://doi.org/10.1016/S0379-7112(97)00041-6.

31. Floyd, J.E., *Comparison of CFAST and FDS for fire simulation with the HDR T51 and T52 tests*. 2002, National Institute of Standards and Technology: Gaithersburg, Maryland.

32. Morinishi, Y., et al. *Fully Conservative Higher Order Finite Difference Schemes for Incompressible Flow*. Journal of Computational Physics, 1998. **143**, 90-124 DOI: https://doi.org/10.1006/jcph.1998.5962.

33. Patankar, S.V., *Numerical heat transfer and fluid flow*. 1980, New York: McGraw-Hill.

34. Maulik, R. and O. San *Explicit and implicit LES closures for Burgers turbulence*. Journal of Computational and Applied Mathematics, 2018. **327**, 12-40 DOI: https://doi.org/10.1016/j.cam.2017.06.003.

35. Pope, S.B., *Turbulent flows*. 2000, Cambridge: Cambridge University Press.

36. Hostikka, S., *Development of fire simulation models for radiative heat transfer and probabilistic risk assessment*. 2008, VTT Technical Research Centre of Finland: Espoo, Finland.

37. Jahna, W., G. Reina, and J.L. Toreroa, *The Effect of Model Parameters on the Simulation of Fire Dynamics*, in *Fire Safety Science – Proceedings of the Ninth International Symposium* B. Karlsson, Editor. 2008, International Association for Fire Safety Science Karlsruhe University, Karlsruhe. p. 1341-1352.

38. Hoffmann, N. and N.C. Markatos *Thermal radiation effects on fires in enclosures*. Applied Mathematical Modelling, 1988. **12**, 129-140 DOI: https://doi.org/10.1016/0307-904X(88)90004-2.

39. Kennedy, I.M. *Models of soot formation and oxidation*. Progress in Energy and Combustion Science, 1997. **23**, 95-132 DOI: https://doi.org/10.1016/S0360-1285(97)00007-5.

40. Overholt, K.J., J.E. Floyd, and O.A. Ezekoye *Computational Modeling and Validation of Aerosol Deposition in Ventilation Ducts*. Fire Technology, 2016. **52**, 149-166 DOI: 10.1007/s10694-014-0414-5.

41. Jahn, W., G. Rein, and J.L. Torero, *11, Posteriori modelling of Fire Test One*, in *The Dalmarnock Fire Tests: Experiments and Modelling*, G. Rein, C.A. Empis, and R. Carvel, Editors. 2007, School of Engineering and Electronics, University of Edinburgh: Edinburgh, UK.

42. Guigay, G., et al., *The Use of CFD Calculations to Evaluate Fire-Fighting Tactics in a Possible Backdraft Situation.* Fire Technology, 2009. **45**(3): p. 287-311.

43. Averill, J.D., et al., *Report on residential fireground field experiments*, in *NIST Technical Note 1661*, B. Robinson, Editor. 2010, National Institute of Standards and Technology: Gaithersburg, MD. p. 104.

44. Alarifi, A.A., et al., *Effects of fire-fighting on a fully developed compartment fire: Temperatures and emissions.* Fire Safety Journal, 2014. **68**: p. 71-80.

45. Palm, A., M. Kumm, and H. Ingason, *Full Scale Firefighting Tests in the Tistbrottet Mine.* Fire Technology, 2016. **52**(5): p. 1519-1537.

46. Babrauskas, V., *Effective heat of combustion for flaming combustion of conifers.* Canadian Journal of Forest Research, 2006. **36**(3): p. 659-663.

47. Janssens, M., *Calorimetry*, in *SFPE Handbook of Fire Protection Engineering*, M.J. Hurley, et al., Editors. 2016, Springer New York: New York, NY. p. 905-951.

48. Byström, A., et al., *Full-scale experimental and numerical studies on compartment fire under low ambient temperature.* Building and Environment, 2012. **51**: p. 255-262.

49. Cheng, X.-d., et al., *Numerical Study on Temperature Distribution of Structural Components Exposed to Travelling Fire.* Procedia Engineering, 2014. **71**: p. 166-172.

50. Pope, N.D. and C.G. Bailey, *Quantitative comparison of FDS and parametric fire curves with post-flashover compartment fire test data.* Fire Safety Journal, 2006. **41**(2): p. 99-110.

51. Weinschenk, C.G., K.J. Overholt, and D. Madrzykowski, *Simulation of an Attic Fire in a Wood Frame Residential Structure, Chicago, IL.* Fire Technology, 2016. **52**(6): p. 1629-1658.

52. Heskestad, G. and M.A. Delichatsios, *Update: The initial convective flow in fire.* Fire Safety Journal, 1989. **15**(6): p. 471-475.

53. Janssens, M., *Rate of heat release of wood products.* Fire Safety Journal, 1991. **17**(3): p. 217-238.

54. Bwalya, A.C., E. Zalok, and G. Hajisophocleous, *Design fires for commercial premises: results of phase 1*. 2006, Institute for Research in Construction, National Research Council Canada: Canada.

55. Saber, H.H. and A. Kashef. *CFD simulations for fully-developed fires in a room under different ventilation conditions*. in *16th Annual Conference of the CFD Society of Canada*. 2008. Saskatoon, Saskatchewan: National Research Council Canada.

56. Lee, B.T., *Heat Release Rate Characteristics of Some Combustible Fuel Sources in Nuclear Power Plants*. 1985, National Bureau of Standards: Gaithersburg, MD.

57. Krasner, L., *Burning Characteristics of Wooden Pallets as a Test Fuel*, in *Progress Report Serial No. 16437*. 1968, Factory Mutual Research Corporation: Norwood, MA.

58. Babrauskas, V., *Heat Release Rates*, in *SFPE Handbook of Fire Protection Engineering*, M.J. Hurley, et al., Editors. 2016, Springer New York: New York, NY. p. 799-904.

59. National Fire Protection Association, *National fire alarm and signaling code*. 2019, National Fire Protection Association: Quincy, MA.

60. Tran, H.C., *Experimental data on wood materials.* Heat release in fires. New York: Elsevier Applied Science, 1992: p. 357-372.

61. Simpson, W.T., *Equilibrium moisture content of wood in outdoor locations in the United States and worldwide*. 1998, United States Department of Agriculture: Washington, DC. p. 11.

62. Weather and Climate. *Average humidity in Durban*. 2019; Available from: https://weather-and-climate.com/average-monthly-Humidity-perc,durban,South-Africa.

63. Climate-Data.org. *Climate Durban*. Available from: https://en.climate-data.org/africa/south-africa/kwazulu-natal/durban-511/.

64. Campbell, R. *U.S. Firefighter Injuries on the Fireground, 2010–2014*. Fire Technology, 2018. **54**, 461-477 DOI: 10.1007/s10694-017-0692-9.

65. Austin, C.C., G. Dussault, and D.J. Ecobichon, *Municipal firefighter exposure groups, time spent at fires and use of self-contained-breathing-apparatus.* American Journal of Industrial Medicine, 2001. **40**(6): p. 683-692.

66. Yan Jiang, Y., et al., *An integrated numerical simulator for thermal performance assessments of firefighters' protective clothing.* Fire Safety Journal, 2010. **45**(5): p. 314-326.

67. Lawson, J.R., *Fire fighters' protective clothing and thermal environments of structural fire fighting*, in *NISTIR 5804*. 1996, National Institute of Standards and Technology: Gaithersburg, MD.

68. Jin, L., et al. *New Approaches to Evaluate the Performance of Firefighter Protective Clothing Materials*. Fire Technology, 2018. 1-25 DOI: 10.1007/s10694-018-0730-2.

69. Walker, A., R. Pope, and R.M. Orr *The impact of fire suppression tasks on firefighter hydration: a critical review with consideration of the utility of reported hydration measures*. Annals of Occupational and Environmental Medicine, 2016. **28**, 63 DOI: 10.1186/s40557-016-0152-x.

70. Barr, D., W. Gregson, and T. Reilly *The thermal ergonomics of firefighting reviewed*. Applied Ergonomics, 2010. **41**, 161-172 DOI: https://doi.org/10.1016/j.apergo.2009.07.001.

71. Moran, D.S., A. Shitzer, and K.B. Pandolf *A physiological strain index to evaluate heat stress*. American Journal of Physiology-Regulatory, Integrative and Comparative Physiology, 1998. **275**, R129-R134 DOI: 10.1152/ajpregu.1998.275.1.R129.

72. McQuerry, M., R. Barker, and E. DenHartog *Relationship between novel design modifications and heat stress relief in structural firefighters' protective clothing*. Applied Ergonomics, 2018. **70**, 260-268 DOI: https://doi.org/10.1016/j.apergo.2018.03.004.

73. Lee, Y.M. and R.L. Barker, *Effect of moisture on the thermal protective performance of heat-resistant fabrics.* Journal of Fire Sciences, 1986. **4**(5): p. 315-331.

74. Barker, R.L., et al., *Effects of moisture on the thermal protective performance of firefighter protective clothing in low-level radiant heat exposures.* Textile Research Journal, 2006. **76**(1): p. 27-31.

75. Office of the Deputy Prime Minister, *Physiological Assessment of Firefighting, Search and Rescue in the Built Environment*, in *Fire Research Technical Report*. 2004, Optimal Performance Limited On behalf of the Office of the Deputy Prime Minister: London.

76. Fahy, R.F., *US firefighter deaths related to training, 2001-2010*. 2012, National Fire Protection Association: Quincy, MA.

77. Donnelly, M.K., et al., *Thermal environment for electronic equipment used by first responders*. 2006, National Institute of Standards and Technology: Gaithersburg, MD.

78. Krasny, J., J.A. Rockett, and D. Huang, *Protecting fire fighters exposed in room fires: Comparison of results of bench scale test for thermal protection and conditions during room flashover.* Fire Technology, 1988. **24**(1): p. 5-19.

79. Fahy, R.F., *US firefighter deaths related to training, 1996-2005*. 2006, National Fire Protection Association: Quincy, MA.

80. Traina, N., et al., *Occupant Tenability in Single Family Homes: Part I—Impact of Structure Type, Fire Location and Interior Doors Prior to Fire Department Arrival.* Fire Technology, 2017. **53**(4): p. 1589-1610.

81. Su, J.Z., et al., *Unprotected Floor Assemblies and Tenability Conditions in a Test House Under Two Basement Fire Scenarios.* Fire Technology, 2011. **47**(3): p. 631-664.

82. Purser, D.A. and J.L. McAllister, *Assessment of Hazards to Occupants from Smoke, Toxic Gases, and Heat*, in *SFPE Handbook of Fire Protection Engineering*, M.J. Hurley, et al., Editors. 2016, Springer New York: New York, NY. p. 2308-2428.

83. Svensson, S., *Experimental Study of Fire Ventilation During Fire Fighting Operations.* Fire Technology, 2001. **37**(1): p. 69-85.

84. Gómez, R. and L.C. Cancio, *Management of Burn Wounds in the Emergency Department.* Emergency Medicine Clinics of North America, 2007. **25**(1): p. 135-146.

85. Guanquan, C. and S. Jinhua, *The Effect of Pre-movement Time and Occupant Density on Evacuation Time.* Journal of Fire Sciences, 2006. **24**(3): p. 237-259.

86. National Fire Protection Association, *Standard on protective ensembles for structural fire fighting and proximity fire fighting*. 2018, National Fire Protection Association: Quincy, MA.

87. Berenson, P.J., A.P. Gagge, and J.B. Pierce, *Temperature*, in *Bioastronautics Data Book*, J.F. Parker Jr and V.R. West, Editors. 1973, National Aeronautics and Space Administration: Washington, DC.

88. Song, G., S. Mandal, and R.M. Rossi, *Development of high performance thermal protective clothing*, in *Thermal Protective Clothing for Firefighters*. 2017, Woodhead Publishing: Duxford, UK. p. 46-75.

89. Lawson, J.R., W.E. Mell, and K. Prasad, *A Heat Transfer Model for Firefighters' Protective Clothing, Continued Developments in Protective Clothing Modeling.* Fire Technology, 2010. **46**(4): p. 833-841.

90. S O'Sullivan, S.J., *Human vulnerability to thermal radiation offshore*. 2004, Health & Safety Laboratory: Buxton.

91. Su, Y., et al., *Developing a test device to analyze heat transfer through firefighter protective clothing.* International Journal of Thermal Sciences, 2019. **138**: p. 1-11.

92. Abbott, N.J. and S. Schulman, *Protection From Fire: Nonflammable Fabrics and Coatings*.* Journal of Coated Fabrics, 1976. **6**(1): p. 48-64.

93. Foster, J. and G. Roberts, *Measurements of the firefighting environment*. 1994, Department for Communities and Local Government United Kingdom. p. 1-20.

94. Coletta, G., et al., *The Development of Criteria for Firefighter's Gloves: Glove Criteria and Test Methods. Volume II*. Vol. II. 1976, Cambirdge, MA: Arthur D. Little, Inc.

95. Federal Emergency Management Agency/United States Fire Administration, *Minimum Standards on Structural Fire Fighting Protective Clothing and Equipment: A Guide for Fire Service Education and Procurement*. 1992, United States Fire Administration: Emmitsburg, MD.

96. Behnke, W.P., *Predicting flash fire protection of clothing from laboratory tests using second-degree burn to rate performance.* Fire and Materials, 1984. **8**(2): p. 57-63.

97. Peacock, R.D., et al., *Protecting fire fighters exposed in room fires, part 2: Performance of turnout coat materials under actual fire conditions.* Fire Technology, 1990. **26**(3): p. 202-222.

98. Kim, H.-J. and D. Lilley. *Heat release rates of burning items in fires*. in *38th Aerospace Sciences Meeting and Exhibit*. 2000. Reno, NV: American Institute of Aeronautics and Astronautics.

99. Lawson, J.R., W.D. Walton, and W.H. Twilley, *Fire performance of furnishings as measured in the NBS furniture calorimeter. Part 1*. 1984, U.S. Department of Commerce: Washington, DC.

100. McGrattan, K., et al., *Fire Dynamics Simulator Technical Reference Guide Volume 3: Validation*. 2017, National Institute of Standards and Technology: Gaithersburg, MD.

101. U.S. Fire Administration. *U.S. fire statistics*. 2019; Available from: https://www.usfa.fema.gov/data/statistics/#tab-3.

102. Incidents attended by fire and rescue services. 2017; Available from: https://data.gov.uk/dataset/bcce7434-0b1a-4700-96b9-fcff8eef4dc0/fire-statistics-incidents-attended.

103. Statistics Canada, *Fire statistics in Canada, Selected Observations from the National Fire Information Database 2005 to 2014*. 2017, Canadian Association of Fire Chiefs.

104. Incident-based fire statistics by type of fire incident and type of structure. 2019; Available from: https://www150.statcan.gc.ca/t1/tbl1/en/tv.action?pid=3510019201&pickMembers%5B0%5D=1.3.

105. Weinschenk, C., R. Nicks, and O.A. Ezekoye, *Analysis of Fireground Standard Operating Guidelines/Procedures Compliance for Austin Fire Department.* Fire Technology, 2008. **44**(1): p. 39-64.

106. ASHRAE, *2013 ASHRAE HANDBOOK FUNDAMENTALS*. SI ed. 2013, Atlanta, GA: ASHRAE.

107. Drysdale, D., *An introduction to fire dynamics*. Third ed. 2011, West Sussex: John Wiley & Sons.

108. Khan, M.M., A. Tewarson, and M. Chaos, *Combustion Characteristics of Materials and Generation of Fire Products*, in *SFPE Handbook of Fire Protection Engineering*, M.J. Hurley, et al., Editors. 2016, Springer New York: New York, NY. p. 1143-1232.

109. Hurley, M., *Appendix 3. Fuel Properties and Combustion Data*, in *SFPE handbook of fire protection engineering*, D. Gottuk, et al., Editors. 2016, Springer New York. p. 3437-3475.

110. Alpert, R.L., *Ceiling Jet Flows*, in *SFPE Handbook of Fire Protection Engineering*, M.J. Hurley, et al., Editors. 2016, Springer New York: New York, NY. p. 429-454.

111. Floyd, J., K. Overholt, and O. Ezekoye, *Soot Deposition and Gravitational Settling Modeling and the Impact of Particle Size and Agglomeration*, in *Fire Safety Science – Proceedings of the Eleventh International Symposium* D. Nilsson, P.v. Hees, and R. Jansson, Editors. 2014, International Association for Fire Safety Science University of Canterbury, Christchurch. p. 376-388.

112. Butler, K.M. and G.W. Mulholland, *Generation and Transport of Smoke Components.* Fire Technology, 2004. **40**(2): p. 149-176.

113. Lautenberger, C., et al., *Radiation Heat Transfer*, in *SFPE Handbook of Fire Protection Engineering*, M.J. Hurley, et al., Editors. 2016, Springer New York: New York, NY. p. 102-137.

114. Jahn, W., G. Rein, and J.L. Torero, *A posteriori modelling of the growth phase of Dalmarnock Fire Test One.* Building and Environment, 2011. **46**(5): p. 1065-1073.

115. Eskom confirms another full day of load shedding. 2018; Available from: https://www.fin24.com/Economy/Eskom/eskom-confirms-another-full-day-of-load-shedding-20181206.

116. Fire and Emergency Planning Directorate, *Compartment fires and tactical ventilation*. Fire service manual. Vol. 2. 1997, Norwich: The Stationery Office.

117. Mayfield, C. and D. Hopkin, *Design fires for use in fire safety engineering*. 2011, Garston, Watford: IHS BRE Press.

APPENDIX A

Table 39: First floor – individual room critical heat flux using measuring devices at 1.5 m above the floor

Room Entry Time After Ignition	**Individual room critical heat flux (kW/m^2)**						
	A1	**B1**	**C1**	**D1**	**E1**	**G1**	**G2**
0 seconds	0.56	0.56	0.56	0.56	0.56	0.56	0.56
100 seconds	0.61	0.61	0.61	0.61	0.61	0.61	0.61
200 seconds	0.67	0.67	0.67	0.67	0.67	0.67	0.67
300 seconds	0.73	0.73	0.73	0.73	0.73	0.73	0.73
400 seconds	0.81	0.81	0.81	0.81	0.81	0.81	0.81
500 seconds	0.92	0.92	0.92	0.92	0.92	0.92	0.92
600 seconds	1.05	1.05	1.05	1.05	1.05	1.05	1.05
700 seconds	1.22	1.22	1.22	1.22	1.22	1.22	1.22
	H1	**H2**	**H3**	**I1**	**J1**	**K1**	
0 seconds	0.56	0.56	0.56	0.56	0.56	0.56	
100 seconds	0.61	0.61	0.61	0.61	0.61	0.61	
200 seconds	0.67	0.67	0.67	0.67	0.67	0.67	
300 seconds	0.73	0.73	0.73	0.73	0.73	0.73	
400 seconds	0.81	0.81	0.81	0.81	0.81	0.81	
500 seconds	0.92	0.92	0.92	0.92	0.92	0.92	
600 seconds	1.05	1.05	1.05	1.05	1.05	1.05	
700 seconds	1.22	1.22	1.22	1.22	1.22	1.22	

Table 40: First floor – location of critical heat flux in the burn room using measuring devices at 1.5 m above the floor

Location Entry Time After Ignition	**Location critical heat flux (kW/m^2)**				
	F1	**F2**	**F3**	**F4**	**F5**
0 seconds	1.71	1.70	2.03	2.50	2.59
100 seconds	2.19	2.18	2.72	3.68	3.83
200 seconds	2.91	2.92	3.76	6.00	6.26
300 seconds	3.66	3.76	5.03	9.24	10.84
400 seconds	3.13	3.15	4.94	10.06	13.11
500 seconds	1.73	1.58	3.24	5.93	8.81
600 seconds	1.05	1.05	2.14	3.68	4.58
700 seconds	1.22	1.22	1.46	2.28	2.66
800 seconds	1.47	1.47	1.47	1.47	1.47
900 seconds	1.84	1.84	1.84	1.84	1.84
1,000 seconds	2.44	2.44	2.44	2.44	2.44
1,100 seconds	3.66	3.66	3.66	3.66	3.66
1,200 seconds	7.32	7.32	7.32	7.32	7.32

Table 41: First floor – individual room critical heat flux using measuring devices at 2.0 m above the floor

Room Entry Time After Ignition	**Individual room critical heat flux (kW/m^2)**						
	A2	**B2**	**C2**	**D2**	**E2**	**G4**	**G12**
0 seconds	0.56	0.56	0.56	0.56	0.56	0.56	0.56
100 seconds	0.61	0.61	0.61	0.61	0.61	0.61	0.61
200 seconds	0.67	0.67	0.67	0.67	0.67	0.67	0.67
300 seconds	0.73	0.73	0.73	0.73	0.73	0.73	0.73
400 seconds	0.81	0.81	0.81	0.81	0.81	0.81	0.81
500 seconds	0.92	0.92	0.92	0.92	0.92	0.92	0.92
600 seconds	1.05	1.05	1.05	1.05	1.05	1.05	1.05
700 seconds	1.22	1.22	1.22	1.22	1.22	1.22	1.22
	H2	**I2**	**J2**	**K2**	**L2**	**M2**	
0 seconds	0.56	0.56	0.56	0.56	0.56	0.56	
100 seconds	0.61	0.61	0.61	0.61	0.61	0.61	
200 seconds	0.67	0.67	0.67	0.67	0.67	0.67	
300 seconds	0.73	0.73	0.73	0.73	0.73	0.73	
400 seconds	0.81	0.81	0.81	0.81	0.81	0.81	
500 seconds	0.92	0.92	0.92	0.92	0.92	0.92	
600 seconds	1.05	1.05	1.05	1.05	1.05	1.05	
700 seconds	1.22	1.22	1.22	1.22	1.22	1.22	

Table 42: First floor – location of critical heat flux in the burn room using measuring devices at 2.0 m above the floor

Location Entry Time After Ignition	**Critical heat flux at location (kW/m^2)**				
	F1	**F2**	**F3**	**F4**	**F5**
0 seconds	1.77	1.76	1.94	2.25	2.31
100 seconds	2.31	2.29	2.61	3.20	3.32
200 seconds	3.18	3.13	3.71	5.17	5.47
300 seconds	4.37	4.24	5.27	8.81	10.06
400 seconds	4.00	3.76	5.27	10.44	13.42
500 seconds	1.97	1.81	3.00	4.66	6.48
600 seconds	1.05	1.05	1.74	2.36	2.75
700 seconds	1.22	1.22	1.22	1.33	1.44
800 seconds	1.47	1.47	1.47	1.47	1.47
900 seconds	1.84	1.84	1.84	1.84	1.84
1,000 seconds	2.44	2.44	2.44	2.44	2.44
1,100 seconds	3.66	3.66	3.66	3.66	3.66
1,200 seconds	7.32	7.32	7.32	7.32	7.32

Table 43: Ground floor – location of critical heat flux using measuring devices at 1.5 m above the floor

Location Entry Time After Ignition	**Critical heat flux at location (kW/m^2)**					
	A1	**A2**	**A3**	**A4**	**B1**	**B2**
0 seconds	8.81	3.50	2.18	1.53	8.54	3.01
100 seconds	12.81	4.55	2.79	1.78	11.74	3.73
200 seconds	13.75	5.42	3.10	1.81	12.25	4.24
300 seconds	14.83	5.47	3.01	1.38	13.74	4.40
400 seconds	13.75	4.99	2.26	0.81	12.81	4.21
500 seconds	13.11	4.11	1.32	0.92	11.99	3.44
600 seconds	11.99	2.80	1.05	1.05	10.63	2.50
700 seconds	9.72	2.12	1.22	1.22	8.81	1.90
800 seconds	8.54	1.68	1.47	1.47	7.94	1.47
900 seconds	7.42	1.84	1.84	1.84	7.04	1.84
1,000 seconds	6.00	2.44	2.44	2.44	5.87	2.44
1,100 seconds	4.94	3.66	3.66	3.66	4.82	3.66
1,200 seconds	7.32	7.32	7.32	7.32	7.32	7.32
	B3	**C1**	**C2**	**C3**	**C4**	**D1**
0 seconds	1.31	8.95	2.71	1.49	1.28	9.55
100 seconds	1.45	10.44	2.89	1.66	1.40	11.74
200 seconds	1.42	9.89	2.86	1.59	1.27	11.05
300 seconds	1.17	10.44	2.82	1.32	1.02	11.99
400 seconds	0.81	9.72	2.55	0.95	0.81	10.84
500 seconds	0.92	8.95	2.14	0.92	0.92	10.06
600 seconds	1.05	8.54	1.81	1.05	1.05	9.55
700 seconds	1.22	7.13	1.53	1.22	1.22	7.94
800 seconds	1.47	6.63	1.47	1.47	1.47	7.42
900 seconds	1.84	6.06	1.84	1.84	1.84	6.71
1,000 seconds	2.44	5.27	2.44	2.44	2.44	5.75
1,100 seconds	3.66	4.44	3.66	3.66	3.66	4.90
1,200 seconds	7.32	7.32	7.32	7.32	7.32	7.32

Table 44: Ground floor – location of critical heat flux using measuring devices at 2.0 m above the floor

Location Entry Time After Ignition	**Critical heat flux at location (kW/m^2)**					
	A1	**A2**	**A3**	**A4**	**B1**	**B2**
0 seconds	9.72	3.81	2.31	1.97	9.55	3.06
100 seconds	16.10	5.17	3.01	2.44	14.45	3.81
200 seconds	18.18	6.19	3.40	2.62	14.83	4.40
300 seconds	19.43	6.33	3.33	2.41	17.61	4.54
400 seconds	18.18	5.75	2.68	1.48	16.10	4.34
500 seconds	17.08	4.82	1.59	0.92	15.23	3.52
600 seconds	15.23	3.10	1.05	1.05	12.81	2.52
700 seconds	11.27	2.19	1.22	1.22	9.55	1.81
800 seconds	9.55	1.63	1.47	1.47	8.67	1.47
900 seconds	7.94	1.84	1.84	1.84	7.32	1.84
1,000 seconds	5.93	2.44	2.44	2.44	5.75	2.44
1,100 seconds	4.51	3.66	3.66	3.66	4.37	3.66
1,200 seconds	7.32	7.32	7.32	7.32	7.32	7.32
	B3	**C1**	**C2**	**C3**	**C4**	**D1**
0 seconds	1.49	9.89	2.78	1.69	1.52	10.63
100 seconds	1.67	11.05	2.89	1.94	1.73	13.11
200 seconds	1.70	9.89	2.85	1.94	1.69	11.74
300 seconds	1.48	10.63	2.79	1.71	1.42	12.81
400 seconds	1.09	9.89	2.48	1.23	1.00	11.74
500 seconds	0.92	9.24	2.05	0.92	0.92	11.05
600 seconds	1.05	8.54	1.69	1.05	1.05	10.06
700 seconds	1.22	7.04	1.38	1.22	1.22	7.94
800 seconds	1.47	6.55	1.47	1.47	1.47	7.42
900 seconds	1.84	5.81	1.84	1.84	1.84	6.48
1,000 seconds	2.44	4.90	2.44	2.44	2.44	5.37
1,100 seconds	3.66	3.86	3.66	3.66	3.66	4.27
1,200 seconds	7.32	7.32	7.32	7.32	7.32	7.32